Function and Clearance of Conformers of the Prion Protein

Inaugural-Dissertation

zur

Erlangung des Doktorgrades der

Mathematisch-Naturwissenschaftlichen Fakultät

der Heinrich-Heine-Universität Düsseldorf

vorgelegt von

Janine Monique Muyrers

aus Aachen

Mai 2008

Aus dem Institut für Neuropathologie

der Heinrich-Heine-Universität Düsseldorf

Gedruckt mit der Genehmigung der

Mathematisch-Naturwissenschaftlichen Fakultät der

Heinrich-Heine-Universität Düsseldorf

Referent: PD. Dr. C. Korth

Korreferent: Prof. Dr. D. Willbold

Tag der mündlichen Prüfung: 16.06.2008

Table of contents

1 Introduction

1.1 Prion Protein

Prions (**pro**teinaceous, **in**fectious particles) are unprecedented infectious pathogens that cause prion diseases. Prion diseases are a group of neurodegenerative diseases that include Creutzfeldt-Jakob disease (CJD), Gerstmann-Straussler-Scheinker syndrome (GSS), fatal familial insomnia and Kuru in humans, bovine spongiform encephalopathy in cattle and scrapie in sheep. These diseases are characterized by the triad of spongiform change, neuronal loss and reactive gliosis (Kretzschmar*, et al.*, 1996). They are caused by the conversion of the normal cellular isoforms of the prion protein (PrP^{C}) into the scrapie isoform (PrP^{Sc}) through a posttranslational process Prusiner, 1998, which is stimulated by PrP^{Sc} itself (Fig. 1) (McKinley*, et al.*, 1983). The conversion is thought to take place either directly at the plasma membrane or in the early compartments of the endocytic pathway, e.g. caveolae or rafts, specialized regions in sphingolipids, cholesterol, and glycosyl phosphaticyl-inositol-anchored (Vey *et al.*, 1996; Naslavsky et al., 1997, Taraboulos *et al.*, 1995; Nunziante et al., 2003). The exact mechanism of the conversion is still enigmatic, although two models are currently in consideration. The first model favors a crystallization reaction, where PrP^{Sc} acts as the crystal seed. Newly converted PrP^{Sc} molecules are added to that seed, forming PrP^{Sc} aggregates (Come*, et al.*, 1993). The second model postulates a template-assisted conversion with intermediates, possibly PrP^{C}·PrP^{Sc} heterodimer complexes (Prusiner*, et al.*, 1998).

Although PrP^{C} and PrP^{Sc} are chemically identical, the biophysical features of PrP^{Sc} are drastically different in respect to solubility, structure and stability.

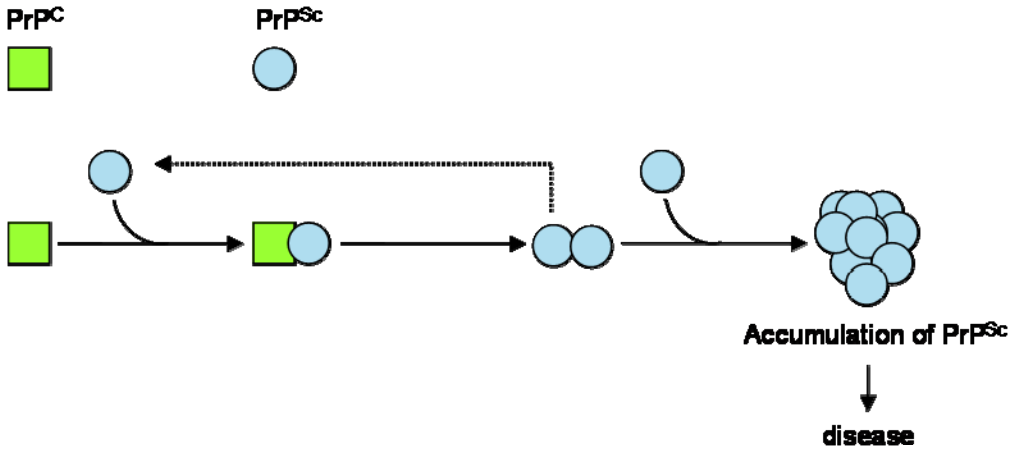

Fig. 1 Conversion of PrP^C to PrP^{Sc} The cellular prion protein PrP^C is converted into PrP^{Sc}. PrP^{Sc} in turn stimulates the conversion of further PrP^C molecules leading to the accumulation of PrP^{Sc} which consequently causes neurodegeneration.

So a portion of the α-helical and coil structure of PrP^C is refolded during the conversion into β sheet (Pan*, et al.*, 1993), which invests the conformation of PrP^{Sc} with an extreme stability. This stability makes PrP^{Sc} in turn highly resistant to chemical, heat or enzymatic degradation. Additionally the formation of β sheet rich structures is always correlated with oligomerization thereby facilitating PrP^{Sc} accumulation (Riesner, 2003). Taken together, PrP^{Sc} is characterized by rich β sheet structures, a tendency for polymerization into very large amyloidic structures (prion rods), resistance to Proteinase K digestion and detergent insolubility. Furthermore protease-sensitive PrP^{Sc} molecules that form low molecular weight aggregates (as small as 600 kDa) have been identified (Safar *et al.*, 1998; Tzaban*, et al.*, 2002). PrP^{Sc}, while transmissible (i.e. “infectious”), is not intrinsically pathological, because animals do not develop prion disease if their endogenous PrP gene is missing (Brandner *et al.*, 1996). PrP^C is a highly conserved 33-35 kDa glycophosphatidylinositol-anchored membrane protein with two N-linked glycosylation sites.

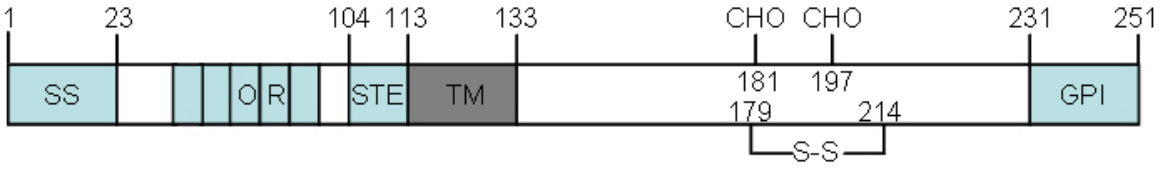

Fig. 2 schematic diagram of the domain structure of PrP The diagram shows the N-terminal signal sequence (SS), the octarepeat region (OR), the stop transfer effector sequence (STE), the potential transmembrane domain (TM), the potential N-linked glycosylation sites (CHO), the disulfide bond (S-S) and the C-terminal GPI anchor sequence Cai*, et al.*, .

The final processed form of PrP contains amino acids 23-231 from the original translation product of 253 amino acids. Peptide 1-22 is cleaved as signal peptide during trafficking, and peptide 232-253 is replaced by the GPI anchor. Asparagine residues 181 and 197 carry highly branched glyosyl groups with sialic acid substitutions. PrP exist in three forms, unglycosylated, with one glycosyl-, and with two glycosyl-groups. A disulfide bridge is formed between Cys 179 and Cys 214. PrP contains two hexarepeats and five octarepeats in its N-terminal region (Prusiner, 1989; Weissmann, 1994). A central hydrophobic domain residues 111-134, termed transmembrane (TM) domain, could serve to span the lipid bi-layer. It can act as a signal-anchor-sequence, directing translocation of the protein across the membrane to generate the different topological isoforms of PrP (Stewart *et al.*, 2001). N-terminal of the TM domain is a charged domain termed stop transfer domain (STE domain), which governs membrane integration of the TM domain (Yost *et al.*, 1990) (Fig. 2).

Mature PrP^C is anchored to the outer surface of the plasma membrane and undergoes endocytosis. The highest levels of PrP^C are found in brain, particularly in the hippocampus, but substantial amounts are also found in heart and skeletal muscles and lesser levels in most of other organs except for liver and pancreas (Weissmann*, et al.*, 1993).

1.2 Bioconformatics - topological heterogeneity of PrP^C

In the 1970's it was considered that protein folding was "spontaneous", i.e. dictated solely by the thermodynamics of protein-protein interactions (Anfinsen et al., 1973). This hypothesis was restricted by Ellis and Hartl, 1996 who discovered families of proteins collectively known as "molecular chaperones", which play roles in folding of newly synthesized proteins. In general, they are believed to work by preventing a protein in an unfolded state from engaging in inappropriate or undesired interactions, thereby allowing the opportunity for correct interactions to take place, resulting in proper folding. The current paradigm for the majority of researchers could be stated as: "Each protein has one final folded form and performs one function in the cell". The bioconformatic hypothesis of V. Lingappa refers to a new view of protein biogenesis and folding. The key tenets of this hypothesis are heterogeneous outcomes of synthesis for some proteins, generating multiple forms of identical amino acid sequence, termed conformers. These different conformers are generated by the effects of transient differences in the environment seen by the growing nascent chain (e.g. including protein-protein interactions, redox differences and others), however they refer to stable conformations unlike the transient switches in conformation in many enzymes. Some of these alternate forms are likely not "mis-folded" but rather alternatively folded, having distinct functions and are allowed by "quality control" machinery to leave the ER at particular times.

The hypothesis of bioconformatics has its origin in the study of biogenesis of the prion protein via *in vitro* translation studies of PrP mRNA on reticulocyte ribosomes in the presence of canine pancreas microsomes. (Hay *et al.*, 1987a; Hay *et al.*, 1987b; De Fea *et al.*, 1994). Whereas all other proteins studied up to that time were classifiable uniquely as one topological type (e.g. as either cytosolic proteins, secretory proteins, integral membrane proteins, or proteins destined to other organelles), the identical full length PrP, made from a homogeneous population of nascent chains, encoded in a single mRNA, was found to result in three topologically distinct isoforms (see Fig.3).

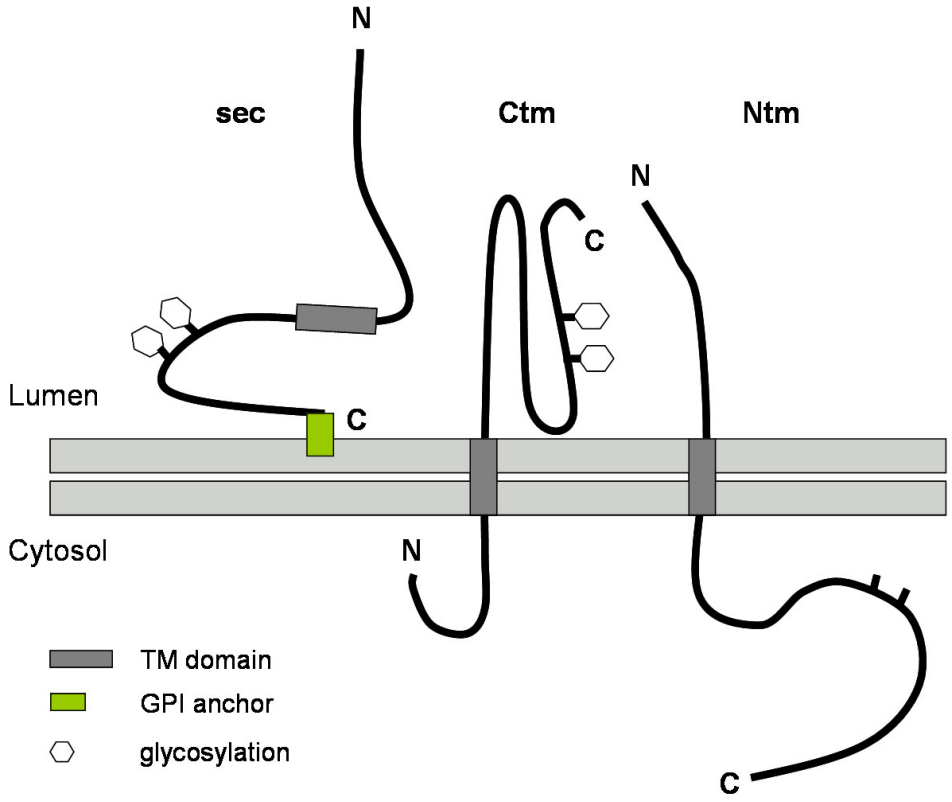

Fig. 3 Model of the three topological isoforms of PrP. The fully translocated secretory PrP (sec) is attached to the membrane via a C-terminal (C) GPI anchor; ^{Ctm}PrP (Ctm) spans the membrane with the transmembrane domain (TM domain) so that its C-terminus is luminal oriented. ^{Ntm}PrP (Ntm) spans the membrane with the transmembrane domain (TM domain) resulting in a luminal oriented N-terminus

One form is entirely translocated into the ER lumen and hence is termed secretory form (^{Sec}PrP) (Hay *et al.*, 1987b). This topology is consistent with most of what is known about PrP^{C}, which is on the cell surface, tethered to the membrane by a glycolipid anchor (Lehmann and Harris, 1995) and whose cleavage results in release from the cell (Stahl *et al.*, 1987). This conformer and also its N-terminally truncated forms, termed C1 and C2 (Vincent *et al.*, 2001; Sunyach *et al.*, 2007) are the prominently detected forms found under normal physiological conditions (Hegde *et al.*, 1998; Stewart and Harris, 2005). The C-terminal fragments were produced by endopro-teolytic cleavage within the N-terminal domain of PrP^{C}. Cleavage occurs at position 110/111, thereby generating C1 and N1 products and around residue 90 yields C2 and N2 fragments (Sunyach *et al.*, 2007).

The second form, termed ^{Ctm}PrP (C-trans transmembrane) spans the membrane once via a conserved, hydrophobic segment encompassing residues 111-134 (transmembrane domain), with the C-terminus on the exofacial surface (Hegde *et al.*, 1998). A third topological variant denoted ^{Ntm}PrP (N-trans transmembrane), spans the membrane via the same hydrophobic domain, but in the opposite orientation with the N terminus on the exofacial surface (Hegde *et al.*, 1998). There is evidence that the relative proportion of the three topological variants are determined by a region of nine hydrophobic acids, termed the stop transfer effector (STE), adjacent to the transmembrane domain of PrP (Lopez *et al.*, 1990; Yost *et al.*, 1990; Hegde *et al.*, 1998). Mutations, deletions, or insertions within these domains can alter the relative amount of each topological form of PrP that is synthesized at the ER (Yost *et al.*, 1990). A possible role of PrP topology in neurodegeneration is discussed, data of Hegde (Hegde *et al.*, 1998) indicate that ^{Ctm}PrP preferring mutations of PrP cause spontaneous neurodegenerative disease in mice and humans. For example the A117V mutation (alanine (A) to valine (V) substitution at position 117), which is causative for neurodegeneration in Gerstmann-Straussler-Scheinker syndrome, based in increased production of ^{Ctm}PrP at the ER membrane.

Tab. 1 Different topological isoforms of PrP

term	structure	topology	predicted function
PrP^{Sc}	β-sheets	Secretory/membrane associated	infectious
^{Sec}PrP	α-sheets	secretory	anti-apoptotic
^{Ctm}PrP	α-sheets	transmembrane	pro-apoptotic
^{Ntm}PrP	α-sheets	transmembrane	unknown

1.3 Physiological function of PrP^C

The physiological function of PrP^C is still unknown, although a number of hypotheses have been proposed in the last decade. PrP-null mice develop normally and show no gross behavioural abnormalities (Bueler *et al.*, 1992), albeit alterations in circadian activity and sleep were reported (Tobler *et al.*, 1996). Furthermore, it has been shown that copper binds to the octarepeat-containing N-terminal region of PrP^C, resulting in a suggested antioxidant activity of the protein (Brown *et al.*, 1997). Therefore, a functional role for PrP^C in copper metabolism and cellular protection against oxidative stress has been proposed (Wong *et al.*, 2000). Recent works point to a role for PrP^C in transducing signals. Antibody-mediated cross-linking of PrP^C on the surface of the murine neuronal 1C11-differentiated cell line promotes the dephosphorylation and activation of Fyn kinase (Mouillet-Richard *et al.*, 2000). A further implication of PrP^C in neuronal survival and differentiation is supported by the finding that different signal transduction pathways involved in neurite outgrowth and neuronal survival are elicited by PrP^C (Chen *et al.*, 2003). PrP-/- mice expressing some N-terminal truncations of PrP show severe neurodegeneration soon after birth (Shmerling *et al.*, 1998). Furthermore it has been postulated that PrP^C may be involved in neurotransmitter metabolism and differentiation of hematopoietic stem cell renewal (Zhang *et al.*, 2006). Various reports suggest that PrP^C may be involved in programmed cell death. Some studies support the hypothesis that PrP^C is pro-apoptotic, while other studies suggest an anti-apoptotic role (Roucou *et al.*, 2005, Roucou and LeBlanc, 2005; Kim *et al.*, 2004). These seemingly very diverse conclusions to the physiological function of PrP can be interpreted by the topological heterogeneity of PrP^C (see 1.2).

1.4 PrP assays

1.4.1 PrP^{Sc} assay

To separate between PrP^{C} and PrP^{Sc}, two biochemical tests are usually performed, either alone or in concert. In these tests the separation is based on different biochemical properties of the two PrP isoforms, as the tendency of PrP^{Sc} to aggregation or the partial enzymatic resistance of the core of PrP^{Sc} (PrP27-30). So is high-speed centrifugation used to pellet PrP^{Sc} (routinely used standard conditions are 100000 g for 1 h at 4°C) and proteolysis of the sample with proteinase K used to digest away PrP^{C} (standard proteolysis conditions are 20 µg/ml proteinase K at 37°C for 30 min).

1.4.2 Topological- and conformational PrP assay

Topology of a protein can be assessed by determining whether any regions of the molecule are accessible to protease added to the outside of membrane vesicles. Full protection from exogenous protease indicates complete translocation into the ER lumen. Conversely, digestion of certain domains to yield discrete protease-protected fragments indicates a membrane spanning topology, at which the exact orientation can be clarified by identification of the protected fragments with epitope-specific antibodies. This use of proteases as a probe of topology is distinctly different from the use of proteases as probes of protein conformation (for example, the resistance of PrP^{Sc}). Because the topology assay is carried out in the absence of detergent, the protection from protease is due to an intact membrane barrier (see Fig 4A). First analysis of the topology of *in vitro* translated PrP (topological assay) made by (Hay *et al.*, 1987a) suggested, that two distinct forms can be made at the ER, the fully translocated ^{Sec}PrP and one integral membrane protein spanning the bilayer twice, with defined extracytoplasmatic domains at both the amino and carboxy terminus. Digestion of the transmembrane form with proteases added to the outside of the membrane yielded two fragments: one is carboxy-terminal derived and glycosylated, and the other is amino-terminal and unglycosylated. Continuing analysis of the

proteolytic fragments resulting from topological assay provided evidence for the existence of two different transmembrane forms of PrP, using the difference in antibody reactivity, glycosylation and size of the fragments (Hegde *et al.*, 1998).

In a conformational assay the addition of non-denaturing detergent abolishes all topological differences, so that mild proteolysis is directed towards conformational differences (Fig. 4B) (Hegde *et al.*, 1998).

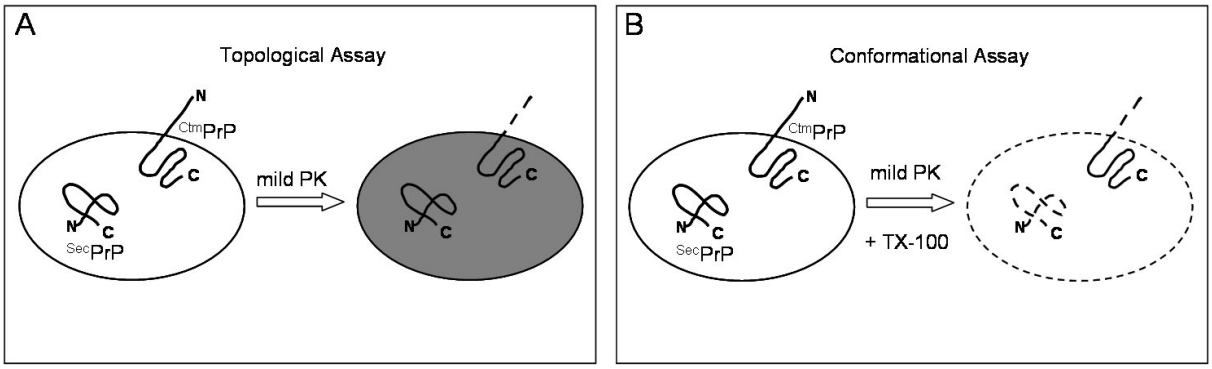

Fig. 4 (A) The topological assay Vesicles shield proteins from proteinase K (PK), therefore protecting ^{Sec}PrP from digestion, whereas the exposed residues of ^{Ctm}PrP signature fragment. **(B) The conformational assay** Addition of non-denaturing detergent abolishes al topological differences, so that PK digestion in this scenario is directed towards conformational differences, where the ^{Ctm}PrP signature fragment remains intact (Saghafi, 2007).

1.4.3 Conformation specific antibodies

The use of conformation specific antibodies enables the distinction between two different conformations. These antibodies can be split in two different categories, truly conformational antibody, i.e. antibodies which recognize a distinct three-dimensional epitope constituted by nonadjacent amino acid residues or indirect conformational antibodies, i.e. antibodies which have a linear epitope that is only exposed in one conformer and buried in all other conformations.

1.5 Protein degradation

As proteins play crucial roles in virtually all biological processes, the finely tuned equilibrium between their synthesis and degradation influences cellular homoeostasis. Protein degradation is a process which plays an important role in cell cycle, signal transduction and in maintaining the integrity of the proper folded state of proteins. There are two mayor types for intracellular protein degradation, a cytosolic degradation by the ubiquitin proteasome system (UPS) and a lysosomal degradation with proteases in acidic organelles.

1.5.1 The ubiquitin proteasome system (UPS)

The UPS is a large multienzyme complex which consists of both substrate-recruiting and substrate-degrading machinery. The substrate-recruiting machinery, which is composed of three enzymes (E1-3) (Hershko and Ciechanover, 1998) polyubiquitylates misfolded or unassembled proteins, so that proteins are recognized by the proteolytic machinery of the UPS, the 26S proteasome (Hough *et al.*, 1986). The 26S proteasome contains a central, barrel-like core particle, the 20S proteasome. Proteolytically active subunits of the 20S proteasome degrade polyubiquitylated proteins via postglutamylpeptide hydrolysis (PGPH), trypsin-like and chymotrypsin-like cleavage (Dick *et al.*, 1998; Smith *et al.*, 2005). In mammalian cells, proteasomes are located throughout the cytoplasm though most highly concentrated at the centrosome (Wigley *et al.*, 1999).

1.5.2 Lysosomal degradation

Lysosomes are the terminal degradative compartments of the endocytic pathway. The degradation of proteins in lysosomes is caused by hydrolytic enzymes (hydrolase) as proteases, lipases and glycosidase, and low pH. They receive extracellular components via endocytosis and intracellular material via autophagy, as well as via the biosynthetic pathway (Sachse *et al.*, 2002; Eskelinen, 2005; Klionsky, 2007; Luzio*, et al.*, 2007).

Autophagy

Autophagy is a pivotal physiological process for survival during starvation, differentiation, and normal growth control and may play a role in various other cellular functions, via the turnover of cellular macromolecules and organelles. It is defined as the process of sequestrating cytoplasmic proteins or even entire organelles into the lytic compartment (Kabeya *et al.*, 2000). Autophagy is on the one hand a housekeeping function because it is involved in cytoplasmic homeostasis by controlling the turnover of long-lived proteins and on the other hand a stimulated process. A great number of extracellular stimuli (hormonal or therapeutical treatment) as well as intracellular stimuli (accumulation of misfolded proteins) are able to modulate the autophagic response (Meijer and Codogno, 2004). The role of autophagy in the genesis or maintenance of neurodegenerative diseases is not clear at this point and seemingly opposing sets of data have been obtained from different neurodegenerative diseases. Autophagy may have a protective role against the development of a number of neurodegenerative diseases, because of its role in the clearance of misfolded proteins. For example the loss of the essential gene Atg7 leads to neurodegeneration, shown in Atg7 lacking mice (Komatsu *et al.*, 2006). On the other hand excessive autophagy may contribute to the pathogenesis of some neurodegenerative disorders such as Huntington's disease and Alzheimer's disease by altering the processing of mutant forms of huntingtin and amyloid precursor protein (Nixon *et al.*, 2000; Qin *et al.*, 2003).

As different the processes are, in which autophagy is involved, as numerous are the signaling pathways which are involved in the control of autophagy, though the mTOR signaling pathway plays a major role in transmitting autophagic stimuli.

mTOR pathway

The mammalian target of rapamycin (mTOR) is a serine-threonine protein kinase that controls a wide spectrum of cellular events in response to various environmental cues, including stimulation by growth factors, changes in nutrient conditions and fluctuations in energy levels (Martin and Hall, 2005; Wullschleger *et al.*, 2006a).

mTOR elicits its pleiotropic function in the context of two distinct multicomplexes termed mTOR complex 1 (mTORC1) and mTOR complex 2 (mTORC2) (Loewith *et al.*, 2002; Jacinto *et al.*, 2004). The mTORC2 contains TOR in association with the protein AVO3/rictor and LST8, and controls the actin cytoskeleton (Jacinto *et al.*, 2004). Its output is insensitive to rapamycin (Sarbassov *et al.*, 2004) and will not be considered further here. mTORC1 is comprised of TOR in association with the proteins raptor (Hara *et al.*, 2002) and LST8, and its output is inhibited by the bacterial macrolide rapamycin in complex with FKBP12 (Loewith *et al.*, 2002; Hara *et al.*, 2002). The major upstream regulators of mTORC1 are the Tuberous Sclerosis heterodimers (TSC1/TSC2) which activate the Ras-like small GTPase rheb by stimulating the intrinsic GTPase activity of rheb and, thus, negatively regulate rheb function. Conversely, inactivation of the TSC1/TSC2 complex results in accumulation of GTP-bound rheb, which activates mTORC1 (Manning and Cantley, 2003; Li *et al.*, 2004). Additionally, rheb antagonizes the activity of FKBP38, a member of the FK506-binding protein (FKBP) family, which acts as an endogenous inhibitor of mTOR (Bai *et al.*, 2007). Taken together, rheb serves as a regulator of mTOR activity.

Downstream of mTOR the two effectors eukaryotic initiation factor 4E (eIF4E) and the ribosomal S6 kinase 1 (S6K1) propagate the signals integrated by mTOR. S6K1 in turn phosphorylates mTOR (Holz and Blenis, 2005).

mTOR regulates a diverse array of cellular processes, including autophagy, cell size regulation, cell proliferation, protein sythesis and metabolism, and ribosom biogenesis (see Fig. 5).

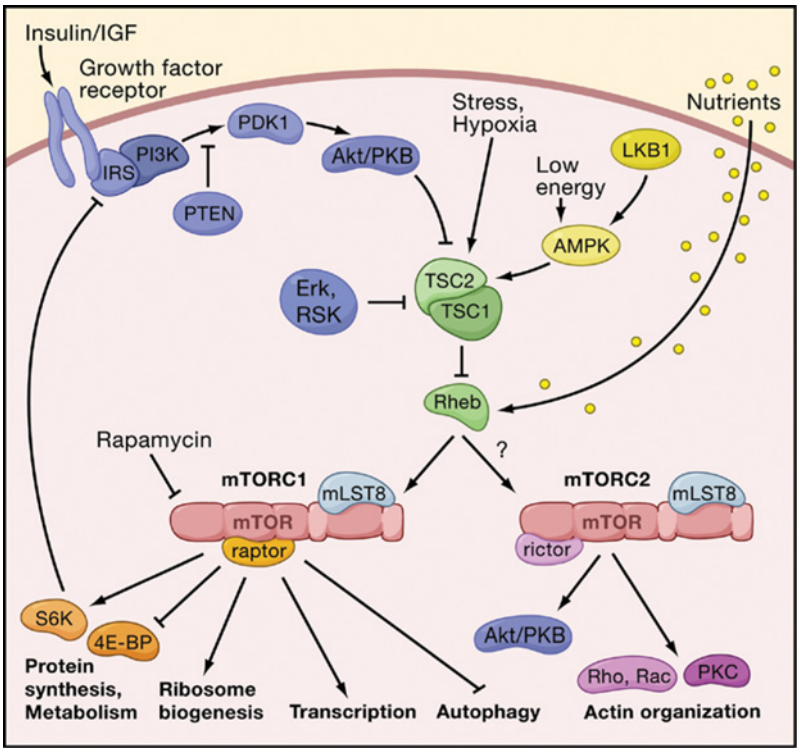

Fig. 5 Model of the mTOR Signaling Network in Mammalian Cells The mTOR signaling network consists of two major branches, each mediated by a specific mTOR complex (mTORC). Rapamycin-sensitive mTORC1 controls several pathways that collectively determine the mass (size) of the cell. Rapamycin-insensitive mTORC2 controls the actin cytoskeleton and thereby determines the shape of the cell. mTORC1 and possibly mTORC2 respond to growth factors (insulin/IGF), energy status of the cell, nutrients (amino acids), and stress. mTORC1 (and likely mTORC2) are multimeric, although are drawn as monomers. Arrows represent activation, whereas bars represent inhibition. Wullschleger*, et al.*, 2006b

1.5.3 Clearance of PrP^{Sc}

At least two ways of PrP^{Sc} reduction are known, first the reduction of PrP^{Sc} via interference of *de novo* formation of prions and second the degradation of pre-existing PrP^{Sc} via the lysosomal system.

A variety of experimental approaches for interfering with prion conversion have been reported. Some of them target PrP^{C}, as the conversion can be blocked by removing substrate for the process. This can be achieved by preventing the PrP^{C} expression (Prusiner, 1998; Weissmann *et al.*, 2001; Tilly *et al.*, 2003) or by inhibiting its transport to the plasma membrane (Gilch *et al.*, 2003). Chemical chaperones are thought to interfere with the interaction of PrP^{Sc} with complexes consisting of PrP^{C} and folding intermediates (Tatzelt *et al.*, 1996). Such substances include ß sheet breakers, anti-PrP aptamers, and anti-PrP antibodies (Head and Ironside, 2000; Enari *et al.*, 2001; Heppner *et al.*, 2001; Peretz *et al.*, 2001; Sigurdsson *et al.*, 2002; Gilch *et al.*, 2003; White *et al.*, 2003; Donofrio *et al.*, 2005). Only very few compounds like branched polyamines directly target PrP^{Sc}, increasing its intracellular clearance (Supattapone *et al.*, 1999; Winklhofer and Tatzelt 2000; Supattapone *et al.*, 2001).

Compounds like the tyrosine kinase inhibitor STI571 on the other hand did not interfere with the *de novo* formation of PrP^{Sc} but activates the lysosomal degradation of pre-existing PrP^{Sc}, lowering the half-life of PrP^{Sc} (Ertmer *et al.*, 2004).

1.6 Objectives

The physiological function of the cellular prion protein PrP^{C} is still unclear as controversial functions (toxic and protective) have been proposed. These results could be explained by the fact that PrP^{C} can adopt several stable conformations, which was shown in *in vitro* translation studies.

Also, the molecular mechanisms which are involved in the clearance of the misfolded and aggregated PrP^{Sc} are not definitely established. In this thesis, I set out to overcome these difficulties by characterizing the different conformers of PrP.

The objectives of this thesis were:

1. To demonstrate the heterogeneity of the prion protein in vivo with the help of monoclonal antibodies each specific for one transmembrane isoform of PrP^{C}.

2. To characterize ^{Ntm}PrP isoform and find hints to its function with the help of the ^{Ntm}PrP specific mAb 19B10.

3. To demonstrate the excistence and function of CtmPrP in wild typ mice.

4. To demonstrate which signal transduction pathway(s) regulates the clearance of PrP^{Sc}.

2 Material and Methods

2.1 Reagents

All reagents, enzymes and antibodies used in this thesis were obtained from Sigma-Aldrich (Taufkirchen, Germany), Fluka/Sigma-Aldrich (Taufkirchen, Germany), Roth (Karlsruhe, Germany), Invitrogen (Karlsruhe, Germany), Duchefa (Haarlem, Netherlands), Merck (VWR, Darmstadt, Germany), OXOID (Wesel, Germany), Amersham (Freiburg, Germany), Kindler (Freiburg, Germany), Qiagen (Hilden, Germany), Biontex (Martinsried, Germany), Fermentas (St. Leon-Rot, Germany), Chemicon (Hofheim, Germany), Natutec (Frankfurt, Germany), Cell Signaling/Invitrogen (Karlsruhe, Germany), Biorad (München ,Germany), Pierce/Perbio (Bonn, Germany), New England Biolabs (Frankfurt, Germany) BD Biosciences Clontech (Heidelberg, Germany), Anaspec (San Jose CA, USA), LC Laboratories (Woburn, MA, USA), Vector Laboratories Inc. (Burlingane, CA, USA) and Biozol (Eching, Germany).

Chemicals

Acetone $\geq 99.5\%$	Sigma
Brij	Fluka
Bromphenolblue	Sigma
BSA (bovine serum albumin) $\geq 98\%$	Sigma
Carbenicillin (Carb) $> 90\%$	Duchefa
Chloramphenicol (CAM) $> 98\%$	Duchefa
CTAB (Cetryl-trimethy-ammonium bromide)	Fluka
DAB (Diamino benzidine)	Vector
DMSO (Dimethylsulfoxide)	Sigma

DOC (Deoxycholic acid) ≥ 99%	Sigma
Glucose	Sigma
EDTA (Ethylene-diamine-tetra-acetic acid)	Apple Chem
Formalin	Merck
Glycerol (75304)	Invitrogen
Glycine ≥ 99%	Sigma
CH_5N_3 HCl (guanidine hydrochloride)	Sigma
HEPES (4-(2-Hydroxyethyl)piperazin-1-ethansulfonsäure ≥ 99.5% (3375)	Sigma
H_2O_2 (Hydrogen peroxide)	Sigma
IPTG(Isopropyl ß-D-1-thiogalactopyranoside) > 99%	Duchefa
KAc (Potassium acetate) ≥ 99%	Sigma
KCl (Potassium chloride) ≥ 99%	Sigma
KH_2PO_4 (Monopotassium phosphate) ≥ 99%	Sigma
Lysozyme 95%	Sigma
$MgCl_2$ (Magnesium chloride)	VWR Prolabo
$MgSO_4$ (Magnesium sulfate)	Sigma
β -Mercaptoethanol	Sigma
MES (2-(N-morpholino)ethanesulfonic acid) ≥ 99.5%	Fluka
Methanol p.a.	Merck
NaCl (Sodium chloride) (13423)	Fluka
Na_2HPO_4 (Sodium hydrogen phosphate)	Sigma
Nonidet P40 (NP40)	Sigma
Octyl-glucopyranoside (75083)	Fluka
Paraffin	Merck
PFA (Paraformaldehyde)	Sigma

PMSF (Phenylmethylsulfonyl fluoride) ≥ 98.5%	Sigma
Quinacrine	Sigma
Rapamycin	LC Laboratories
Rotiphorese® Gel 30 (37.5:1)	Roth
Saponine	Sigma
Sarcosyl (N-Laurolsarcosine) (L5777)	Sigma
SDS (sodium dodecyl sulfate) ≥ 99%	Roth
Skim Milk Powder	OXOID
Sucrose ≥ 99.5%	Sigma
TCA (trichloroacetic acid) ≥ 99%	Sigma
TCEP (Tris(2-carboxyethyl)phosphine)	Sigma
TRIS (tris-(hydroxymethyl)-amino methane)	Merck
Triton®X-100 (T9284)	Sigma
Bacto-tryptone	Fluka
TWEEN®20 (P5927)	Sigma
TEMED 99%	Roth
α- Tocopherol succinate	Sigma
Urea ≥ 99.5%	Fluka
Xylol p.a.	Merck
bacto-yeast extract	Fluka
Criterion Tris-HCl gel 4-20%	Biorad
Criterion Tris-HCl gel 7.5%	Biorad
Criterion Tris-Tricine gel 10-20%	Biorad
ECL Western Blotting Detection Reagents	Amersham
Eukitt	Kindler

HiPerfect transfection reagent	Qiagen
Metafectene transfection reagent	Biontex
Ni-NTA Agarose	Qiagen
PageRuler™ Prestained Protein Ladder	Fermentas
ProLong® Gold + DAPI Antifade reagent	Invitrogen
Protein A-Agarose Fast Flow (P3476)	Sigma
Protein G-Agarose Fast Flow (P4691)	Sigma
Proteinase inhibitor complete EDTA-free	Roche
Tricine Loading Buffer (161-0739)	Biorad
Tricine Running Buffer	Biorad

Kits

ApopTag® Peroxidase *In Situ* Apoptosis Kit (S7100)	Chemicon
DC Protein Assay (500-0114)	BioRad
In Situ Cell Death Detection Kit, Fluorescein	Roche
QIAGEN Plasmid Midi and Maxi Kit	Qiagen
QIAprep Spin Miniprep Kit	Qiagen
QIAquick Gel Extraction Kit	Qiagen
SulfoLink®Kit (44895)	Pierce

Enzymes

BamHI (restriction enzyme)	NEB
EcoRI (restriction enzyme)	NEB
HindIII (restriction enzyme)	NEB

KpnI (restriction enzyme)	NEB
XbaI (restriction enzyme)	NEB
DNAse I	Roche
RNAse	Zymo Research
PNGaseF (P0704S)	NEB
Proteinase K (1.24568.0100)	Merck

Material

Blotting paper GB003 0,8 mm	Whatman
Hyperfilm ECL	Amersham
Protran® BA83 nitrocellulose membrane 0.2 µm	Whatman
PVDF Immobilon-P Transfer Membrane 0.45 µm (IPVH00010)	Millipore
SuperFrost Plus® adhesion microscope slides	Mänzel-Gläser

Buffers

Lysis buffer pH7.4

10 mM	Tris-HCl pH7.4
150 mM	NaCl
0.5%	TX-100
0.5%	DOC

VRL buffer

50 mM	HEPES pH 7.5
100 mM	KAc
5 mM	$MgCl_2$
250 mM	Sucrose

PBS (Phosphate buffered Saline)

137 mM	NaCl
2.7mM	KCl
10 mM	Na_2HPO_4
2 mM	KH_2PO_4

PBS-T buffer

137 mM	NaCl
2.7 mM	KCl
10 mM	Na_2HPO_4
2 mM	KH_2PO_4
0.05%	Tween 20

TBS (Tris-buffered Saline)

25 mM	Tris
137 mM	NaCl
2.7 mM	KCl

TBS-T buffer

25 mM	Tris
137 mM	NaCl
2.7 mM	KCl
0.1%	Tween 20

Sample buffer IP 19B10

50 mM	HEPES pH 7.5
300 mM	NaCl
5 mM	EDTA
0.6%	Nonidet P40 (NP40)
0.3%	Sarcosyl

Incubation buffer IP 19C3

20 mM	HEPES pH 7.5
0.5 M	NaCl
20%	Glycerol
30 mM	Octyl-glucopyranoside
1%	TX-100

Washingbuffer IP19C3

20 mM	HEPES pH 7.5
0.5 M	NaCl
20%	Glycerol
0.3%	Sarcosyl
1%	TX-100

HBS buffer

20 mM	HEPES pH7.4
150 mM	NaCl

4% Paraformaldehyde (PFA)

4%	PFA
1 x	PBS

TNS buffer

10 mM	Tris, pH 7.5
150 mM	NaCl
1%	Sarcosyl
1 mM	$MgCl_2$

2.2 DNA methods

2.2.1 General procedures (DNA)

Unless stated otherwise, all methods including DNA cloning and purification, PCR, sequencing and agarose gel electrophoresis were performed according to standard protocols (Maniatis, 1989) and manufacturer's instructions.

2.2.2 DNA Constructs

Plasmids containing the PrP mature domain with prolactin (Prl), signal mutant of prolactin (Prl SN-> QT - substitutions: S20N, Q21T) and immunoglobulin G (IgG) signal sequence were generously provided by V. Lingappa (Ott and Lingappa, 2004). Constructs for cell culture experiments were engineered by subcloning the open reading frame of SHaPrP fused to the different signal sequences from SP64 (Promega, Madison,WI, USA) into pcDNA3.1+ (Invitrogen) by utilizing HindIII and BamHI sites. Plasmids containing SHaPrP and the mutants KHII (substitutions: K1110I, H111I) and ΔSTE (deletion of the STE domain, Δ103-114) were also generously provided by V. Lingappa (S. Saghafi, 2007).

Human Ras homolog enriched in brain (rheb) and its mutant rhebS20N were a generous gift of J. Avruch, Harvard Medical School (Long, 2005 #32). PCR amplified inserts were cloned into the dual expression vector pBudCE4.1 under the control of the EF-1α promotor using BglII and NotI sites which were introduced in advance by polymerase chain reaction (PCR). The pBudCE4.1 plasmid already MHM2 PrP under the control of the CMV promotor (kind gift of S. Grubenbecher). rheb and rhebS20N were also cloned into pcDNA3.1+ (Invitrogen) and pEGFPC1 (CLONTECH) using BamHI and XbaI restriction sites.

The single chain antibodies (scFvAB) of 19B10 and W226, which were engineered by R. Leliveld, were subcloned into the eukaryotic expression vector pcDNA3.1+

(Invitrogen). The Igκ chain leader sequence (NCBI: X91670, (Donofrio, 2005 #5)), which specifies for secretion of heterologous proteins (Donofrio, 2005 #5), was introduced amino-terminal and unique KpnI/ EcoRI (scFv19B10 and scFvW226) were N-/C-terminal introduced by PCR. The resulting Igκ scFvW226 was again amplified by PCR to introduce an N-terminal HindIII site, since the scFvW226 construct contains an internal KpnI.

2.2.3 Primer

name	Sequence 5´-> 3´	bp	Tm °C
Prl(bov)-PrPFOR	cccaagcttatggacagcaaaggttctcgcag	32	70.8
IgGPrPFOR	cccaagcttatggatatctggatcttcctgttcatcc	37	70.6
moPrPHindIIIREV			
IgκscFv19B10FOR	aaaaaaggtacccatatggagacagacacactcctgctatgggta ctgctgctctgggttccaggttccactggtgacatggcggaggtccag	93	84.4
IgκscFv19B10REV	ccggaattctctagaagccggatctcagtggtggtg	36	74.0
IgκscFvW226HFOR	aaaaaaaagcttggtacccatatggagacagac	33	65.8
RhebNotFOR	aaaaaagcggccgcatgccgcagtcc	26	69.5
RhebBglREV	aaaaaaagatcttcacatcaccgagcat	28	60.7

2.3 Microbiological culture

2.3.1 Bacteria

DH5α Subcloning Efficiency™ DH5™ Competent *E. coli*	Invitrogen
BL21 Rosetta™(lambda DE3) Competent *E. coli*	Novagen
E. coli bacterial strain JM109	Promega

2.3.2 Media

2 x YT medium

1.6%	Bacto-tryptone
1.0%	Bacto-yeast extract
0.5%	NaCl

Luria Bertani (LB) medium

1.0%	Bacto-tryptone
0.5%	Bacto-yeast extract
1.0%	NaCl

SOC medium

2.0%	Bacto-tryptone
0.5%	Bacto-yeast extract
10 mM	NaCl
2.5 mM	KCl
10 mM	$MgSO_4$
20 mM	Glucose

2.3.3 Preparation of chemical competent *E. coli*

Preparation of chemical competent *E. coli* was performed according to standard protocol (Hanahan, 1983).

2.3.4 Transformation of chemical competent *E.coli* (Hanahan, 1991)

1. 50 µL competent cells were thaw on ice.
2. 100-500 ng plasmid DNA was added and gently mixed.
3. Cells were incubated on ice for 30 min.
4. Cells were heat shocked for 45 sec at 42°C and subsequently incubated 2 min on ice.
5. 1 mL SOC medium was added and cells were incubated at 37°C on a shaker for 1h.
6. Cells were plated on appropriate supplemented solid media and incubated overnight at 37°C.

2.4 Protein methods

2.4.1 General procedures (protein)

Unless stated otherwise, methods including SDS polyacrylamide gel electrophoresis (SDS-PAGE) and western blotting were performed according to standard protocols (Maniatis, 1989) and manufacturer's instructions.

2.4.2 Preparation of brain homogenate

10% (w/v) brain homogenate was prepared from frozen brain pieces or fresh brain by homogenizing brain in ice-cold VRL homogenization buffer with a Potter homogenizer. Aliquots were shock frozen in liquid nitrogen and stored at -80°C.

2.4.3 Immunoprecipitation (IP)

Since the protocol varied for every ligand, IP protocols are listed separately.

IP (1) 19B10

1. 20 µL protein G agarose beads (SIGMA) (per sample) were incubated in 1 mL 19B10 hybridoma cell supernatant 2 h at RT or over night at 4°C with gentle agitation and were washed afterwards 2 x in lysis buffer.
2. Homogenate was diluted to a final concentration of 0.5% (v/v) in lysis buffer/ proteinase inhibitor (PI).
3. Preclearing: homogenate was centrifuged 5 min at 12000 x g at RT.
4. S1 homogenate was added to the 20 µL PG-19B10 agarose and incubated 2 h at RT or overnight at 4°C.
5. Beads were washed 3 x in 1 mL lysis buffer.
6. The precipitated prion protein was eluted from the protein G (PG)-19B10 agarose by denaturing 5 min at 99°C in 2 x Lämmli buffer without ß-mercaptoethanol.

IP (2) 19B10 native vs. denatured homogenate

Homogenate was denatured by:

1. Adding 2% SDS and boiling 20 min at 99°C.
2. Adding 10 mM DTT and incubating 5 min at RT.
3. Adding 20 mM Iodoacetamid and incubating 5 min at RT.

Before application to the PG -19B10 beads, homogenate was diluted to a final concentration of 0.2% SDS in lysis buffer.

Serial IP (3) 6H4-19B10

1. Preparation of PG - 19B10 beads see IP(1)19B10.
2. KCB55 cells were lysed in 2 mL lysis buffer/PI per flask.
3. Preclearing: cell lysate was centrifuged at 12000 x g at RT for 5 min.

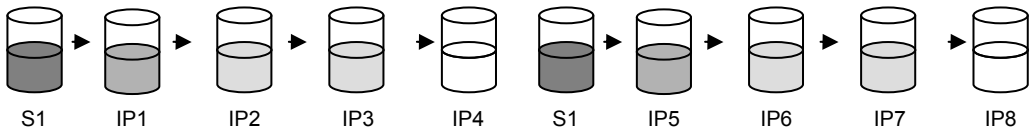

4. IP1 and IP5: 1 mL S1 lysate was added to 20 µL PG - 6H4 and incubated for 2 h at RT with gentle agitation.
5. Beads were spinned down for a few seconds and the supernatant (SUP) from IP1 was added to fresh PG - 6H4 beads (IP2). SUP from IP5 was added to fresh PG - 6H4 beads (IP6) and incubated for 2 h at RT with gentle agitation. Beads from IP1 and IP5 were washed 3 x with 1 mL lysis buffer and stored on ice.
6. IP2 and IP6 were spinned down for a few seconds and SUP from IP2 was added to fresh PG beads (IP3). SUP from IP6 was added to fresh PG beads (IP7) and incubated for 2 h at RT with gentle agitation. Beads from IP2 and IP6 were washed 3 x with 1 mL lysis buffer and stored on ice.
7. IP3 and IP7 were spinned down for a few seconds and SUP from IP3 was added to fresh PG - 6H4 beads (IP4). SUP from IP7 was added to fresh PG-19B10 beads (IP8) and incubated for 2h at RT with gentle agitation. Beads from IP3 and IP7 were washed 3 x with 1 mL lysis buffer and stored on ice.
8. IP4 and IP8 were spinned down for a few seconds and SUP was discarded. Beads from IP4 and IP8 were washed 3 x with 1 mL lysis buffer
9. To each sample, 15 µL 2 x Lämmli buffer without ß-mercaptoethanol (ßME) was added and samples were denatured for 5 min at 99°C.

IP (4) scFv19B10 (pull down of ^{Ntm}PrP ligands)

Coupling of scFvAb to N-hydroxylsulfosuccimide (NHS) -activated-Sepharose

1. NHS-Sepharose was washed 2 x in 1 mM HCl.
2. NHS-Sepharose was washed 2 x in binding buffer (1 x PBS, 1% TX100, 40 mM $NaPO_4$ pH 7.5).
3. 2 µg scFvAb/µL NHS-Sepharose and 40 mM $NaPO_4$ pH 7.5 (final concentration) +1% TX100 (final concentration) was added and incubated for 3 h at RT with gentle agitation. (The scFvAb was immobilized on NHS-Sepharose by covalent attachment of its primary amino groups to the activated NHS group of the NHS-Sepharose by forming a stable amide linkage.)
4. 50 mM glycine was added for 30 min at RT so that the remaining free binding sites of the NHS-Sepharose were blocked.
5. Sepharose beads were washed 5 x in binding buffer.
6. Sepharose beads were washed 2 x in sample buffer (50 mM HEPES pH 7.0, 300 mM NaCl, 5 mM EDTA, 0.6% NP40, 0.3% sarcosyl).
7. As negative control, NHS-Sepharose was washed as described in step1 + 2 followed by steps 4 – 6.

IP scFv19B10

1. Preclearing: fractionated human brain homogenate was incubated with 1 mL blocked NHS-Sepharose over night at 4°C with gentle agitation to precipitate proteins which bind unspecific to NHS-sepharose.

2. NHS-Sepharose beads were pelleted for 10 min 2500 x g centrifugation.
3. Supernatant was transferred to scFv19B10 Sepharose beads and incubated 24 h at 4°C with gentle agitation and NHS Sepharose beads were washed 2 x with sample buffer and stored at 4°C.
4. After 24 h incubation scFv19B10 Sepharose beads were spinned down for 10 min at 2500 x g and washed 2 x with sample buffer.
5. Proteins from scFv19B10 pull down and preclearing were first eluted 2 x with 250 µL 100 mM glycine pH2.5 and afterwards 2 x with 250 µL 100 mM Tris pH 8.5, 1% SDS. Samples eluted with same Elution buffer were pooled and immediately precipitated with TCA.

TCA Precipitation

1. ½ volume of 50% TCA was added to the eluates and incubated 30 min on ice.
2. Eluat was centrifuged at 4°C for 15 min at 22000 x g and supernatant was carefully removed.
3. The pellet was washed with 1 mL cold acetone, centrifuged at 4°C for 15 min at 22000 x g and all supernatant was carefully removed.
4. Pellet was air dried, subsequent resuspended in 30 µL 2 x Lämmli buffer with ß-ME and denatured 5 min at 99°C.

Eluted proteins were separated by a 4-20% Tris-Glycine SDS PAGE and stained with Colloidal Blue staining kit performed according to manufacturer's instructions.

Protein patterns between preclearing (with blocked NHS Sepharose) and scFv19B10 pull down were compared and protein bands only present in scFv19B10 pull down were cut out. Selected bands were analyzed by mass spectrometry (by Bruce Onisko, University of California, Berkley).

Co-IP (5) scFv19B10 RTN3a and NogoB

1. Coupling of scFvAb to NHS-activated-Sepharose was performed as described in IP (4) scFv19B10.
2. Homogenate was diluted to a final concentration of 0.5% (v/v) in sample buffer.
3. S1 homogenate was added to the 2 µL PG-19B10 agarose and incubated 2 h at RT or over night at 4°C
4. Beads were washed 3 x in 1 mL sample buffer.
5. The precipitated proteins were eluted from the scFv19B10 sepharose by denaturing 5 min at 99°C in 2 x Lämmli buffer without ß-ME.

Optimized IP (6) 19C3

1. 500 µL protein A agarose beads (SIGMA) (batch) were incubated in 50 mL 19C3 hybridoma cell supernatant over night at 4°C with gentle agitation and were washed afterwards 3 x in PBS.
2. Homogenate was diluted to a final concentration of 0.2% - 2% (v/v) in incubation buffer (20 mM HEPES pH 7.5, 0.5 M NaCl, 20% glycerol, 30 mM octyl-glucopyranoside, 1% TX-100).
3. Preclearing: homogenate was centrifuged for 20 min at 22.000 x g at 4°C.
4. S1 homogenate was added to the 20 µL PA-19C3 agarose and incubated 2 h at RT.
5. Beads were washed 1 x in 500 µL incubation buffer and 2 x 1 mL in washing buffer (20 mM HEPES pH7.5, 0.5 M NaCl, 20% Glycerol, 0.3% sarcosyl, 1% TX-100).
6. The precipitated protein was eluted from the PA - 19C3 agarose by denaturing 5 min at 99°C in 2 x Lämmli buffer without ß-ME.

IP19C3 (7) combined with Conformational PrP^C assay (cold Proteinase K (PK) digest followed by PNGase F digest)

The conformational assay was performed with minor changes as previously described (Hegde, 1998 #52).

IP19C3

1. IP (6)19C3 was performed as described before (1400 µL 2% homogenate (KHII, ΔSTE, FVB) incubated with 60 µL PA -19C3). In addition beads were washed in a final step 2 x in VRL buffer with 0.5% TX-100.
2. IP 19C3 was divided in halves, one half was used for cold PK digest, the other half was again divided in halves and stored on ice until further use.

Cold PK digest

1. 10 µL VRL buffer with 0.5% TX-100 was added to the 30 µL beads, or 20 µL VRL buffer with 0.5% TX-100 was added to 20 µL S1 homogenate.
2. Sample was treated with 0.25 mg/mL auto digested PK and incubated 1 h on ice at 4°C.
3. 1 mM fresh PMSF in DMSO was added to the beads/homogenate to terminate the PK reaction. The sample was subsequently incubated on ice for 10 min.
4. PK digest was divided in halves, one half was used for PNGase F digest the other half was stored on ice until further use.

PNGase F digest

1. Protein was eluted from the beads (PK digested or undigested) by adding 1% SDS and 2% ß-ME in 50 mM Tris pH 8.0 and incubating for 15 min at 37°C.
2. Supernatant was transferred into new tubes and diluted with 50 mM Tris pH 8.0, 1% TX-100 to a final concentration of 0.5% SDS, 1% ß-ME and denatured for 2 min at 99°C.
3. After cooling down to RT deglycosylation was performed with 200 u PNGase F (New England Biolabs) per sample overnight at 37°C.

Tricine loading buffer was added to all samples and samples were boiled for 5 min at 99°C. Proteins were separated by 10-20% Tris-Tricine-SDS-PAGE in Tricine running buffer.

2.5 Antibodies

2.5.1 Antibodies

rabαActin (A2066)	Sigma
rabα-c-myc	BD Clontech
rabα-APG7 (CT) (54230)	Anaspec
mαc-myc 9E10	G.I.Evan *et al*., 1985
Phospho-mTOR (Ser2448) antibody (2971)	Cell Signaling
Phospho-mTOR (Ser2481) antibody (2974)	Cell Signaling
mα^{Ntm}PrP 19B10	Korth unpublished
mα^{Ctm}PrP 19C3	Korth unpublished
mαPrP W226	Petsch unpublished
Phospho-p70 S6 Kinase (Thr389) (108D2) Rabbit mAb	Cell Signaling
Phospho-p70 S6 Kinase (Thr421/Ser424) antibody	Cell Signaling
RHEB antibody (ab 25873)	Biozol

ImmunoPure® Goat αmIgG + IgM, (H+L), POD Conjugated (31444)	Pierce
mouse TrueBlot™ ULTRA: Horseradish Peroxidase αmIgG (18-8817)	NatuTec
biotinylated anti-mouse IgG (H+L), affinity purified (BA-2000)	Biozol
α-mIgG (Fc SPECIFIC) FITC CONJUGATE antibody (F5387)	Sigma
goatα-m IgG Alex Fluor 594 (A-11005)	Molecular Probes
ImmunoPure® Goat αrabIgG POD (31460)	Pierce
goatαrabIgG, HRP-linked antibody (7074)	Cell Signaling

2.5.2 Production of polyclonal antibodies

1. Prior to first immunization, preimmune serum was collected from the rabbit (New Zealand White Rabbit).
2. First immunization: 100 µg all-RTN (Reticulon) peptide (NH2-KELRRLFLVDDLVDSLKC-COOH), linked to KLH (keyhole limpet hemocyanin) suspended in RIBI Adjuvant (Sigma), was injected subcutaneously.
3. Second and third immunizations were performed within four weeks after the first boost.
4. The induced immune response was examined in western blotting-analysis comparing preimmune serum vs. all RTN antiserum.

2.5.3 Expression of recombinant scFvAb in *E. coli*

scFv19B10 expression in *E. coli* BL21 (lambda DE3)

1. day 1: starter culture: 2 x 20 mL 2 x YT, 0.2% glucose, 10 mM $MgCl_2$, 200 µg/µL Carb, 34 µg/mL CAM medium were inoculated with single colonies of fresh scFv19B10-myc-his transformed *E. coli* BL21 (lambda DE3) Rosetta cells and grown over night in a 37°C shaker.
2. day 2: the main cultures (2 x 500 mL 2 x YT 0.2% glucose, 10 mM $MgCl_2$, 100 µg/µL Carb, 34 µg/mL CAM) were inoculated with the starter cultures and grown to an OD_{600} ~ 1.3.
3. Cultures were cooled to a temperature of 25°C in ice water.

4. The protein expression was induced by the application of 1 mM IPTG.
5. Cultures were grown for 3 h at 25°C.
6. Cultures were harvested by spinning down for 15 min at 3000 x g.
7. Supernatant was discarded and the pellet was shock frozen in liquid nitrogen.
8. Pellets were defrosted on ice and resuspended in 20 mL 20 mM Tris pH 8.0, 5 mM EDTA, 1 mg/mL lysozyme, 1 mM fresh PMSF for lysis.
9. 1% TX-100 was added and mixed well.
10. 20 mM $MgCl_2$ and 400 u DNAseI was added and incubated for 15 min at RT shaking/rotating on wheel.
11. Lysate was filled up to 50 mL with 20 mM Tris pH 8.0/ 5 mM imidazole/ 500 mM NaCl/ 10 mM $CaCl_2$/ 1% TX100/ 1 mM PMSF (final concentration).
12. Lysate was cleared by centrifugation for 20 min at 20.000 x g at RT.
13. The supernatant contained the soluble protein solution, the pellet was discarded.

2.5.4 Antibody purification

Immobilized metal affinity chromatography (IMAC) (C.F. Ford, 1991)

His_6-tagged scFv19B10 Ab purification on a nickel-nitrilotriacetic acid (Ni-NTA) column:

1. The Ni-NTA column was equilibrated with 10 column volumes (CV) equilibration buffer (20 mM Tris pH 8.0, 5 mM imidazole, 500 mM NaCl, 1% TX100).
2. The soluble protein solution was applied to the column by gravity flow. The histidine residues of the His_6 tag of the protein bound to the Ni-ions of the Ni-NTA column.
3. The column was washed with 10 CV equilibration buffer.
4. The column was washed with 10 CV washing buffer 1 (20 mM Tris pH 8.0, 50 mM imidazole, 500 mM NaCl, 1% TX100).
5. The column was washed with 10 CV washing buffer 2 (20 mM Tris pH 8.0, 5 mM imidazole, 1 M NaCl).
6. The protein was eluted with 5 CV elution buffer (20 mM Tris pH 8.0, 300 mM imidazole, 300 mM NaCl) by competitive displacement with imidazole.
7. Protein quantification OD_{280} (with Nanodrop® peq lab).
8. 2 mM EDTA and 1 mM PMSF were added immediately.
9. The eluate was dialyzed overnight against 20 mM Tris pH 8.0, 1 mM EDTA 1:200.

Ion-exchange chromatography (IEC)

Purification of scFv19B10myc-His_6 on a Q-Sepharose-High-Performance (HP)-column (anion exchanger). Separation of polar molecules based on the charge properties of the molecule.

1. The Q-Sepharose-HP-column was connected to the BioLogic LP (low-pressure) chromatography system (BIORAD).
2. The column was equilibrated with buffer A (20 mM Tris pH 8.0, 1 mM EDTA).
3. The IMAC purified and dialyzed scFv19B10 Ab was slowly applied on the column with a syringe so that the negative charged scFvAb could bind to the positive charged stationary phase.
4. The column was washed with 30 mL buffer A.
5. The protein was eluted with 40 mL of a gradient from buffer A to B (A>B 0-100%) (buffer B: 20 mM Tris pH 8.0, 1 mM EDTA, 500 mM NaCl). Eluates were fractioned in 1.5 mL fractions.
6. The column was cleared with buffer B followed by 5 M guanidinehydrochlorid and finally with buffer A.

Affinity chromatography

Purification of 19B10 Ab on a Protein G column (affinity-purification)

1. 20 mM Tris pH 8.0 and 2 mM EDTA were added to the 19B10 hybridoma cell supernatant.
2. The supernatant was sterile filtrated with stericups (Millipore).
3. The protein G column was connected to the BioLogic LP (low-pressure) chromatography system (BIORAD) and washed with TBS buffer.
4. 19B10 hybridoma cell supernatant was applied to the column (speed 0.5 mL/min). (Protein G precipitates 19B10 Ab out of the hybridoma cell supernatant by binding to the Fc region of the Ab.)
5. The column was washed with 50 mL TBS buffer.
6. The protein was eluted with elution buffer (low pH and high salt) (100 mM glycine pH 2.5, 500 mM NaCl).
7. The eluate was immediately neutralized with 200 mM Tris pH 8.5.
8. 1 mM EDTA was added.

Affinity purification of polyclonal rabα-allRTN Ab (SulfoLink)

Unless stated otherwise procedure was performed according to manufacturer's instructions (SulfoLink®Kit PIERCE).

1. 4.5 mg allRTN peptide was solved in 1 mL coupling buffer.

2. Disulfide bonds of the peptides were reduced with 1 mM Tris (2-carboxyethyl) phosphine (TCEP), to have free (reduced) sulfhydryls for immobilization.
3. SulfoLink column was equilibrated to RT.
4. 8 mL coupling buffer was applied to the column by gravity flow.
5. Peptide + 2 mL coupling buffer was applied to the column and the closed column was mixed by rocking at RT for 15 min.
6. The column was incubated for additional 30 min at RT without mixing.
7. After incubation column was opened and flow through was saved.
8. Column was washed with 6 mL coupling buffer.
9. 15.8 mg L-cysteine-HCl in 2 mL coupling buffer was applied to the column. The closed column was mixed by rocking at RT for 15 min and subsequent incubated 30 min at RT without mixing.
10. Column was washed with 12 mL washing buffer.
11. Column was washed with 6 mL PBS buffer.
12. 1.5 mL α-allRTN rabbit anitserum + 200 µL PBS buffer was applied to the column by gravity flow.
13. Bottom column cap was replaced and 500 µL PBS buffer were added.
14. Column was incubated 1 h at RT.
15. Steps 12-14 repeated with the rest of the serum.
16. Column was washed with 12 mL PBS buffer.
17. Ab was eluted with 100 mM glycine pH 2.5 and immediately neutralized with 200 mM Tris pH 8.5.

2.6 Cell culture

2.6.1 Cell lines

N2a	mouse neuroblastoma cells (Olmsted et al., 1970)
scN2a	mouse neuroblastoma cells, infected with the RML strain of mouse adapted scrapie prions and subcloned (Bosque and Prusiner, 2000)
WACII	human neuroblastoma cells (Zhang et al. 2001)
NLF	human neuroblastoma cells (Schwab, 1983)
19B10	α-^{Ntm}PrP Ab producing hybridoma cells (Korth, unpublished)
19C3	α-^{Ctm}PrP Ab producing hybridoma cells (Breil, unpublished)
W226	α-PrP Ab producing hybridoma cells (Petsch, unpublished)
9E10	α-c-mycAb producing hybridoma cells

2.6.2 Media and reagents

WACII, NLF

RPMI 1640	Invitrogen
1% L-Glutamine 200 mM concentrate (100x)	PAA
10% Fetal Bovine Serum "GOLD"	PAA

N2a, ScN2a

Minimum Essential Medium (MEM) with Earle's Salts	Invitrogen
1% L-Glutamine 200 mM concentrate (100x)	PAA
1% Penicillin-Streptomycin (100x)	Invitrogen
10% Fetal Bovine Serum "GOLD"	PAA

19B10, 19C3, W226, 9E10

Minimum Essential Medium (MEM) with Earle's Salts	Invitrogen
1% L-Glutamine 200mM concentrate (100x)	PAA
1% Penicillin-Streptomycin (100x)	Invitrogen
10% Fetal Bovine Serum "GOLD"	PAA
2% HT-Supplement (50x)	Invitrogen

19C3

Protein-Free-Hybridoma Medium (PFHM)	Invitrogen
1% L-Glutamine 200 mM concentrate (100x)	PAA

Dulbecco's Phosphate Buffered Saline (D-PBS) (1X)	Invitrogen
Trypsin-EDTA (0,05% Trypsin, EDTA·4Na) (1X)	Invitrogen

2.6.3 Culture conditions

Cells were grown at 37°C and 5% CO_2 in a cell incubator (Binder).

2.6.4 Transfection

Transient transfection with Metafectene (N2a-, WACII-, NLF-cells)

1. The day before transfection, cells were seeded in 6 cm plates or for immunofluorescence staining on sterile cover slips at a density of approx. 50%.
2. On the day of transfection, x µg DNA and x µL Metafectene (see table x) were each diluted in MEM medium without serum. (Metafectene was vortexed before use.)

plate	Metafectene µL/sample	DNA µg/sample
24 well	1.2	0.4
6 well	3.5	0.75
6 cm	7	1.5
10 cm	17.5	3.75

3. The diluted DNA and the transfection reagent were mixed and incubated for 15 min at RT to form DNA-lipid complexes.
4. The medium of the cells was changed.
5. The complexes were added drop-wise onto the cells. The plate was gently swirled to ensure uniform distribution of the transfection complexes.
6. The medium was changed 5-8 h after transfection.

Transient transfection with HiPerfect (ScN2a cells)

1. The day before transfection, cells were seeded in 6 cm plates at a density of approx. 50%.
2. On the day of transfection, 20 µL HiPerfect was diluted in 30 µL HBS buffer (20 mM HEPES pH 7.4, 150 mM NaCl) and incubated for 5 min at RT. (HiPerfect was mixed before use.)
3. 1.3 µg DNA was diluted in 50 µL HBS buffer.

4. The diluted DNA and transfection reagent were mixed and incubated for 15 min at RT to form complexes.
7. The medium of the cells was changed.
8. The complexes were added drop-wise onto the cells. The plate was gently swirled to ensure uniform distribution of the transfection complexes.

Transfection of siRNA (ScN2a cells)

Mm_Apg7l_1_ HP siRNA	TS: TAG CAT CAT CTT TGA AGT GAA
Mm_Apg7l_4_ HP siRNA	TS: AAG GTC AAA GGA CAA AGA TAA
Mm_Map1lc3a_3_HP siRNA	TS: CCG GCG CCG CCT GCAACT CAA

siRNAs (from Qiagen) with target sequence (TS)

1. The day before transfection, cells were seeded in 6cm plates at a density of approx. 50%.
2. siRNA was solved and pretreated according to the manufacturer's instructions (Qiagen).
3. 50 nmol siRNA was diluted in 100 µL MEM medium without serum. If two siRNAs were combined in one experiment, 50 nmol of each siRNA were used.
4. 20 µL HiPerfect was added.
5. The siRNA - transfection reagent mix was mixed and incubated for 15 min at RT to form complexes.
6. The complexes were added drop-wise onto the cells. The plate was gently swirled to ensure uniform distribution of the transfection complexes.
7. Medium was exchanged two days after transfection.
8. Cells were lysed in lysis buffer 48 h, 72 h or 96 h after transfection.
9. The protein concentration of the lysates was measured (DC Protein Assay, Biorad) and adjusted to provide equal protein amount.
10. Protein knock-down was tested by western blotting and detection with specific antibodies.
11. The influence of the protein knock-down on the amount PrP^{Sc} of was examined with a PrP^{Sc} assay.

2.6.5 Immunofluorescence of transient transfected N2a

Surface staining

1. 48 h after transfection cells were briefly rinsed in PBS.
2. Cells were fixed in 4% PFA in PBS for 10 min on ice.

3. Cells were washed 1x in PBS.
4. Cells were incubated in primary antibody (19B10 SUP, W226 SUP, 3F4 SUP, 19C3 SUP), diluted 1:1 in 2% BSA in PBS for 1 h at RT.
5. Cells were washed 3 x in PBS.
6. Cells were incubated in secondary antibody (α-mFITC), diluted 1:200 in 2% BSA in PBS for 30 min at RT in the dark.
7. Cells were washed 3 x in PBS in the dark.
8. Cells on cover slips were mounted upside down on a drop of glycerol or ProLong® Gold + DAPI Antifade reagent (Invitrogen) on glass slides and sealed with nail varnish.

Intracellular staining

1. 48 h after transfection cells were briefly rinsed in PBS.
2. Cells were permeabilized by incubating in 0.5% saponine in PBS for 30 min at RT.
3. Cells were fixed in 4% PFA in PBS for 10 min on ice.
4. Cells were washed 1 x in 0.5% saponine in PBS
5. Cells were incubated in primary antibody (19B10 SUP, W226 SUP, 3F4 SUP, 19C3 SUP), diluted 1:1 in 0.5% saponine + 2% BSA in PBS for 1 h at RT.
6. Cells were washed 3 x in 0.5% saponine in PBS.
7. Cells were incubated in secondary antibody (α-mFITC), diluted 1:200 in 0.5% saponine + 2% BSA in PBS for 30 min at RT in the dark.
8. Cells were washed 3 x in 0.5% saponine in PBS in the dark.
9. Cells on coverslips were mounted upside down on a drop of glycerol or ProLong® Gold + DAPI Antifade reagent (Invitrogen) on glass slides and sealed with nail varnish.

Combined intracellular staining and TUNEL staining

With *In Situ* Cell Death Detection Kit, Fluorescein (Roche)

1. Cells were fixed in 4% PFA in PBS for 1 h at RT.
2. Cells were washed 2 x in PBS.
3. Cells were permeabilized by incubation in 0.5% saponine in PBS for 30 min at RT.
4. Cells were incubated in primary antibody (19C3 SUP, MEM), diluted 1:1 in 0.5% saponine + 2% BSA in PBS for 2 h at RT.
5. Cells were washed 3 x in 0.5% saponine in PBS.
6. As positive control, cells were DNAseI digested (4 u) in 50 mM Tris p H 7 .5 / 1 mg/mL BSA for 10 min at RT to induce DNA strand breaks.
7. TUNEL reaction was performed according to manufacturer's instructions.
8. The secondary antibody α-mALEXA-FLUOR (red) was diluted 1:100 with the TUNEL mix and incubated together with the TUNEL reaction for 1 h at 37°C in a dark, humidified chamber.
9. Cells were washed 3 x in PBS.

10. Cells on cover slips were mounted upside down on a drop of glycerol on glass slides and sealed with nail varnish.

2.6.6 Immunohistochemistry

Fixation, processing and embedding was automatically performed in a Tissue-Tek VIP (Sakura).

Fixation: Perfused brains were fixed in 4% formalin 2 h at 40°C.

Processing: Brains were dehydrated in an ascending ethanol series

1. 70% ethanol 1 h 40°C
2. 70% ethanol 1 h 40°C
3. 96% ethanol 1 h 40°C
4. 96.6% ethanol 1 h 40°C
5. 100% ethanol 30 min 40°C
6. 100% ethanol 30 min 40°C
7. 100% ethanol 1 h 40°C
8. 100% xylol 1 h 40°C
9. 100% xylol 1 h 40°C

Embedding: Brains were embedded 4 x in paraffin for 30 min at 60°C.

Sectioning

1. 4 µm thin sections were cut on a microtome.
2. Sections were transferred into a hot water bath (60°C) with A. dest.
3. Sections were placed on Superfrost Plus slides.
4. The remaining Aqua dest. was absorbed with a filter paper.
5. Sections were dried over night at 60°C.

Staining

1. Sections were deparaffinized in xylol 2 x for 5 min and 2 x 5 min in 100% EtOH.
2. Endogenous peroxidase activity was inactivated by 0.3% H_2O_2/methanol treatment for 20 min in the dark.
3. Sections were rehydrated in a descending ethanol series (2 x 100% EtOH, 2 x 95% EtOH, 2 x 70% EtOH, 2 x A.dest)
4. Sections were boiled for 20 min in citrate buffer for epitope retrieval.

5. Sections were rinsed 1 x in Aqua dest. and 1 x in PBST.
6. Sections were incubated with primary antibody, diluted 1:500 (α-c-myc CLONTECH) and 1:10 (W226 SUP) in 2% BSA in PBS, for 2 h at RT in a humidified chamber.
7. Sections were rinsed 3 x in PBST.
8. Secondary antibody biotin-labled α-mIgG (diluted 1:1000 in 2% BSA in PBS) was applied and incubated for 45 min at RT in a humidified chamber.
9. Sections were rinsed 3 x in PBST.
10. Strepavidin-HRP diluted 1:2000 in 2% BSA in PBS was applied and incubated 45 min at RT in a humidified chamber.
11. Sections were rinsed 1 x PBS and 1 x in Aqua dest.
12. DAB solution was applied and incubated for 3-5 min.
13. Sections were rinsed 2 x in Aqua dest.
14. Sections were stained 1 min in hematoxylin solution (stains nuclei blue).
15. Sections were rinsed 2 x in Aqua dest.
16. Sections were incubated 10 min in tap water.
17. Sections were dehydrated in an ascending ethanol series (2 x 70% EtOH, 2 x 95% EtOH2 x 100% EtOH, 2 x 100% xylol each 5 min).
18. Sections were mounted in Eukitt.

2.6.7 TUNEL staining

(with ApopTag® Peroxidase *In Situ* Apoptosis Kit S7100, Chemicon)

1. Sections were deparaffinized in Xylol 3 x for 10 min
2. Sections were hydrated in a descending ethanol series (2 x 100% EtOH 5 min, 1 x 95% EtOH 5 min, 1 x 85% EtOH 5 min, 1 x 70% EtOH 5 min, 2 x Aqua dest. 5 min)
3. Endogenous peroxidase activity was quenched by 0.3% H_2O_2/ methanol treatment for 30 min in the dark.
4. Sections were rinsed 2 x in Aqua dest. and washed 3x in PBST for 5 min.
5. Sections were subjected to proteolysis for 15 min 2 µg/mL PK in 1 x PBS at RT for epitope retrieval.
6. Section were rinsed 3 x in PBST for 5 min.
7. For positive control, one section was pretreated in 30 mM Tris pH 7.2/ 4 mM $MgCl_2$/ 0.1 m M DTT and then DNAseI digested (200 u) for 10 min at RT to cause DNA fragmentation. In a final step the section was washed 3 x in Aqua dest.
8. Remaining liquid was gently wiped off the slides and a circle was made around the sections with an immunoedge pen. Sections were equilibrated in 30 µL equilibration buffer for 10 min in a hydration box at RT and then the equilibration buffer was shaken off.
9. 30 µL TdT enzyme reaction (prepared according to the manufacturer's instructions) was added. A plastic cover slip was placed onto each section and incubated in a hydration box for 1 h at 37°C. Negative control was treated only with the reaction buffer without TdT enzyme.

10. TdT enzyme reaction was removed and the section was incubated in stop solution (prepared according to the manufacturer's instructions) in a hydration box for 40 min at 37°C to stop the enzyme reaction.
11. Sections were rinsed 3 x in PBST.
12. Remaining liquid was gently wiped off, 30 µL ANTI-DIGOXIGENIN was applied and incubated for 30 min in a hydration box at RT.
13. Sections were rinsed 3 x in PBST.
14. Sections were rinsed 1 x in PBS.
15. DAB solution was applied and incubated for 3-5 min.
16. Sections were rinsed 2 x in Aqua dest.
17. Sections were stained 1min in hematoxylin solution (stains nuclei blue).
18. Sections were rinsed 2 x in Aqua dest.
19. Sections were incubated 10 min in tap water.
20. Sections were dehydrated in an ascending ethanol series (2 x 70% EtOH, 2 x 95% EtOH, 2 x 100% EtOH, 2 x 100%Xylol each 5 min).
21. Sections were mounted in Eukitt.

2.6.8 Histoblots

Sectioning

1. Immediately after brain extraction, the brain was embedded in freezing medium and shock-frozen in liquid nitrogen.
2. Glass slides were pre-cooled to -20°C (inside the Cryostat).
3. Frozen brain was sectioned into thin sections of 8 µm using a Cryostat.
4. Sections were placed on glass slides which were pre cooled and defrosted a few seconds before use (for better adherence).
5. Sections were stored cool at -20°C.

Blotting

(According to A. Taraboul, 1992)

1. A 0.2 µm nitrocellulose membrane was wetted in lysis buffer and laid on a double layer of Whatmann paper saturated in lysis buffer.
2. Sections were quickly thawed.
3. Sections were blotted onto nitrocellulose membrane by pressure for 5 min.
4. Membrane was blocked in 5% non fat dry milk in PBST for 1 h at RT.
5. Membrane was washed 2 x in PBST.
6. Membrane was incubated in primary antibody (19B10 SUP, W226 SUP, 19C3 SUP, MEM), diluted 1:1 in PBST for 2 h at RT.
7. Membrane was washed 3 x in PBST for 10 min.
8. Membrane was incubated in secondary antibody α-mHRP, diluted 1:40,000 in PBST for 1 h at RT.
9. Membrane was washed 3 x in PBST for 10 min.

10. Substrate (ECL - enhanced chemiluminescence) was added.
11. Exposure on x-ray film.

2.7 Animal experiments

Animal experiments were performed by Professor Lothar Stitz from Tübingen.

1. 1 mg of scFv 19B10 Ab, 1 mg scFv 19B10 Ab + Pertussis toxin or PBS (mock) were injected intraperitoneal in Tg20 mice.
2. Mice were perfused 1 h after injection with 4% formalin.

2.8 PrP assays

2.8.1 Biochemical detection of PrP^{Sc} (PrP^{Sc} assay) Cell lysates were proteolyzed at 37°C for 30 min with 20 µg/mL proteinase K.

1. The reaction was terminated with 2 mM phenylmethylsulfonyl fluoride (PMSF).
2. The lysates were centrifuged at 4°C for 45 min at 100000 x g in an ultracentrifuge (Beckman Coulter, Fullerton, CA, USA).
3. Pellets were denatured in 2 x Lämmli buffer 5 min at 99°C.
4. Sodium dodecyl sulfate- polyacrylamide gel-electrophoresis (SDS-PAGE) and immunoblotting were performed according to standard techniques. Immunoblots were first incubated with the monoclonal α-PrP antibody W226 (generously provided by B. Petsch), afterwards with α-mouse IgG-HRP antibody and developed with ECL.

2.8.2 Conformational PrP^{C} assay

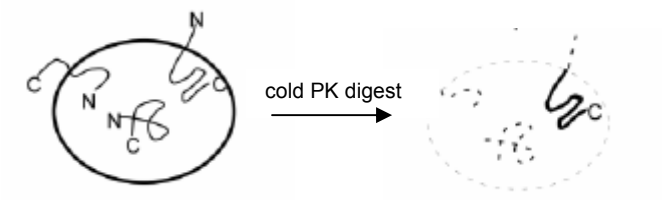

Cold PK digest

1. 10% brain homogenate was rapidly thawed and diluted to a final concentration of 2% in cold VRL buffer with 0.5% TX-100.
2. Preclearing: homogenate was centrifuged 20 min 22000 x g at 4°C.
3. 20 µL VRL buffer with 0.5% TX-100 was added to 20 µL S1 homogenate.
4. Sample was treated with 0.25 mg/mL auto digested PK and incubated 1 h on ice at 4°C.
5. 1 mM fresh PMSF in DMSO was added to the homogenate to terminate the PK reaction and subsequently incubated for 10 min on ice.

PNGase F digest

PNGase F digest was performed subsequent to cold PK digest to distinguish ^{Ctm}PrP from the C1 fragment of PrP.

4. 1% SDS and 2% ß-ME in 50 mM Tris pH 8.0 were added to the PK digest and incubated for 15 min at 37°C.
5. Sample was diluted with 50 mM Tris pH 8.0, 1% TX-100 to a final concentration of 0.5% SDS, 1% ß-ME and denatured for 2 min at 99°C.
6. After cooling down to RT, deglycosylation was performed with 200 u PNGase F per sample over night at 37°C.

2.8.3 PrP^{Sc} inhibition assay in ScN2a cells (compounds)

1. A confluent 10 cm dish was splitted and a drop of cells was pipetted into a 6 cm dish.
2. After 4-6 h, when cells had settled down, they were treated with different concentrations of α-tocopherol succinate, quinacrine and rapamycin.
3. Medium was exchanged every second day, together with the compounds.
4. Cells were lysed with lysis buffer after 7 day treatment, having achieved about 80% confluence.
5. The protein concentration of the lysates was measured (DC Protein Assay, BioRad) and adjusted.
6. For verification of the compound-based inhibition of PrP^{Sc}, a PrP^{Sc} assay was performed as described before.

2.8.4 PrP^{Sc} inhibition assay in ScN2a cells (mAb)

1. A confluent 10 cm dish was split and a drop of cells was pipetted into a 6 cm dish.
2. After 4-6 h, when cells had settled down, cells were treated with different mAb (fresh hybridoma supernatant of 40,000 cells).

3. Medium was exchanged every second day, together with fresh Ab (half medium: half hybridoma supernatant).
4. Cells were lysed with lysis buffer after 7 day treatment, having achieved about 80% confluence.
5. The protein concentration of the lysates was measured (DC Protein Assay, BioRad) and adjusted to provide equal protein amounts.
6. For verification of the Ab-based inhibition of PrP^{Sc}, a PrP^{Sc} assay was performed as described before.

2.8.5 Sizing of PrP^{Sc} aggregates via sucrose gradient centrifugation

1. ScN2a cells were treated for one week with 10 nM rapamycin.
2. Untreated and rapamycin treated cells were scraped in 1 mL PBS/10cm dish.
3. Cells were centrifuged 5 min at 1.000 x g at 4°C
4. Cell pellets were lysed in 1 mL TNS buffer (10 mM Tris, pH 7.5, 1% sarcosyl, 150 mM NaCl, 1 mM $MgCl_2$) and 20 u DNAseI and incubated 30 min on ice.
5. The sucrose density gradient was prepared by layering successive decreasing sucrose density solutions (700 µL of 60%, 30%, 25%, 20%, 15%, 10% sucrose in TNS buffer).
6. 400 µL lysate was applied to the top of the gradient.
7. The tubes were centrifuged over night at 200000 x g (swinging bucket MLS-50) at 4°C.
8. Immediately after centrifugation, seven fractions were collected. 20 µL of each fraction was separated by SDS-PAGE and PrP^{Sc} aggregates were detected by western blotting.

3 Results

3.1 Topological isoforms of the Prion Protein

In vitro translation experiments suggested that the population of PrP^{C} is conformational heterogeneous (Hegde *et al.,* 1998). Sensitive detection of these PrP^{C} isoforms *in vivo* has been limited due to the absence of high affinity monoclonal antibodies (mAb).

In this thesis two monoclonal mouse antibodies 19B10 (mAb19B10) and 19C3 (mAb19C3) were characterized which specifically recognizes two conformers of PrP^{C}, ^{Ntm}PrP and ^{Ctm}PrP.

3.1.1 Characterization of the ^{Ntm}PrP specific murine mAb19B10

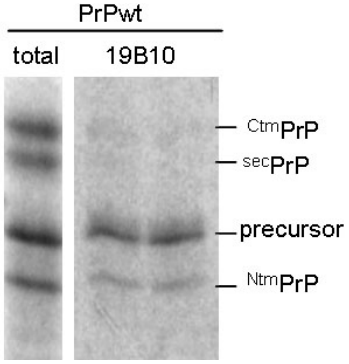

Fig. 6 mAb19B10 is specific for ^{Ntm}PrP. Autoradiography of *in vitro* translated total PrP wild type (wt) (left lane) and an immunoprecipitation (IP) with the conformation specific monoclonal antibody 19B10 of *in vitro* translated PrPwild type (right lane). 19B10 precipitated specifically only the Ntm conformer and a precursor of PrP, but not ^{Ctm}PrP and ^{sec}PrP.

The murine mAb 19B10, which was screened against recombinant mouse PrP, specifically recognized a conformational epitope in an unglycosylated PrP species that overlaped with ^{Ntm}PrP from *in vitro* translation studies (Fig. 6) (C. Korth and Lingappa unpublished data).

To find more evidence for the specific conformational epitope of mAb19B10 IPs from native or denatured human brain homogenate were performed (Fig. 7).

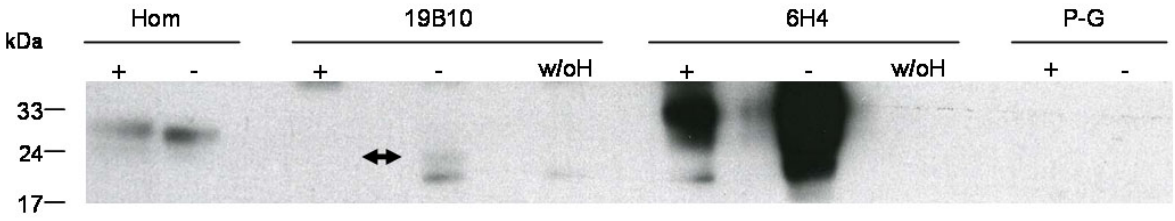

Fig. 7 mAb19B10 specifically recognizes a conformational epitope of PrP. Western blot analysis of an immunoprecipitation with the mAb19B10 and general α-PrP mAb 6H4 from denatured (2 %SDS, 10 mM DTT, 20 mM Iodoacetamid, 20 min 95°C) (+) and native (-) respectively without human homogenate (w/oH). Arrow: ^{Ntm}PrP

The fact that 19B10 only recognized native PrP but not denatured PrP compared to 6H4 which precipitated both, confirmed the first results of a conformational epitope from *in vitro* translation studies.

An alternative approach was searched to demonstrate the ability of the mAb 19B10 to detect a specific subpopulation of PrP (^{Ntm}PrP). The performance of a serial immunoprecipitation with the mAb 6H4, which so far was regarded as an universal PrP antibody and the ^{Ntm}PrP specific mAb 19B10 should prove the hypothesis that different conformers of the prion protein exist in wild type mouse. The principle of a serial IP is that if there are two conformers of a protein, they can be distinguished with two conformation specific mAb (see Fig. 8). The depletion of a given sample (brain homogenate) with one antibody for one conformer will still leave the other conformer in solution. A mAb recognizing the second conformer will be able to pull down the remaining conformer even if the sample has been depleted with the first conformer.

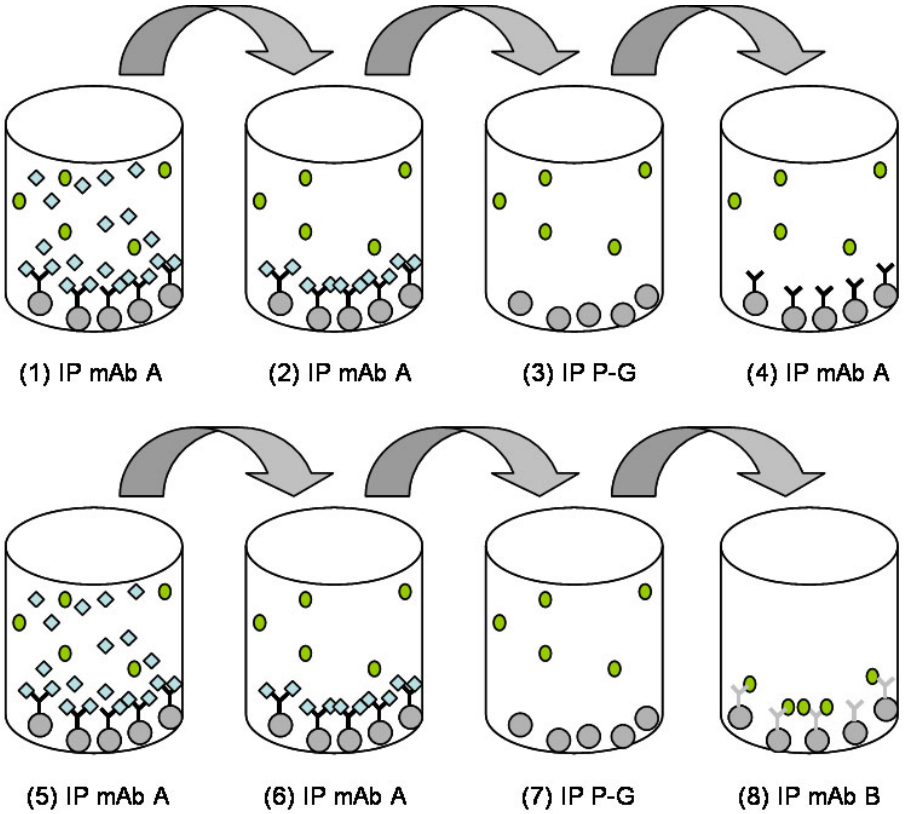

Fig. 8 Schematic diagram of two serial IPs. Quadrangles represent one conformer of a protein, circles represents a different conformer of the protein. In serial IP the supernatant of an IP (1 or 5) with mAb A will be transferred to new IP (2 or 6) with the same mAb. This step will be repeated until antibody A has completely precipitated one specific conformer of the protein out of the supernatant. To exclude a false positive result of unspecific bound protein to protein G beads (P-G) the supernatant will be incubated with P-G alone (3 or 7). In a last step the supernatant will be incubated either again with mAb A (4) or with mAb B (8). In IP 4 the Ab A will be not able to precipitate protein out of the homogenate in contrast to IP (8) with Ab B which will pull down the remaining conformer.

Until now different conformers of PrP were only detected in the cell free system. The western blot analysis of this serial IP (Fig. 9) showed that mAb19B10 could precipitate unglycosylated PrP out of supernatant which was used in two previous IPs with 6H4. Therefore 6H4 was not able to precipitate PrP out of supernatant which was used in two previous IPs with this antibody. This implied that 6H4 did not recognize the PrP conformer which, however, was recognized by 19B10.

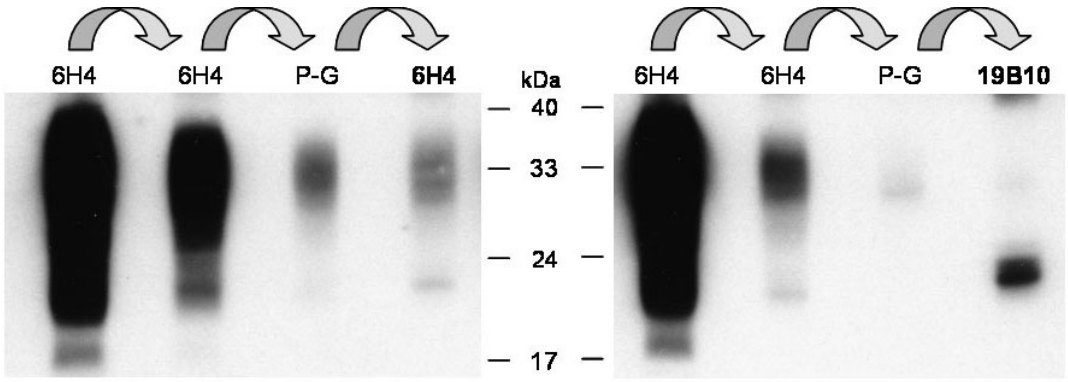

Fig. 9 mAb19B10 precipitates a subpopulation of PrP which is not recognized by 6H4. Western blot analysis of a serial IP from human brain homogenates with the monoclonal "universal" α-PrP antibody 6H4, the conformation specific α-^{Ntm}PrP mAb 19B10 and as a control with protein G (P-G) alone. Blot was probed with the α-PrP antibody W226. The “universal” mAb 6H4 did not depleted the 19B10 antigen from brain homogenates.

3.2 Expression pattern of ^{Ntm}PrP

Expression of ^{Ntm}PrP in undifferentiated and differentiated fetal cord stem cells

In (Fig. 10) the expression of ^{Ntm}PrP in undifferentiated and differentiated fetal cord stem cells (generously provided by Prof. Dr. Hans-Werner Müller, Neurological Clinic, Heinrich-Heine-university Düsseldorf, germany) was examined by IPs with mAb19B10. It was discovered that the amount of ^{Ntm}PrP was considerably higher in undifferentiated than in differentiated fetal cord stem cells. In comparison, the amount of PrP precipitated by 6H4 was not significantly different between undifferentiated and differentiated fetal cord stem cells. The differentiation dependent decrease in expression could point to a putative role of ^{Ntm}PrP in the embryonic development.

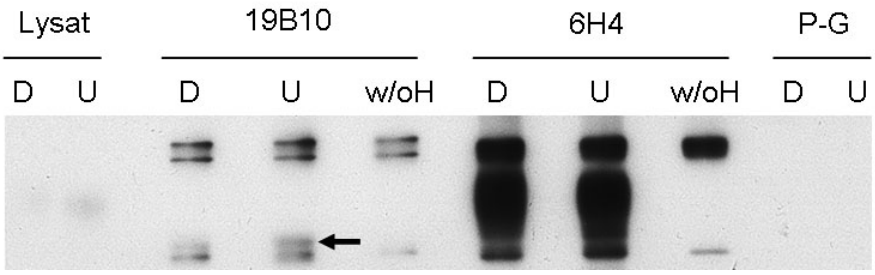

Fig. 10 ^{Ntm}PrP shows a differentiation- dependent decrease in expression. Western blot analysis of an IP with the PrP specific antibodies 19B10 and 6H4 from cell lysates of differentiated (D), undifferentiated (U) fetal cord stem cells and without lysate (M). The IP with Protein G (P-G) alone and the IP without homogenate (w/oH) served as negative controls. ^{Ntm}PrP expression was increased in undifferentiated compared to differentiated fetal cord stem cells. Arrow: ^{Ntm}PrP

Expression of ^{Ntm}PrP from embryonic development to senescence

Due to the fact that ^{Ntm}PrP showed a differentiation-dependent decrease in expression, I hypothesized that ^{Ntm}PrP could play a role in the embryonic development.

To test this hypothesis the expression pattern of ^{Ntm}PrP was examined at different stages during the embryonic development and compared to postnatal stages. Immunoprecipitations of murine brain homogenates at embryonic day 14, 16 and 18, and postnatal day 2, 10, 241 and 322 with the ^{Ntm}PrP specific mAb 19B10 were performed as described in chapter 2.4.2 (IP1). The western blots of the precipitated PrP and the precleared brain homogenates (Fig. 11) showed that ^{Ntm}PrP as well as PrP^{C} expression increased during development. ^{Ntm}PrP expression did not exclusively increase in embryonic development compared to expression of PrP^{C}.

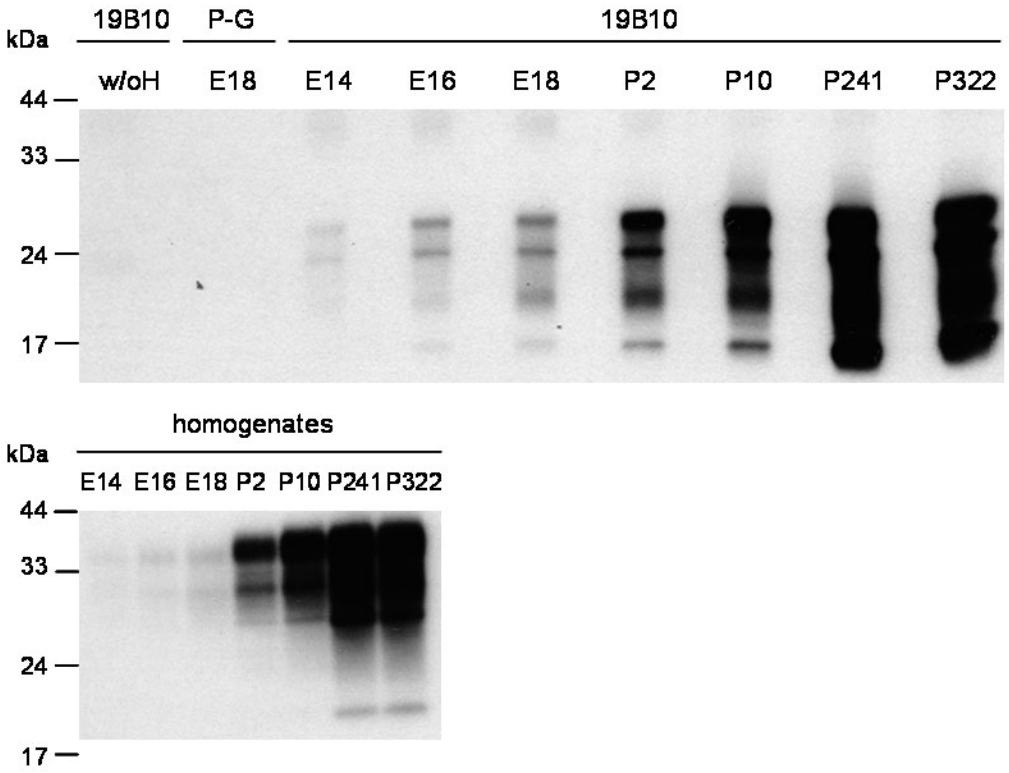

Fig. 11 ^{Ntm}PrP and PrP^{C} show an age-dependent increase in expression. Western blot analysis of an IP with mAb19B10 from murine brain homogenates embryonic (E) day 14-16 and postnatal (P) day 2-322. IP 19B10 without homogenate (w/oH) and IP P-G without antibody served as negative controls. Western Blot was probed with the α-PrP Ab W226.

The identification of a specific expression pattern of ^{Ntm}PrP in mouse brain using 19B10 staining of histoblots was not successful, due to the high background compared to the faint signal of 19B10. The inefficient binding of 19B10 could be explained by the fact that the antibody only detected native PrP and that the conformation was probably changed during the blotting and/or staining procedure. In contrast, the staining with mAbW226 which has a linear epitope, showed a distinct pattern (Fig. 12). To identify also a distinct staining pattern for ^{Ntm}PrP, the protocol for the histoblot would have to be optimized regarding optimal non denaturing conditions.

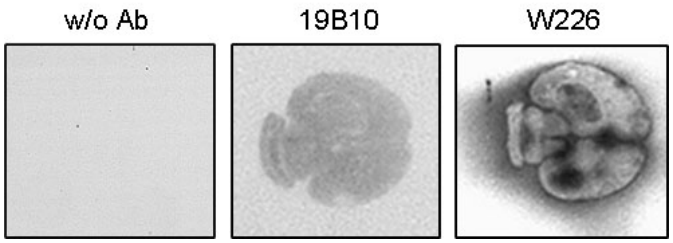

Fig. 12 Histoblots of C57/BL6 wild type mice brain sections stained with mAb19B10, mAbW226 and without antibody (w/oAb) depicted the expression pattern of PrP in brain.

Cellular localization of ^{Ntm}PrP

It was described that PrP^{C} is linked to the extracellular side of the plasma membrane by its C-terminal glycosylphosphatidylinositol anchor (Stahl *et al*., 1991). The fact that PrP^{C} can adopt several stable conformations, i.e. the secretory GPI-anchored ^{sec}PrP and the two transmembrane isoforms ^{Ntm}PrP and ^{Ctm}PrP raised the question if all three conformers are located at the cell surface or if this is only true for ^{sec}PrP. Therefore the cellular localization of ^{Ntm}PrP and ^{Ctm}PrP was investigated by taking advantage of signal swapped PrP constructs which favored in each case one conformer (Ott and Lingappa, 2004). The substitution of the PrP signal sequence with that of a mutated Prolactin (Prl mut) signal sequence resulted in a significant increase in the ^{Ntm}PrP fraction whereas an IgG signal sequence resulted in an increase in the ^{Ctm}PrP fraction.

Murine neuroblastoma cells (N2a) were transfected with the two transmembrane conformation favoring constructs pcDNA3.1 Prl(mut) PrP and pcDNA3.1 IgG PrP, pcDNA3.1 PrPwild type and as mock control with pcDNA3.1 alone. An immunofluorescence staining (intracellular and surface) of wild type, ^{Ntm}PrP or ^{Ctm}PrP overexpressing cells was conducted with the ^{Ntm}PrP specific mAb 19B10 and a universal α-PrP mAb W226, 48h after transfection (protocol see chapter 2.6.5).

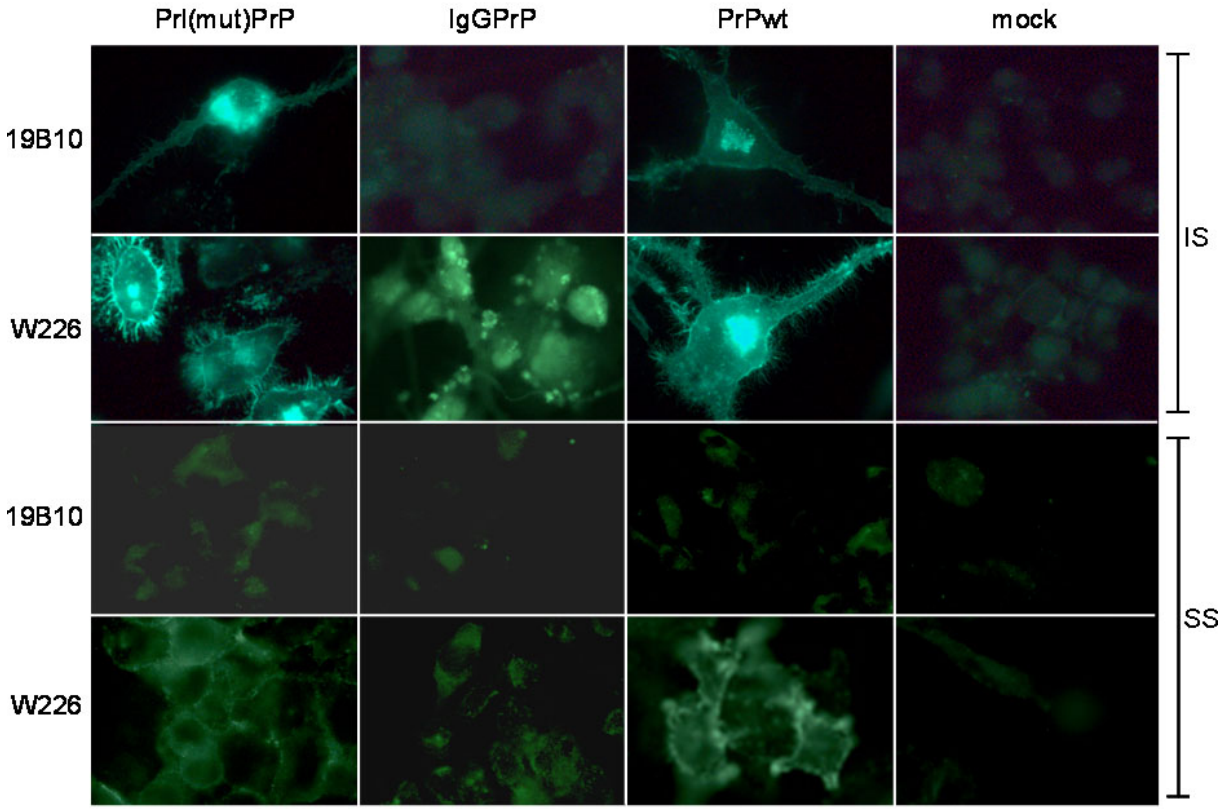

Fig. 13 ^{Ntm}PrP is located exclusively intracellular. Immunofluorescence staining of ^{Ntm}PrP (Prl(mut)PrP: PrP with mutated Prolactin signal sequence), ^{Ctm}PrP (IgGPrP: PrP with IgG signal sequence) (Ott and Lingappa, 2004) and PrPwild type overexpressing N2a cells. As mock control cells were transfected with pcDNA3.1.The intracellular (IS) and surface staining (SS) was performed with mABs 19B10 and W226. 19B10 antigen is solely intracellular located whereas the W226 antigen ("general"PrP) is additionally located at the cell surface.

Fig. 13 demonstrated that ^{Ntm}PrP was exclusively located intracellular (intracellular 19B10 staining), whereas the major fraction of PrP was located at the plasma membrane (surface W226 staining). ^{Ctm}PrP aggregated in immunoreactive clusters (intracellular W226 staining).

3.2.1 Experiments with single chain fragment of mAb 19B10 (scFv19B10)

Full length antibodies have many disadvantages because of there large size that limit their efficiency as a therapeutical tool. By contrast recombinant antibodies offer several advantages which make them suitable for a wide variety of applications. They can easily be modified by recombinant DNA techniques, can be reliably purified and are much smaller in size than full length antibodies. scFv (single chain variable

fragment) antibodies are one type of recombinant antibodies which are engineered homogeneous molecules of the heavy and light chain variable regions of the full length antibodies.

Validation of scFv19B10 function

To validate the functionality of the single chain fragment (scFv) of 19B10 a competition experiment was conducted (Fig. 14). For that purpose a high excess of unbound scFv19B10 was added to an immunoprecipitation with 19B10 bound to protein G agarose. After 2 h incubation time the supernatant was discarded and the beads were washed with lysis buffer several times to remove all unbound scFv19B10. The IPs with and without addition of scFv19B10 were compared regarding to the amount of precipitated PrP. The addition of a 5 fold molar excess of scFv19B10 resulted in a lower amount of precipitated PrP by 19B10, due to a competition with the scFv19B10. This result supplied evidence for the functionality of the scFv19B10.

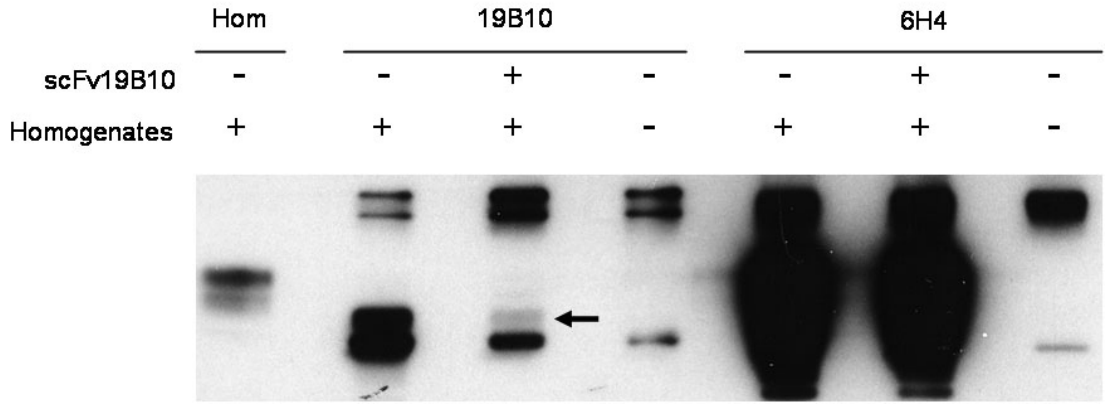

Fig. 14 scFv19B10 competes with mAb19B10 for ^{Ntm}PrP – scFv19B10 is functional. Western blot analysis of an IP with the PrP specific antibodies 19B10 and 6H4 and murine brain homogenate (Hom). Partially a high excess of unbound scFv19B10 was added to the immunoprecipitation (addition of scFv19B10 as indicated above) to have a competition with 19B10. Arrow: ^{Ntm}PrP

Examination of the ability of scFv19B10 to pass the blood brain barrier

It has been shown that mAbs directed primarily against PrP^{C} prevent *de novo* scrapie infection and abrogate prion infectivity and PrP^{Sc} from chronically scrapie-infected neuroblastoma cells (Enari*, et al.*, 2001).

The PrP^{Sc} level is determined by a steady state equilibrium between formation and degradation, so that the depletion of PrP^{C} by the binding of the anti PrP^{C} antibody can interrupt the propagation of PrP^{Sc} (Enari *et al.*, 2001). To implement this strategy of PrP^{Sc} depletion from cell culture to animal experiments the obstacle of the blood brain barrier has to be overcome, because a direct injection in the brain is therapeutically not applicable. Full length mAbs are not able to pass the blood brain barrier, because of there size. In this experiment we tested if the single chain fragment of the mAb19B10 was able to pass the blood brain barrier, because of its extremely reduced size (approx. 30 kDa) compared to the full length Ab (approx. 150 kDa). 1 mg scFv19B10 or 1 mg scFv19B10 and pertussis toxin or PBS were injected to Tg20 mice. Mice were perfused with formalin 3 h after injection, brains were removed and embedded in paraffin as described in chapter 2.6.6. Brain sections were probed with an anti-myc antibody which recognized the myc tag of the scFv19B10. Compared to controls (PBS mock inoculation and without c-myc Ab staining) scFv19B10 and scFv19B10 + Pertussis toxin inoculated mouse brain sections showed a faint brown staining (DAB) especially at the outer layers, suggested the presence of scFv19B10 in the brain. This were only preliminary data and a definite proof could not be given, because the experiment was only done once, because of limited resources. Pertussis toxin, an exotoxin produced by the bacterium *Bordetella pertussis*, which is described to open the blood brain barrier (Amiel, 1976; Bruckener *et al.*, 2003) , had no detectable influence on the permeability of scFv19B10 across the blood brain barrier.

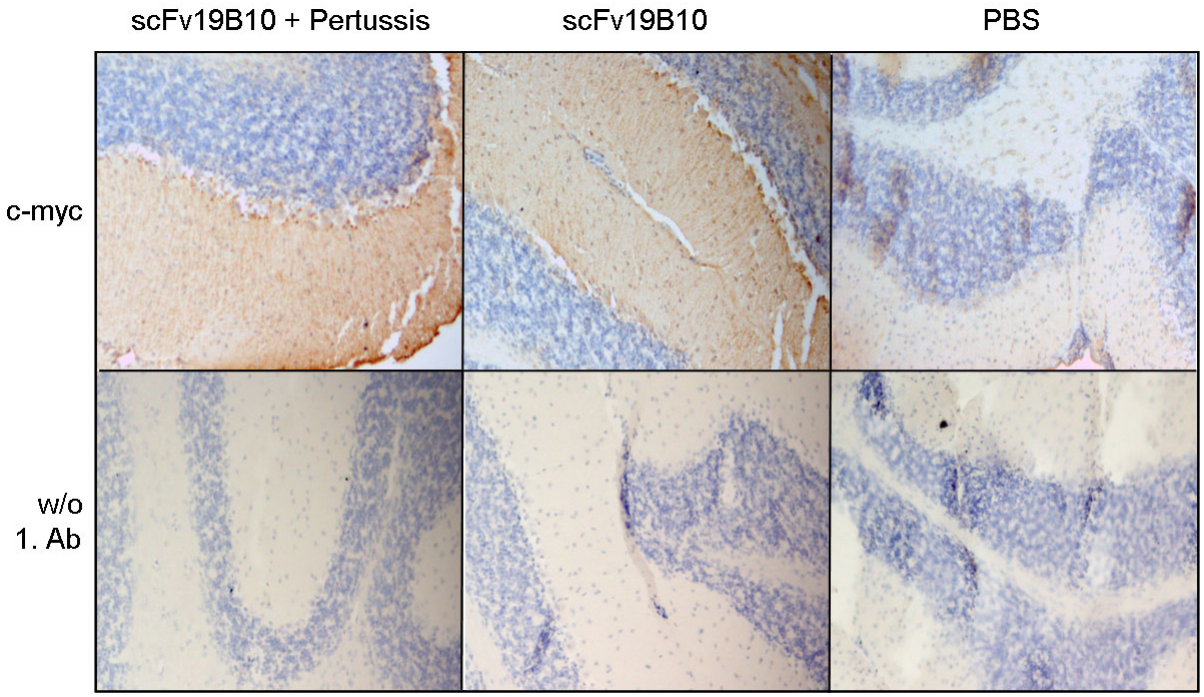

Fig. 15 scFv19B10 passes the blood brain barrier DAB staining of formalin-fixed brain sections of scFv19B10 and scFv19B10 + Pertussis toxin inoculated Tg20 mice probed with anti c-myc Ab. scFv19B10 was detected in brain sections. scFv19B10 passed the blood brain barrier.

TUNEL assay of scFv19B10 inoculated Tg20 mice

It is known form literature, that on one hand treatment with antibodies to PrP^{C} can antagonize PrP^{Sc} propagation, on the other hand the cross-linking of PrP^{C} by bivalent anti-PrP antibodies is neurotoxic (Solforosi *et al.*, 2004). In this approach we investigated if the inoculation of Tg20 mice with a single chain fragment of 19B10 resulted in an increased rate of apoptosis. A TUNEL staining of paraffin brain sections showed no increase of apoptotic cell in scFv19B10 treated mice compared to mock (PBS) treated mice, i.e. the treatment with scFv19B10 did not trigged apoptosis in Tg20 mice.

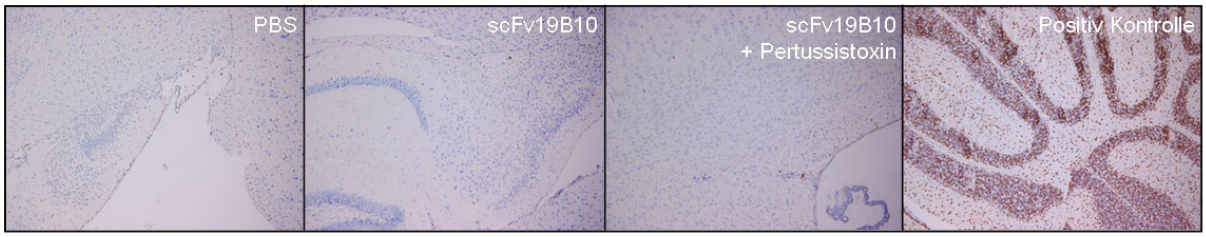

Fig. 16 Treatment with scFv19B10 does not induce apoptosis in Tg20 mice. TUNEL (brown) and hematoxylin (blue) staining of formalin-fixed perfused brain paraffin sections of scFv19B10 and scFv19B10 + Pertussis toxin inoculated Tg20 mice. There was no increase of apoptotic cells in scFv19B10 or scFv19B10 + Pertussis toxin inoculated Tg20 mice compared to mock (PBS) inoculated mice.

Treatment of ScN2a cells with the mAb19B10

To investigate if the mAb19B10 had the ability to cause clearance of PrP^{Sc} as it was shown for other anti-PrP^{C} Abs, like W226, ScN2a cells were treated for one week with fresh supernatant of 19B10Ab, W226Ab and 9E10Ab-producing hybridoma cells. The non PrP antibody 9E10 (anti c-myc antibody) and fresh hybridoma cell medium served as negative controls. As expected, treatment with W226 resulted in complete clearance of PrP^{Sc} whereas treatment with 19B10 only resulted in a faint reduction of the PrP^{Sc} amount compared to both negative controls.

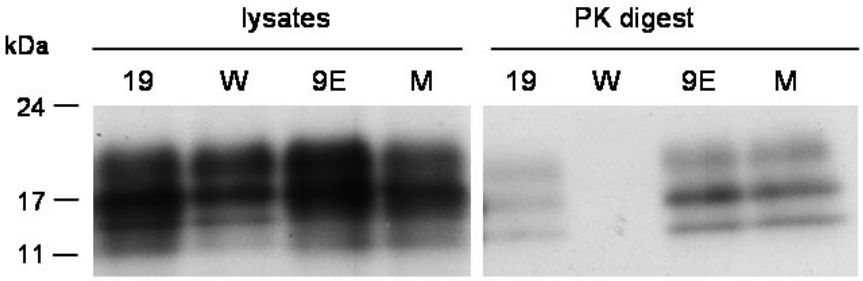

Fig. 17 Treatment of ScN2a cells with 19B10 causes a faint reduction of the PrP^{Sc} amount. Western blot analysis of undigested (lysates) and protease-digested (PK digestion) cell lysate of ScN2a cells depicting the presence or absence of prions (PrP^{Sc}) after one week treatment with the mAb 19B10 (19), W226 (W), and 9E10 (9E). Untreated cell (M) and 9E10 (anti c-myc Ab) served as negative controls.

Expression of Igκ-scFv19B10 in ScN2a cells

To validate the faint reduction of PrP^{Sc} amount in ScN2a cells treated with 19B10Ab an approach was chosen where the single chain fragment of 19B10 and, as positive

control, the single chain fragment of W226 was directly expressed in ScN2a cells. In addition, to assure the secretion of the scFvAbs, an Igκ leader sequence which specifies for the secretion of heterologous proteins, was added to the N-terminal of the protein. Untransfected cells and cells transfected with the empty expression vector (pcDNA3.1) served as negative controls. ScN2a cells were transiently transfected with the Igκ-scFvAb constructs and a PrP^{Sc} assay was performed four days after transfection. Although the control transfection with empty vector caused a reduction in the PrP^{Sc} amount, the expression of Igκ-scFv19B10 resulted in a weak but significant decrease of PrP^{Sc} in ScN2a cells compared to the transfection with empty vector alone. Administration of full length 19B10 and the intracellular expression of scFv19B10 caused a faint reduction of the amount of PrP^{Sc}, but no complete clearance as shown for other anti PrP^{C} antibodies.

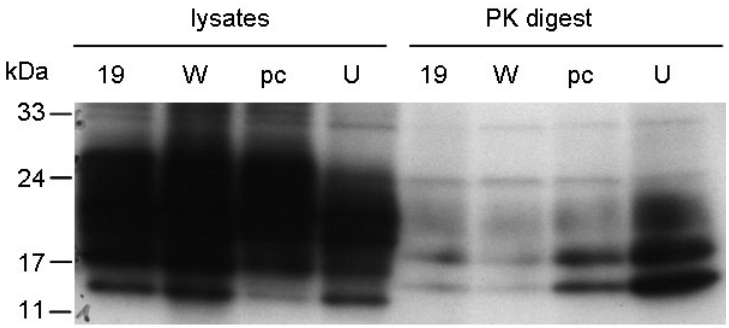

Fig. 18 Expression of Igκ-scFv19B10 in ScN2a cells for 4 days causes a faint reduction of the PrP^{Sc} amount. Western blot analysis of undigested (lysates) and protease-digested (PK digestion) cell lysate of ScN2a cells depicting the presence or absence of prions (PrP^{Sc}) of pcDNAIgκ-scFv19B10 (19), pcDNAIgκ-scFvW226 (W), pcDNA3.1 (pc) transfected cells. Untransfected cells (U) served as negative control.

3.2.2 ^{Ntm}PrP ligands

19B10 pull down experiment

Well characterized specific interaction partners of proteins with unknown function can give hints to their function. Due to the fact that the function of ^{Ntm}PrP is still unknown, a pull down experiment with scFv19B10 was performed to find specific ligands for ^{Ntm}PrP. Therefore scFv19B10 was covalently linked to NHS Sepharose beads as described in chapter 2.4.2 and incubated in human brain homogenate fractions. For

identification of false positive, i.e. unspecific ligands, the homogenate was precleared on blocked NHS Sepharose beads. The proteins eluted from the scFv19B10 pull down and the preclearing were resolved by Tris HCl SDS PAGE and proteins were stained with the colloidal blue staining kit. Protein bands which were only present in the scFv19B10 pull down were cut out and analyzed by mass spectrometry by B. Onisko, University of California, Berkley. Interestingly, only two proteins were detected in the ^{Ntm}PrP precipitated samples that were not nonspecific proteins found also in the negative control (NHS-sepharose beads without antibody). One protein was around 24 kDa and one slightly above 17 kDa. The 24 kDa protein was identified in mass spectrometry analysis as Reticulon3A (RTN3a) and the other protein was identified as Ras-related protein 1a (Rap1a).

Co-immunoprecipitation with scFv19B10

To validate the result from the mass spectrometry and identify RTN3a as a specific ligand for ^{Ntm}PrP, an IP with scFv19B10 was performed and the subsequent western blot analysis of the eluted proteins was probed with an anti RTN3a specific antibody generously provided by Jean-Philippe Löffler, Université de Strasbourg. The anti RTN3aAb specifically detected RTN3a in samples precipitated with scFv19B10 but not in samples precipitated with the anti PrP antibody 6H4 (Fig. 19). This co-immunoprecipitation approved the data from the mass spectrometry and validated RTN3a as ligand for ^{Ntm}PrP.

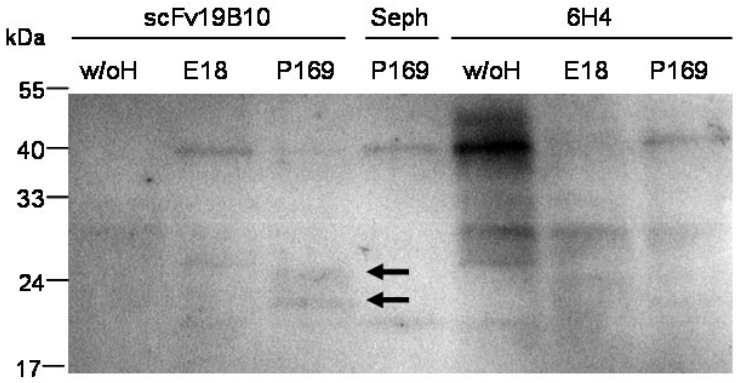

Fig. 19 RTN3a is a ligand of ^{Ntm}PrP. Western blot analysis of a Co-IP with scFv19B10 and the mAb 6H4 from mouse brain homogenates embryonic day 18 (E18) and postnatal day 169 (P169), probed with an α-RTN3 polyclonal antibody. Negative controls: IP scFv19B10 without homogenate (w/oH) and NHS Sepharose beads with homogenate, but without antibody (Seph). scFv19B10 co-precipitated RTN3a. RTN3a was a ligand of ^{Ntm}PrP. Arrows: Reticulon 3a

Members of the reticulon family often interact with each other (Dodd *et al.*, 2005). To investigate if ^{Ntm}PrP also interacts with other members of the reticulon family co-immunoprecipitations with scFv19B10 were performed and the subsequent western blot of the eluted proteins was probed with the anti RTN4Ab LAURA generously provided by Martin Schwab, University of Zurich. In the western blot analysis it could be shown that ^{Ntm}PrP, which was precipitated by scFv19B10, co-precipitated a splicing variant of RTN4A/NogoA, RTN4B/NogoB, from brain homogenate of mice embryonic day 14 and 18. From brain homogenate of two days old mice, scFv19B10 did not co precipitate RTN4B. In contrast to scFv19B10 the control Ab W226 did not co precipitated RTN4B from brain homogenate of mice embryonic day 14.

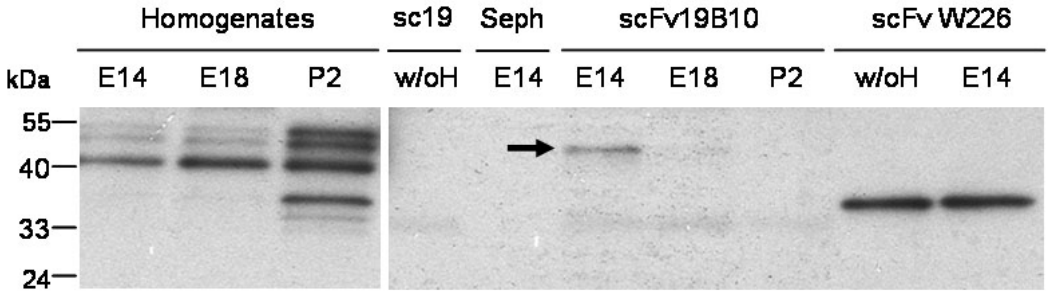

Fig. 20 NogoB is a ligand of ^{Ntm}PrP. Western blot analysis of a Co-Immunoprecipitation with scFv19B10 and the mAb 6H4 as well as mouse brain homogenates at embryonic day 14 (E14), 18 (E18) and postnatal day 2 (P2), probed with the α-RTN4 polyclonal antibody LAURA. scFv19B10 co precipitated RTN4B/NogoB. Arrow: NogoB

3.3 Functional characterization of the ^{Ctm}PrP specific mAb 19C3

The murine mAb19C3 which was generated by immunizing a PrP knockout mouse with recombinant mouse PrP (A. Breil, unpublished data), specifically recognized a linear epitope in a PrP species that overlapped with ^{Ctm}PrP from *in vitro* translation studies (Fig. 21) (these particular experiments were done by Professor V. Lingappa, California Pacific Medical Center, San Francisco and are shown here with his permission for comnpletion of the data set).

The epitope of mAb19C3 was mapped to residues comprising β-strand 2 of PrP. A structural modeling of the different conformers of PrP was done by Prof. Heinrich

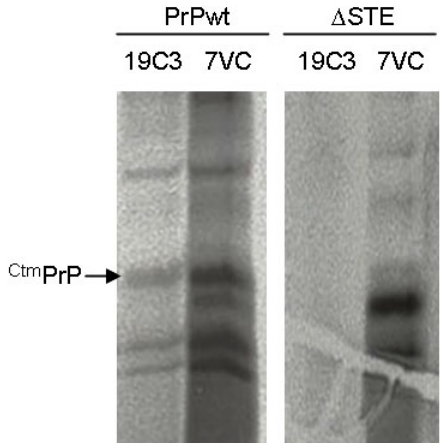

Fig. 21 mAb19C3 is specific for ^{Ctm}PrP. Autoradiography of IP with the two anti PrP Ab 19C3 and 7V3 from *in vitro* translated PrPwild type (left lanes) and ΔSTEPrP (right lanes). In comparison to 7VC which precipitated PrP from PrPwild type as well as from ΔSTEPrP, 19C3 only precipitated ^{Ctm}PrP from wild typePrP, but not from ΔSTEPrP, which predominantly contained ^{sec}PrP.

Sticht. The structure of ^{Ctm}PrP was simply obtained by modelling the novel α-helix (α-TM) according to the prediction of three independent TM prediction programs. Subsequently the stability of the modeled structure was assessed using the Fold-X server. The server indicated that ^{Ctm}PrP was approximately 5-8 kcal/mol less stable than PrP^{C} (due to the lack of β1), which suggested that the N-terminal subdomain became unfolded. The result of such an unfolding is shown in the right picture of Fig. 22, showing that β2 became fully solvent accessible. Of note, this simulation did not consider stabilizing effects that might occur after carbohydrate attachments *in vivo*.

The modeled structure of ^{Ctm}PrP showed that the linear epitope of 19C3 was only exposed at the molecule surface in the Ctm Conformer of PrP, in PrP^{C} this epitope was hidden. To avoid the binding of 19C3 to other PrP conformers than ^{Ctm}PrP it was very important to protect the protein from denaturation. Denaturation could cause the loss of differences in the tertiary structure so that the 19C3 epitope could be exposed to the molecule surface.

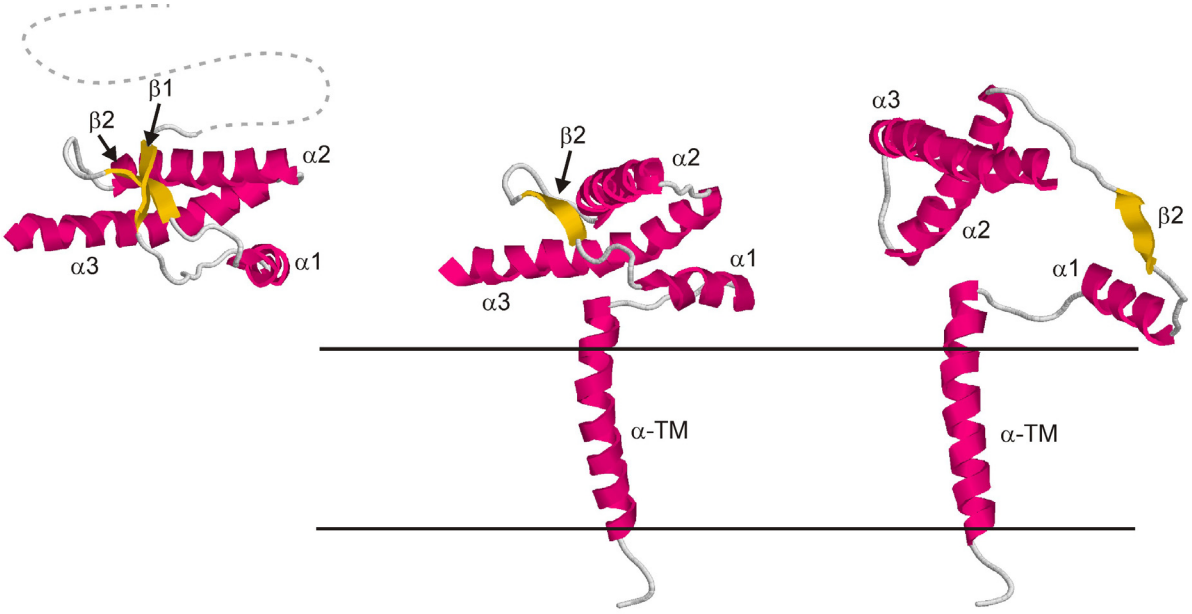

Fig. 22 Structure of ^{Ctm}PrP and PrP^{C}. In PrP^{C} (left picture), the β-strand 2 is buried in the interior of the protein. All N-terminal residues up to Leu125 are disordered (indicated by the grey dashed line). In ^{Ctm}PrP (middle picture) a transmembrane helix (denoted α-TM) is formed by residues 113-135. Note that β-strand 1 is included in this helix. As a consequence, β-strand 2 becomes significantly more solvent accessible by a factor of 2-4 compared to PrP^{C} and hence becomes accessible as epitope. (Heinrich Sticht, with permission).

Optimization of 19C3 immunoprecipitation

Due to the fact that the specific anti ^{Ctm}PrP binding activity of the mAb19C3 depends mainly on the buffer conditions used. 48 different IP incubation buffers were tested sytematically to find the optimal conditions in which 19C3 binds exclusively the Ctm conformer of PrP and non of the other conformers. Different pH values, salts and there concentrations, detergents and there concentration and ± glycerol were tested. IPs were performed as described in chapter 2.4.2 IP(6). Fig. 23 shows western blot

analysis of the different immunoprecipitations. The IPs with 19C3 from KHII homogenate were compared with IPs from Tg20 or 7BHoz or ΔSTE brain homogenates. 7BHoz is a transgenic mouse strain overexpressing wild type. Syrian hamster PrP (SHaPrP) on a $Prnp^{-/-}$ background. KHII (Tg(SHaPrP, KH->II) express a mutant that favors ^{Ctm}PrP conformation as a result of mutations (K110I, H111I) in the topogenic STE domain. The ΔSTE (Tg(SHaPrP, ΔSTE) mice express predominantly the ^{sec}PrP conformer as a result of a deletion of the STE domain residues 104-113. Tg20 mice are transgenic mouse strain overexpressing mouse PrP. The goal was to identify buffer conditions in which 19C3 precipitates more PrP from KHII brain homogenate compared to either Tg20, 7BHoz or ΔSTE brain homogenates. 19C3 had a higher binding activity in NaCl buffer than in $NaSO_4$ buffer and a high salt concentration was better than a low salt concentration. A low pH value led to better results, but not all detergents were soluble at a pH of 6.0; therefore, pH of 7.5 was found to be ideal. The addition of 20% glycerol showed a positive influence on the stability of the conformers. The optimal buffer contained a combination of high salt (0.5 M NaCl), neutral pH (HEPES pH 7.5), 20% glycerol and the two detergents TX-100 (1%) and Octyl-glycopyranoside (30 mM).

Tab. 2 (see on following page) Different buffer conditions tested as 19C3 IP incubation buffer
NC: NaCl, NS: NaSO4, HE: HEPES pH 7.5, MO: MOPS pH 8.5, ME: MES pH 6.0, Gly: glycerol, TX: TX100, CH: CHAPS, CT: CTAB, BR: Brij35, OG: Octylglucopyranoside, SA: Sarcosyl DG: Dodecylglucopyranoside, HpG: Heptylglucopyranoside, HxG: Hexylglucopyranoside, NG: Nonylglucopyranoside, TW: Tween 20, DO: DOC.

POS				NEG

	NCM	NSM	HEmM	MOmM	MEmM	Gly%	TX%	CH%	CT%	BR%	OGmM	NP%	SA.%	DGmM	HpGmM	HxGmM	NGmM	TW%	DO%
1	0.15		20					2											
2	0.50		20					2											
3	0.15			20				2											
4	0.50			20				2											
5	0.15		20			20		2											
6	0.50		20			20		2											
7	0.15			20		20		2											
8	0.50			20		20		2											
9	0.15		20				1												
10	0.50		20				1												
11	0.15			20			1												
12	0.50			20			1												
13	0.15		20			20	1												
14	0.50		20			20	1												
15	0.15			20		20	1												
16	0.50			20		20	1												
17		0.15	20						2										
18		0.50	20						2										
19		0.15	20			20			2										
20		0.50	20			20			2										
21		0.15	20							0.1									
22		0.50	20							0.1									
23		0.15	20			20				0.1									
24		0.50	20			20				0.1									
25		0.15	20								10								
26		0.50	20								10								
27		0.15	20			20					10								
28		0.50	20			20					10								
29	0.50		20			20			2										
30	0.50		20			20				0.1									
31	0.50		20			20					10								
32		0.15	20			20	1												
33	0.50				20	20	1												
34	0.50				20	20	1				10								
35	0.50		20			20	1				10								
36		0.50			20	20	1												
37		0.50			20	20	1				10								
38		0.50	20			20	1				10								
39	0.50		20			20	1				1								
40	0.50		20			20	1				30								
41	0.50		20			20	1						0.3						
42	0.50		20			20	1					0.6							
43	0.50		20			20	1												0.5
44	0.50		20			20	1											0.5	
45	0.5		20			20	1							30					
46	0.5		20			20	1								30				
47	0.5		20			20	1									30			
48	0.5		20			20	1										30		

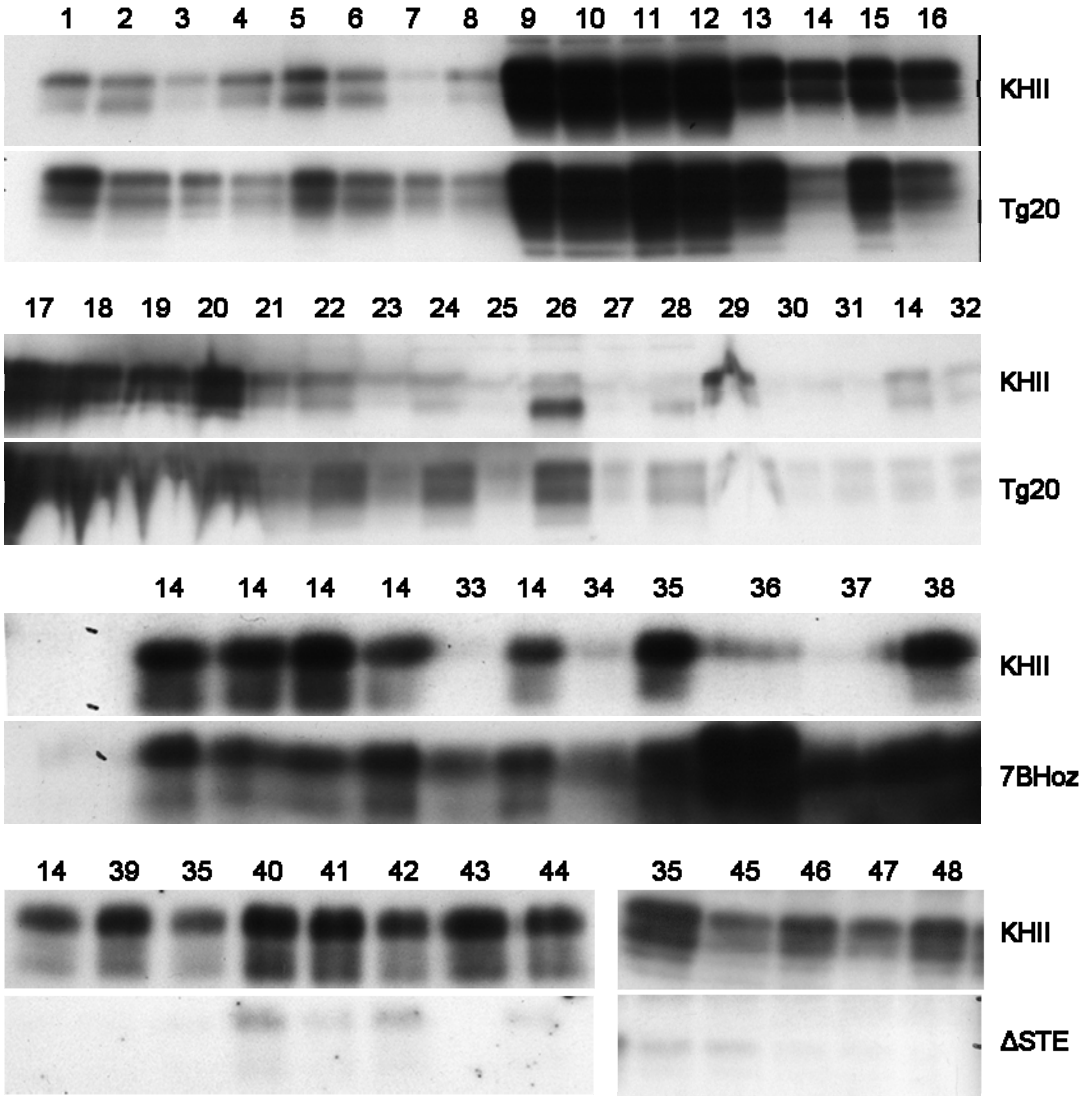

Fig. 23 Optimization of 19C3 incubation buffer conditions. Western blot analysis of IPs with the mAb19C3 and different precleared brain homogenates KHII vs. Tg20, KHII vs. 7BHoz and KHII vs. ΔSTE. Buffer conditions were optimized for ^{Ctm}PrP binding, i.e. 19C3 precipitated more PrP from ^{Ctm}PrP overexpressing Tg(SHaPrP,KHII) mice than from 7BHoz (TgSHaPrP) mice, Tg20 (mPrP overexpression) mice and ΔSTE(Tg(SHaPrP, ΔSTE) mice.

After optimization of the buffer conditions the mAB19C3 was used for immunoprecipitation experiments. 19C3 was able to precipitate a PrP species from tg(SyHaPrP KH110/111II) mice much better than from tg(SyHaPrP) mice overexpressing PrP to about the same level. As expected, 19C3 could not pull down any PrP from tg(SyHaPrP ΔSTE) mice even though, again baseline expression of PrP was about the same. Since ^{Ctm}PrP levels were expected to be much lower in wild type FVB mice, we increased the amount of homogenate used for immunoprecipitation and could observe ^{Ctm}PrP pulled down when 5-10 fold more

homogenate was used (see Fig. 24). This implied that ^{Ctm}PrP was not detected in normal mouse brain until now, because a limited detection. With aid of the ^{Ctm}PrP specific antibody 19C3 it was know possible to bring forward proof for the existence of ^{Ctm}PrP in wild type mouse brain.

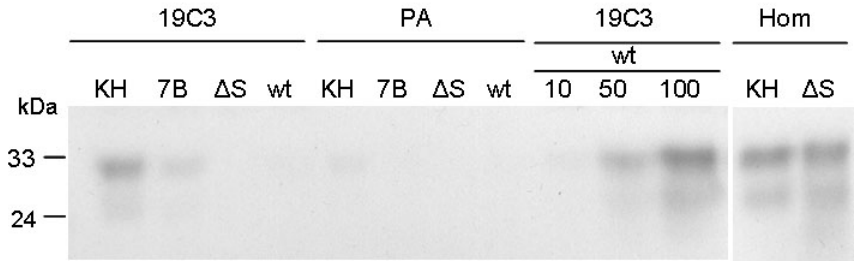

Fig. 24 19C3 precipitates specifically ^{Ctm}PrP - ^{Ctm}PrP exists in wild type mice. Western blot analysis of an IP of mouse and hamster PrP with the mAb 19C3 or protein A Agarose (PA) only and different precleared brain homogenates of (Tg(SHaPrP,KHII) mice (KH), Tg(SHaPrP, ΔSTE) mice (ΔS), 7BHoz mice(TgSHaPrP) (7B), and wild type FVB mice (wt). FVB wild type brain homogenate from 10 µL to 100 µL of a 10 % homogenate in 500 µL IP volume were applied to 19C3 IPs, to find the limit of detection of ^{Ctm}PrP in wild type mice. Blot was probed with the mAbW226.

To demonstrate that the ^{Ctm}PrP pulled down by mAB19C3 corresponded to the species identified by cold PK digestions, we subjected the pulled down material to cold PK digestion. As can be seen in Fig. 25, the pulled down material comprised a cold-PK resistant species that was absent in other homogenates.

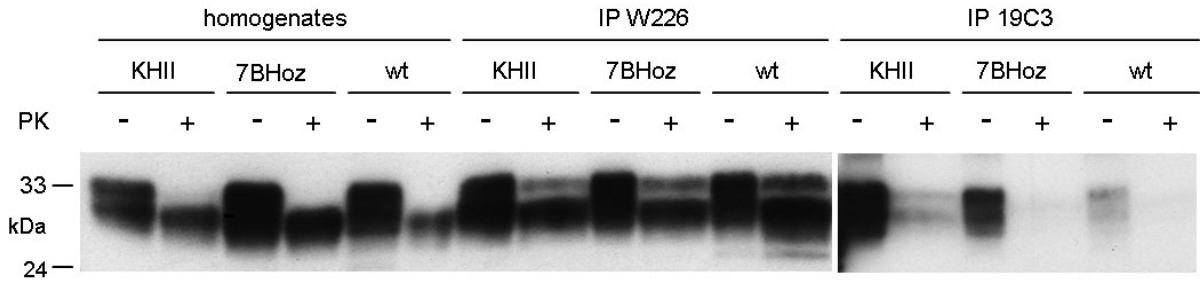

Fig. 25 19C3 precipitates mild PK resistant ^{Ctm}PrP. IP of PrP with mAB 19C3. Precleared homogenates from Tg(SHaPrP,KHII) mice (KHII), Tg(SHaPrP) mice (7BHoz) or wild type FVBwild type mice were immunoprecipitated with mAb 19C3 or mAb 6H4, analyzed by SDS PAGE and immunoblottied with W226. Cold digestion with proteinase K (PK) after the IP or of precleared homogenate (homogenates) is indicated above.

The mild PK digestion alone was not able to identify the 19C3 immunoprecipitated PrP as ^{Ctm}PrP, because the glycosylated forms of the protease-protected fragment of

^{Ctm}PrP and the C1 fragment of PrP could not be differentiated. To overcome this obstacle a PNGase F digestion was performed. Without the highly heterogeneous carbohydrate trees, which were removed by the enzyme PNGase F, the protease-protected fragment of ^{Ctm}PrP should be distinguishable from the C1 fragment of PrP. Remarkably, we found that mAB19C3 did not pull down a commonly seen cold PK-resistant fragment corresponding to a C-terminal fragment of PrP ("C1") (Sunyach *et al.*, 2007), indicating that the 19C3 epitope was not exposed in that PrP fragment and hence fundamentally different from ^{Ctm}PrP (see Fig. 26).

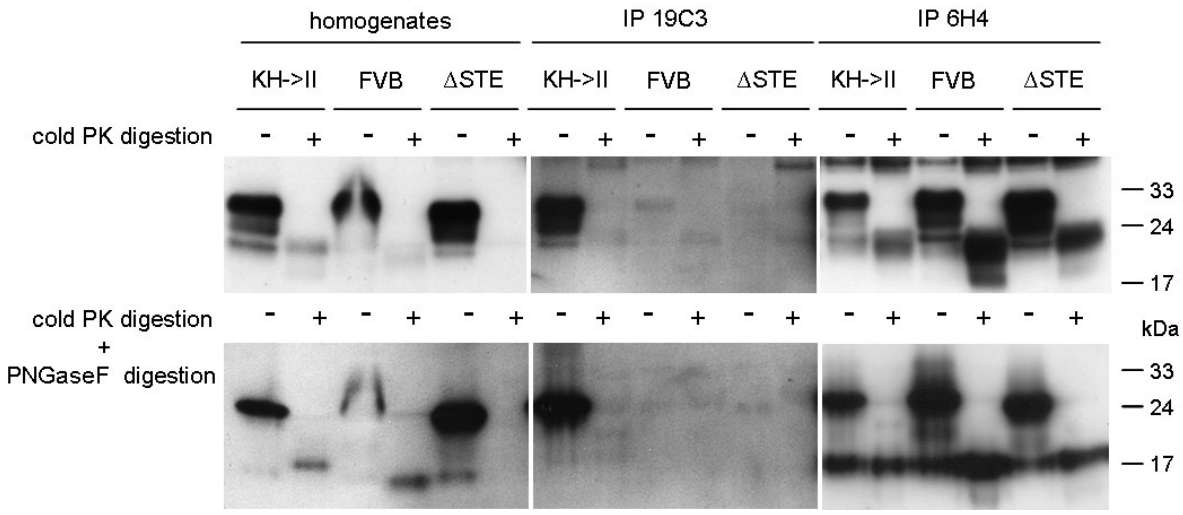

Fig. 26 19C3 precipitates mild PK resistant ^{Ctm}PrP which is distinguishable from the C1 fragment of PrP by deglycosylation. Immunoprecipitation of PrP with mAB19C3. Precleared homogenates from Tg(SHaPrP,KHI)I mice (KHII), Tg(SHaPrP, ΔSTE) mice (ΔSTE) or wild type FVB mice were immunoprecipitated with mAb 19C3 or mAb 6H4 and analyzed by western blot as described. Digestion with Proteinase K and PNGase F after the IP or of precleared homogenate is indicated. Blot was probed with the mAb W226.

Taken together with the further findings these data indicated that the mAb19C3 precipitated specifically the Ctm conformer of PrP.

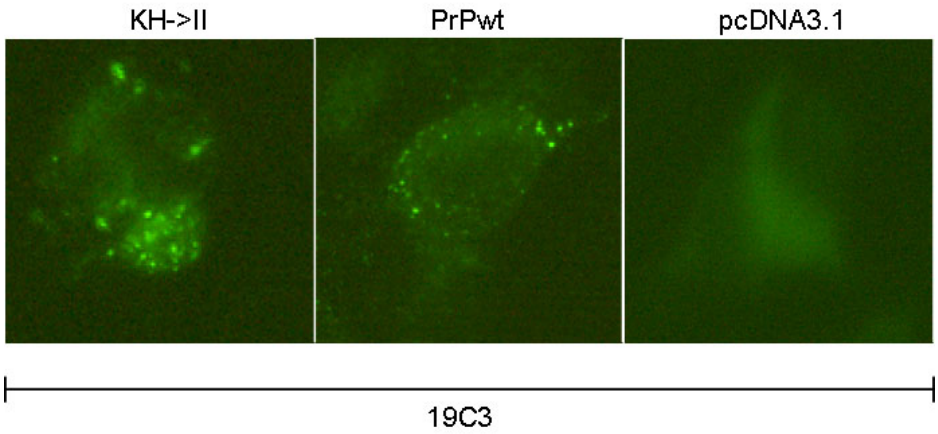

Fig. 27 ^{Ctm}PrP is located intracellular in aggregates. Intracellular immunofluorescence staining of N2a cells expressing KHII or wild type PrP with the PrP specific mAB19C3 was performed as described in methods.

As shown in Fig. 27 it could be demonstrated with the 19C3 immunofluorescence stainings that ^{Ctm}PrP was located intracellularly .

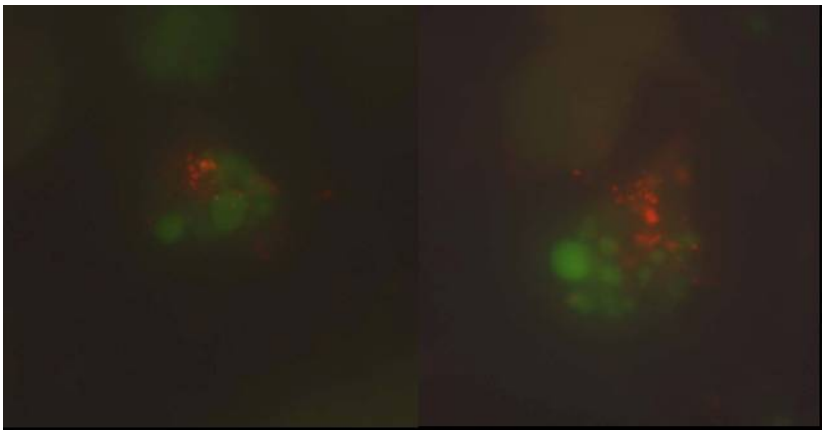

Fig. 28 ^{Ctm}PrP expression induced apoptosis in N2a cells. Intracellular immunofluorescence staining of pcDNA3.1KHII transfected N2a cells with the ^{Ctm}PrP specific mAb19C3 combined with a TUNEL staining. TUNEL staining: green, 19C3 staining red**.**

The overexpression of ^{Ctm}PrP in (Tg(SHaPrP,KHII) mice induces neurodegeneration (Hegde*, et al.*, 1998) by triggering apoptosis (Sam Saghafi, unpublished data). Fig. 28 shows the co-immunofluorescence staining of ^{Ctm}PrP (SHaPrP,KHII pcDNA3.1) overexpressing N2a cells with the ^{Ctm}PrP specific antibody 19C3 and a TUNEL staining. In cells with a strong overexpression of ^{Ctm}PrP stained red by 19C3, DNA fragmentation stained by TUNEL staining (green) was observed.

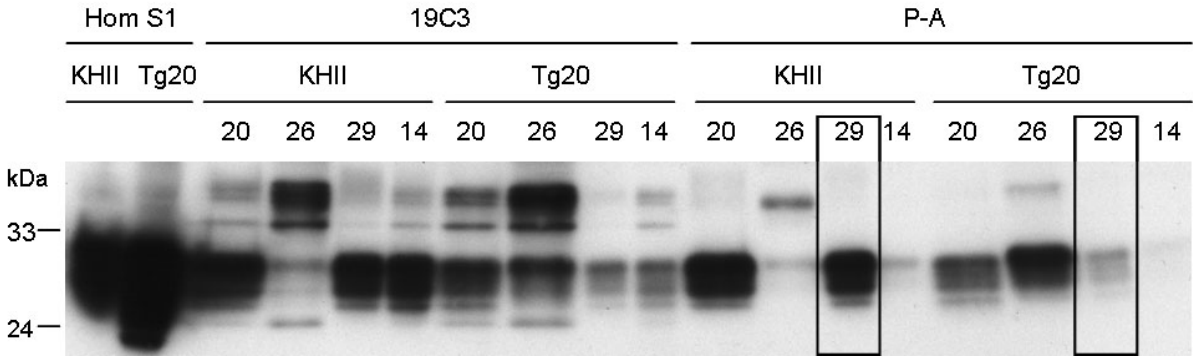

Fig. 29 CTAB buffer precipitates ^{Ctm}PrP buffer without addition of the ^{Ctm}PrP specific mAb 19C3. Western blot analysis of IPs with 19C3 and protein A (P-A) (negative control) with precleared mouse brain homogenates of the ^{Ctm}PrP overexpression mutant (KHII) and the mouse PrP overexpressing transgenic mice (Tg20). Precleared homogenate (Hom S1) served as indicator for the amount of PrP applied to IP. Blot was probed with the mAb W226. Highlighted IPs with protein A (without antibody) and the incubation buffer 29 which included CTAB, showed in comparison to each other a high amount of precipitated PrP in KHII brain homogenate vs. Tg20 brain homogenate.

Remarkably we found that the buffer 29 which contained the detergent CTAB precipitated ^{Ctm}PrP independently of the mAb19C3 with protein A only. Subsequent experiments showed that buffer 29 alone, without protein A precipitated ^{Ctm}PrP. In the next step it was investigated if the ability of the detergent CTAB to precipitate nucleic acids, was involved in the precipitation of ^{Ctm}PrP. It was hypothesized that ^{Ctm}PrP could co-precipitate with associated nucleic acids since the N-terminus of ^{Ctm}PrP is cytosolic and contains nucleic acid binding motifs. To examine this hypothesis a precipitation of ^{Ctm}PrP was performed from undigested and RNAse/DNAse digested precleared homogenates. Interestingly, PrP species precipitated by CTAB were precipitated much less PrP from RNAse/DNAse digested homogenates than from undigested homogenates (Fig. 30).

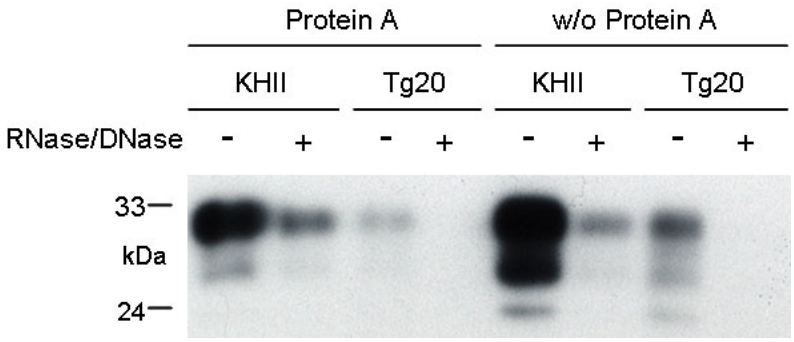

Fig. 30 ^{Ctm}PrP co-precipitated with nucleic acids. Western blot analysis of CTAB precipitated PrP from partially RNAse/DNAse digested mouse brain homogenate from ^{Ctm}PrP (KHII) and mouse PrP-overexpressing mice (Tg20). Blot was probed with the mAb W226.

3.4 Clearance of PrPSc

Previous studies of this laboratory had demonstrated that tocopherols had antiprion effects in ScN2a cells (Korth, Klingenstein, unpublished). It was found that the highly soluble tocopherol derivate α-tocopherol succinate possessed the highest antiprion potency. After treatment of ScN2a cells with α-tocopherol succinate dose-dependent morphology changes were observed. To test if these changes in morphology resulted from the induction of a signal transduction cascade, we probed a variety of compounds known to interfere with signal transduction pathways for antagonizing the effect of α-tocopherol succinate. Rapamycin was identified as such an antagonizing component (Klingenstein, unpublished data).

In this thesis the interaction between α-tocopherol succinate and rapamycin on PrP conversion and/or clearance was investigated in more detail.

3.4.1 Rapamycin antagonizes the antiprion effect of tocopherol succinate

To find the minimum concentration of rapamycin antagonizing the antiprion effect of α-tocopherol succinate, ScN2a cells were treated with different concentrations of rapamycin (1-10 nM) and α-tocopherol succinate (5 µM and 10 µM) over a period of

one week. The undigested and protease-digested cell lysates were analyzed by SDS PAGE and immunoblotting with the α-PrP antibody W226. The western blot analysis in Fig. 31 shows that rapamycin antagonized the antiprion effect of α-tocopherol succinate from 1 nM to higher concentrations.

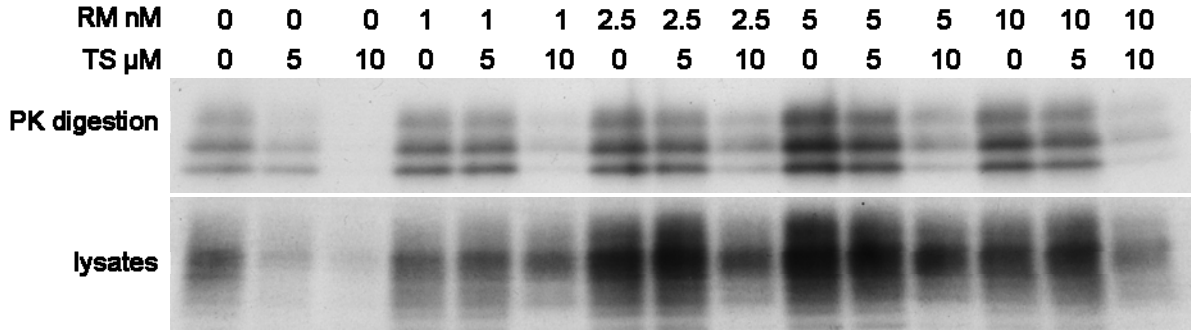

Fig. 31 Rapamycin antagonizes the antiprion effect of α-tocopherol succinate. Western blot analysis of undigested and protease-digested cell lysates of ScN2a cells depicting the presence or absence of prions (PrPSc) after one week treatment with different concentrations of tocopherol succinate (TS) and rapamycin (RM) (concentrations as indicated above). Untreated ScN2a cells served as negative control. Tocopherol succinate showed antiprion activity at a concentration of 10 µM after one week treatment. The antagonizing effect of rapamycin was observed at concentrations of 1nm and higher.

To investigate if α-tocopherol succinate or rapamycin had an effect not only on the clearance of PrP^{Sc} but also on PrP^{C}, uninfected mouse neuroblastoma cells (N2a cells) and human neuroblastoma cells (WAC II) were analyzed after one week treatment with α-tocopherol succinate and rapamycin by immunoblotting with W226 (Fig. 32). The treatment with α-tocopherol succinate caused an increase in the amount of PrP^{C}, whereas the treatment with rapamycin caused a decrease in the amount of PrP^{C}.

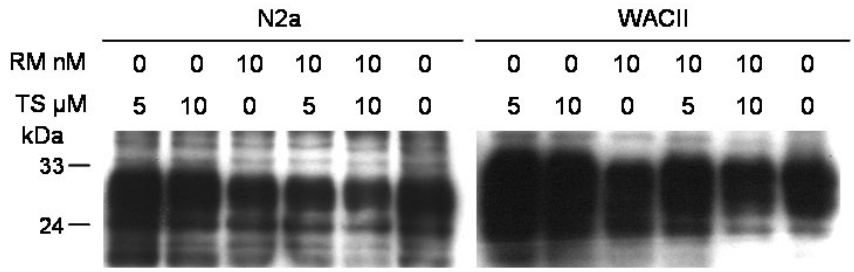

Fig. 32 α-tocopherol succinate causes an increase in PrP^C expression in neuroblastoma cells. Western blot of WACII and N2a cell lysates depicting the amount of PrP^C after one week of treatment with different concentrations of tocopherol succinate (TS) and rapamycin (RM) (concentrations indicated above). Immunoblot was probed with α-W226.The treatment of N2a and WACII cells with tocopherol succinate caused an increase in the amount of PrP^C and the treatment with Rapamycin a decrease in the amount of PrP^C compared to untreated cells.

The changes in morphology caused by α-tocopherol succinate treatment were manifested in a bipolar elongation of the infected neuroblastoma cells (ScN2a), as shown inr Fig. 33 middle image. This phenotypic effect was antagonized by the addition of rapamycin in concentrations which exhibited an antiprion antagonizing effect shown before in western blot analysis. Cells treated with α-tocopherol succinate and rapamycin (right image) showed no differences to untreated cells (left image).

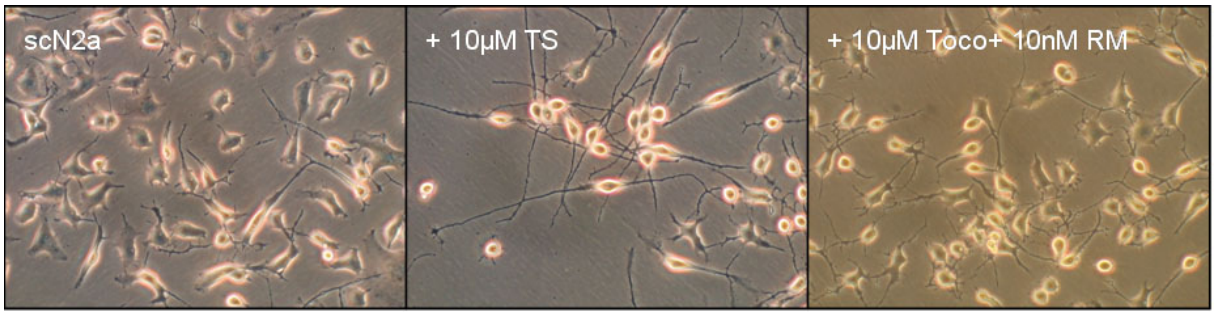

Fig. 33 Tocopherol succinate treatment induces morphological changes in the phenotype of ScN2a. Image of ScN2a cells after 3 days treatment with tocopherol succinate (TS) and rapamycin (RM). Tocopherol succinate treatment induced morphological changes in the phenotype of ScN2a. The simultaneous treatment of tocopherol succinate and rapamycin partially reversed this effect.

Rapamycin is the specific inhibitor of the kinase mTOR (mammalian target of rapamycin). Due to the fact, that rapamycin antagonized the antiprion effect of α-tocopherol succinate and also its effect on the morphology of PrP^{Sc} infected cells, α-tocopherol succinate seamed to act via the mTOR dependent pathway.

To investigate if α-tocopherol succinate had an effect on the phosphorylation status of mTOR or the downstream p70 S6 kinase, ScN2a cells were treated with α-tocopherol succinate and rapamycin in different concentrations and lysed to different time points from 1h up to five days treatment. The effects caused by rapamycin or α-tocopherol succinate treatment were noticeable from 2 h to maximum 1 day of treatment (data only shown for 2 h, 3 h and 1 day of treatment Fig. 34). The western blot (Fig. 34A) shows, that each of the investigated proteins (mTOR and p70 S6 kinase) exhibited alterations only at a single phosphorylation site. For the mTOR kinase the phosphorylation status at Ser 2481 was affected and for the p70 S6 kinase the phosphorylation status at Thr 421 was affected. Treatment of cells with 10 nM rapamycin induced a dephosphorylation of p70 S6 kinase at Thr 421 at a period of time from 2 h to 24 h after addition of rapamycin. A dephosphorylation of mTOR at Ser 2481 induced by rapamycin treatment began not until 3 h of treatment (Fig. 34B) and continued till 24 h of treatment (Fig. 34A). The treatment with α-tocopherol succinate had no significant effect on the phosphorylation of mTOR or S6 Kinase. The decreased phosphorylation of mTOR at Ser 2481 and p70 S6 kinase at Thr 421 compared to untreated cells after 24h of treatment (Fig. 34A) seemed to be a blotting artifact, because this result was not reproducible.

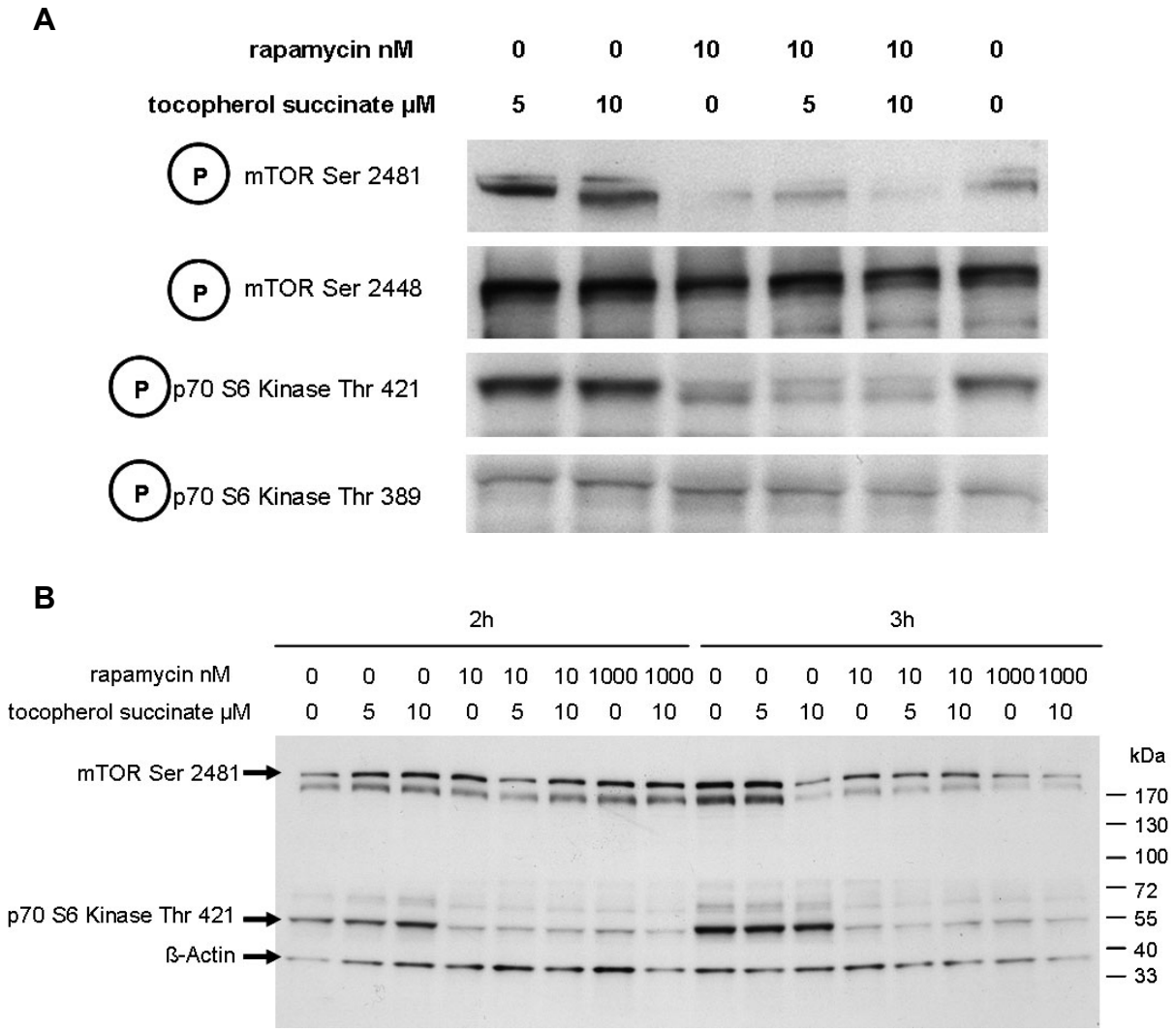

Fig. 34 Tocopherol succinate treatment has no significant effect on the phosphorylation of mTOR and p70 S6 Kinase. Western blot of ScN2a cell lysates depicting the amount of phosphorylated mammalian target of rapamycin (mTOR) Ser 2481 or Ser 2448 and phosphorylated p70 S6 Kinase Thr 421 or Thr 389 after (A) 24 h and (B) 2h and 3h of treatment with different concentrations of tocopherol succinate and rapamycin (concentrations indicated above). Blot was probed with phosphorylation specific antibodies α- mTOR Ser 2481, α- mTOR Ser 2448, α-p70 S6 Kinase Thr 421, α-p70 S6 Kinase Thr 389 and α- ß-actin.

3.4.2 The influence of rheb to the conversion of PrP^C to PrP^{Sc}

The binding of the small GTPase rheb (Ras homolog enriched in brain) to mTOR rescues mTOR from inactivation (Long *et al.*, 2005). In opposition the dominate negative rheb mutant S20N, which also binds to mTOR, causes an inhibition of mTOR due to its lack of kinase activity (Long *et al.*, 2005). Therefore the

overexpression of the rheb mutant S20N should have a comparable effect on mTOR activity as the treatment with rapamycin. The pharmacological approach via rapamycin treatment as well as the genetical approach via overexpression of rhebS20N resulted in an inhibition of mTOR. The overexpression of rheb and the mutant rhebS20N together with MHM2 PrP in ScN2a cells (Fig. 35) should provide evidence if the activation or inactivation of mTOR has an influence on the conversion of PrP^{C} to PrP^{Sc}. MHM2 PrP was coexpressed with rheb, because the introduction of the epitope of mAb 3F4 (Kascasac *et al.,* 1987) into mouse PrP (designated MHM2 PrP) allowed the detection of newly formed PrP^{Sc} against the background of endogenous mouse PrP^{Sc}, which is not recognized by mAb 3F4 (Scott *et al.*, 1992). This enabled the differentiation between a reduced clearance of PrP^{Sc} from a increased conversion of PrP^{C} to PrP^{Sc}.

The western blot analysis of undigested and protease-digested cell lysates of ScN2a cells overexpressing pBud4.1/MHM2 or pBud4.1rhebS20N/MHM2 showed an increased amount of PrP^{Sc} in pBud4.1 rhebS20N/MHM2 transfected ScN2a cells compared to pBud4.1*rheb*/MHM2 or pBud4.1/MHM2 transfected ScN2a cells.

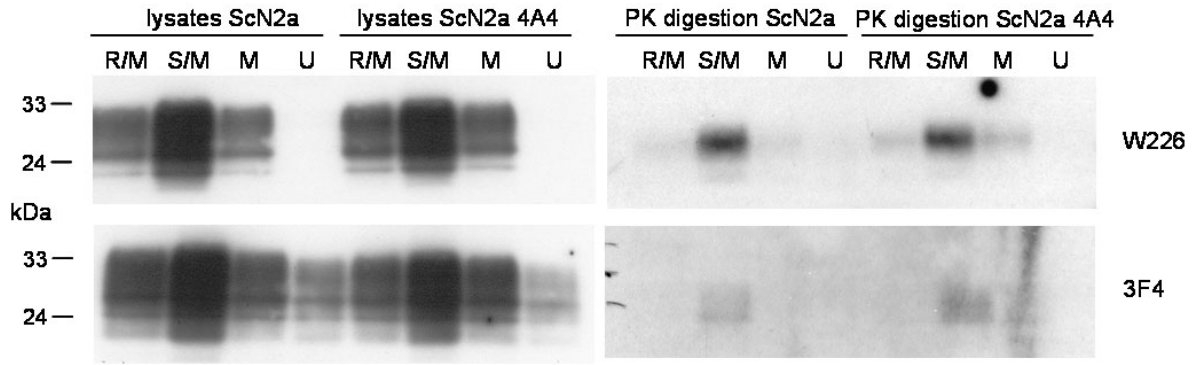

Fig. 35 Inhibition of rheb increases the conversion of PrP^{C} to PrP^{Sc}. Western blot of undigested and protease-digested cell lysates of ScN2a cells and a ScN2a subclone 4A4 depicting the presence or absence of prions (PrP^{Sc}) after overexpression of the chimeric mouse/Syrian hamster construct MHM2 (M) , rheb/MHM2 (R/M) and rhebS20N/MHM2 (S/M). Untreated ScN2a cells (U) served as negative control. Newly converted MHM2 PrP to PrP^{Sc} could be distinguished from endogenous mouse PrP^{Sc} by the Syrian hamster specific monoclonal antibody 3F4. Overexpression of the rheb mutant S20N together with MHM2 PrP increased the amount of newly converted PrP^{Sc} in comparison to the overexpression of the rheb together with MHM2 which had no effect.

Since the antiprion effect of α-tocopherol succinate could be antagonized pharmacologically by rapamycin and rhebS20N was the genetic analogue to rapamycin, the question arised, whether the overexpression of rhebS20N could also antagonize the antiprion effect of α-tocopherol succinate. To answer this question ScN2a cells were transiently transfected with pBud4.1 rhebS20N/MHM2, pBud4.1 MHM2 or pFlag rhebS20N and subsequently treated with different concentrations of α-tocopherol succinate 5 h after transfection. Cells were lysed after 4 days treatment. The western blot analysis of undigested and protease-digested cell lysates probed with mAb 3F4 and mAbW226 shows that in α-tocopherol succinate (10 µM) treated ScN2a cells with rhebS20N overexpressing (together with MHM2 PrP or alone) PrP^{Sc} was not completely cleared compared to MHM2 PrP overexpressing cells. These results suggested that the overexpression of rhebS20N antagonized the antiprion effect of α-tocopherol succinate.

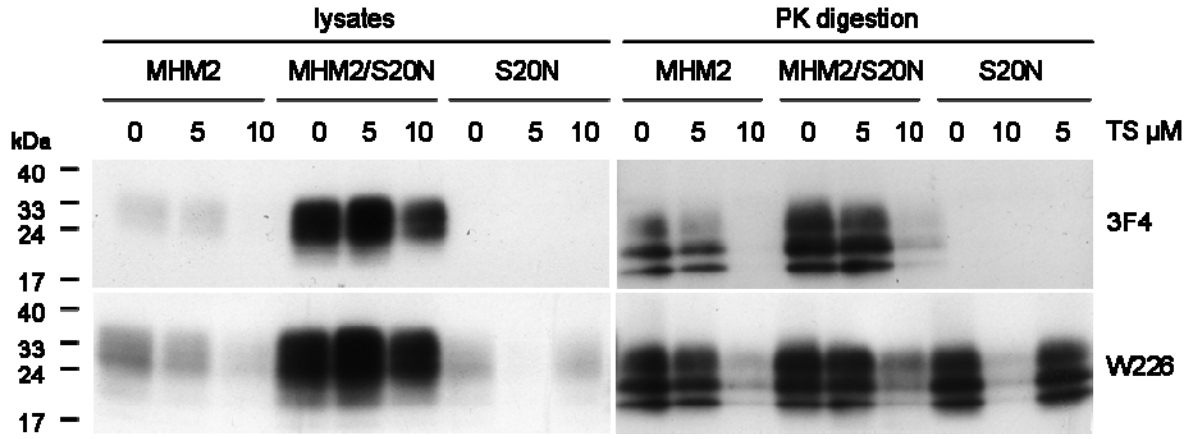

Fig. 36 rhebS20N antagonizes the antiprion effect of α-tocopherol succinate. Western blot of undigested and protease-digested cell lysate of ScN2a cells depicting the presence or absence of prions (PrP^{Sc}) after overexpression of MHM2, MHM2 /rhebS20N or S20N and 4 days treatment with different concentrations of α-tocopherol succinate (TS) (concentrations indicated above). The combined overexpression of the rheb mutant S20N together with MHM2 PrP increased the amount of newly converted PrP^{Sc} in comparison to the single expression of MHM2 or rhebS20N alone, and this effect could partially antagonize the a-tocopherol succinate antiprion effect.

3.4.3 The influence of rheb and the dominate negative mutant of rheb on PrP^{C} expression

Since the overexpression of rhebS20N had an influence on the conversion of PrP^{C} to PrP^{Sc}, could rhebS20N trigger the spontaneous conversion of PrP^{C} to PrP^{Sc} in

untransfected N2a cells? The western blot analysis of undigested and protease-digested cell lysates of N2a cells overexpressing pBud4.1/MHM2, pBud4.1 rhebS20N /MHM2 or pBud4.1*rheb*/MHM2 showed that no spontaneous conversion of PrP^{C} to PrP^{Sc} occurred.

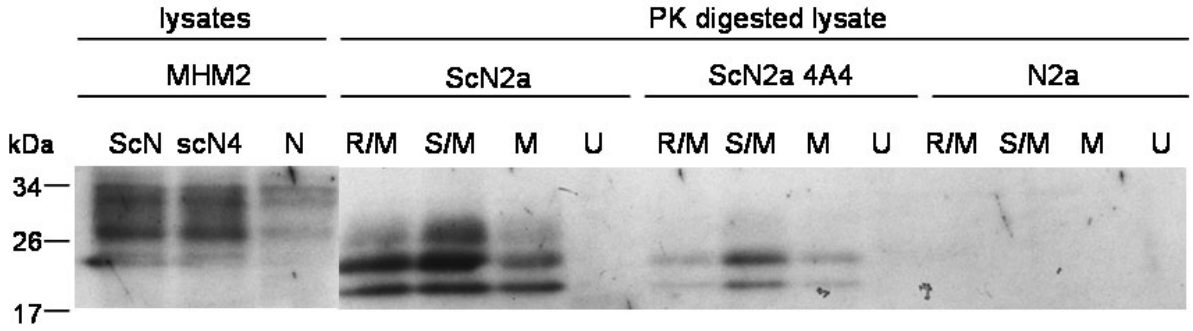

Fig. 37 Inhibition of rheb does not lead to a spontaneous conversion of PrP^{C} to PrP^{Sc} in N2a cells. Western blot of undigested and protease-digested cell lysate of ScN2a (ScN), ScN2a 4A4 (ScN4) and N2a(N) cells depicting the presence or absence of prions (PrP^{Sc}) after overexpression of the chimeric mouse/Syrian 3F4hamster construct MHM2 (M), *rheb*/MHM2 (R/M) and rhebS20N/MHM2 (S/M). Untreated ScN2a cells (U) served as negative control. Immunoblot was probed with hamster specific mAb 3F4. The overexpression of the rheb mutant S20N together with MHM2 PrP in N2a cells had no effect on the amount of newly converted PrP^{Sc} in comparison to the overexpression in ScN2a cells.

Overexpression of rhebS20N in ScN2a cells resulted in increased levels of total PrP as shown in Fig. 35. These results raised the question if overexpression of rhebS20N in uninfected neuroblastoma cells would increase PrP^{C} expression. To answer this question, one murine (N2a) and two human (WAII, NLF) neuroblastoma cell lines were transiently transfected with pcDNA3.1myc *rhebS20N* and pcDNA3.1mycrheb. Cells were lysed 4 days after transfection and analyzed by SDS PAGE and immunoblotting with mAbW226. The western blot in Fig. 38 shows, that there was no difference in the amount of PrP^{C} between transfected and untransfected cells in all three cell lines.

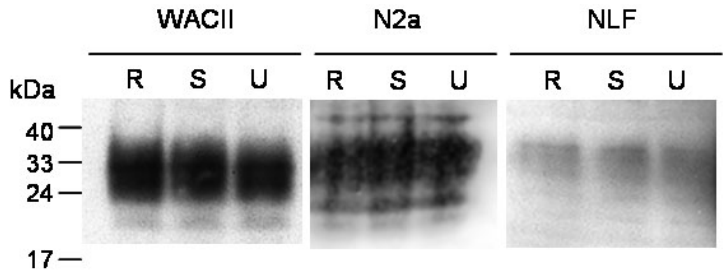

Fig. 38 Overexpression of rheb or the dominate negative mutant of rhebS20N in neuroblastoma cells has no effect on PrP^C expression. Western blot of cell lysates of human neuroblastoma cells WACII and NLF as well as murine neuroblastoma cells N2a transfected with pcDNA3.1myc-rheb (R) and pcDNA3.1myc- rhebS20N (S) constructs. Untransfected cells (U) served as negative control. Cells were lysed 4 days after transfection. Immunoblot was probed with α-PrPAb W226.

3.4.4 The influence of autophagy on the clearance of PrP^{Sc}

The protein kinase mTOR regulates diverse processes in the cell, amongst others autophagy. Autophagy is a catabolic process involving the degradation of a cell's own components through the lysosomal machinery. In scrapie-infected brain, lysosomes and lysosome-related structures are present in abnormally high numbers in neuronal cell processes and these structures contain PrP (Laszlo, *et al* 1992).

To investigate if the antiprion effect of α-tocopherol succinate was caused by inhibition of autophagy via mTOR, an approach was chosen, were autophagy was inhibited by silencing of the two autophagy related proteins Atg7 and LC3 via specific small interfering RNAs (siRNAs).

Atg7 (autophagy-related 7), a member of the E1-like family of proteins, which includes the well-characterized ubiquitin-activating enzymes, is essential for autophagy and its loss leads to the loss of the autophagy marker protein LC3 II (microtubule-associated protein light chain 3) resulting in neurodegeneration (Komatsu*, et al.*, 2006). Fig. 39 shows the western blot of undigested and protease-digested cell lysates of ScN2a cells transfected with LC3 and Atg7 siRNA. The blots with undigested lysates (left blots) were probed with specific antibodies against LC3 and Atg7 and the blots with protease-digested cell lysates (right blots) were probed with the α-PrP Ab W226. An effective silencing of LC3 was shown already after 48 h (The silencing of Atg7 was not as efficient as the silencing of LC3, but phenotypically

the transfected cells looked morbid compared to the mock transfected cells. Unexpectedly the amount of LC3II, which should decrease in absence of Atg7, remained unchanged. This could mean that silencing of Atg7 had been insufficient. The silencing of the autophagy related proteins had no influence on the amount of PrP^{Sc} (Fig. 39, right blots). The amount PrP^{Sc} in untransfected cells was comparable to the amount PrP^{Sc} of siRNA transfected cells.

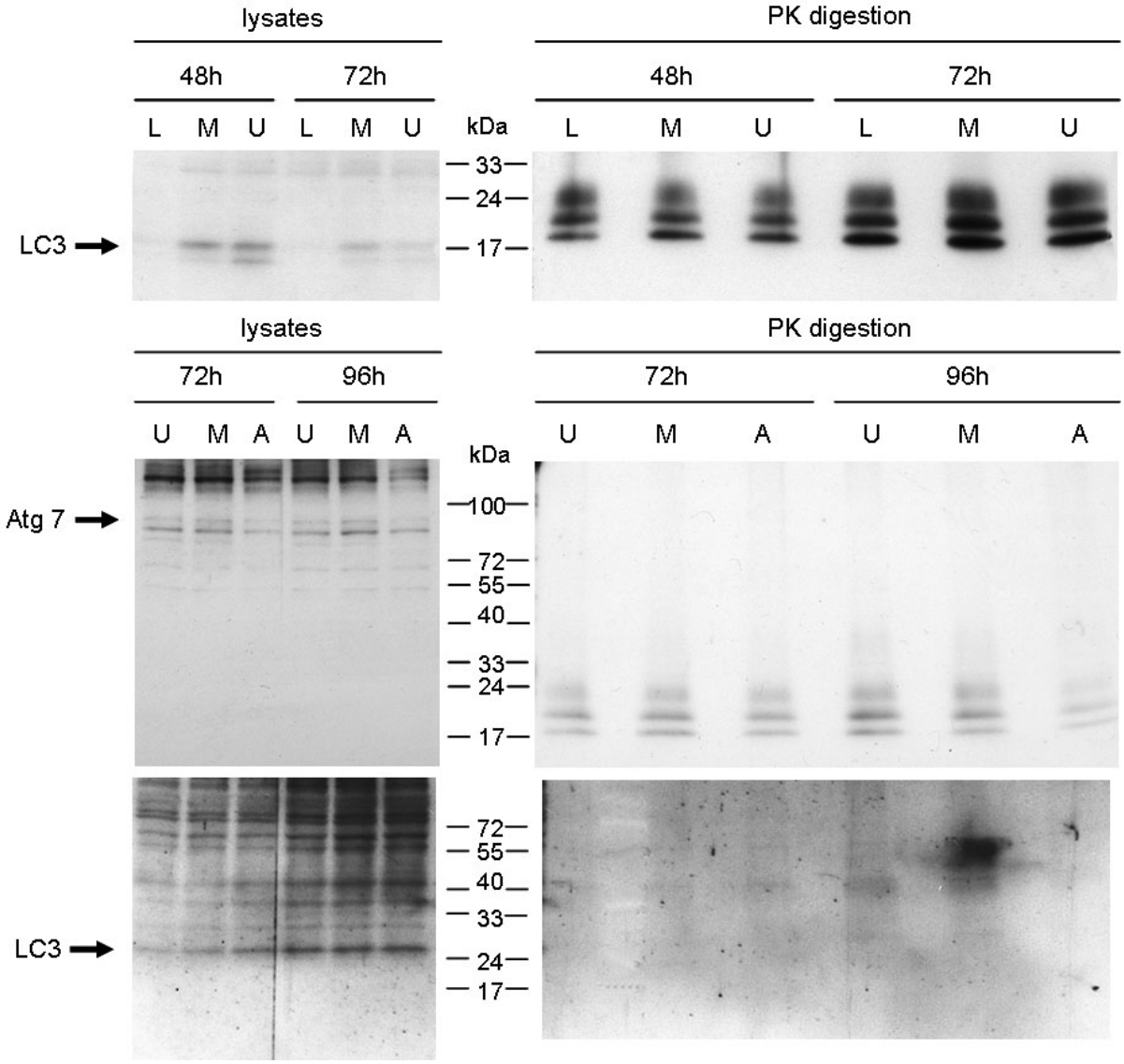

Fig. 39 The silencing of LC3 and Atg7 has no effect on the amount of PrP^{Sc}. Western blot analysis of undigested (lysates) and protease-digested (PK digestion) cell lysate of ScN2a cells depicting the amount of PrP^{Sc} after specific silencing of Atg7 (A) and LC3 (L) two autophagy associated protein by siRNAs. Untransfected (U) and mock siRNA transfected (M) cells served as negative controls. Immunoblots of undigested lysates were probed with α-LC3 polyclonal rabbit serum and α-Apg7 antibody (AnaSpec). Immunoblots of digested lysates were probed with α-PrPAb W226.

Rapamycin, the specific inhibitor of mTOR, induces autophagy by inhibiting the negative regulation of mTOR on autophagy. Increased autophagy could result in the degradation of large PrP^{Sc} aggregates into smaller aggregates and smaller aggregates could be more infectious. This hypothesis was based on studies showing that fragmentation of PrP^{Sc} aggregates by sonification increases converting activity in cell culture (Silveira *et al.*, 2005; Weber *et al*, 2008). To investigate this hypothesis the lysates of rapamycin and untreated ScN2a cells were separated on a sucrose gradient according to protein size. After SDS PAGE and immunoblotting with mAbW226 the fractions of the gradient were analyzed. The western blot analysis in Fig. 40 showed no altered distribution of PrP in the different sucrose gradient fractions between untreated and rapamycin treated cell lysates.

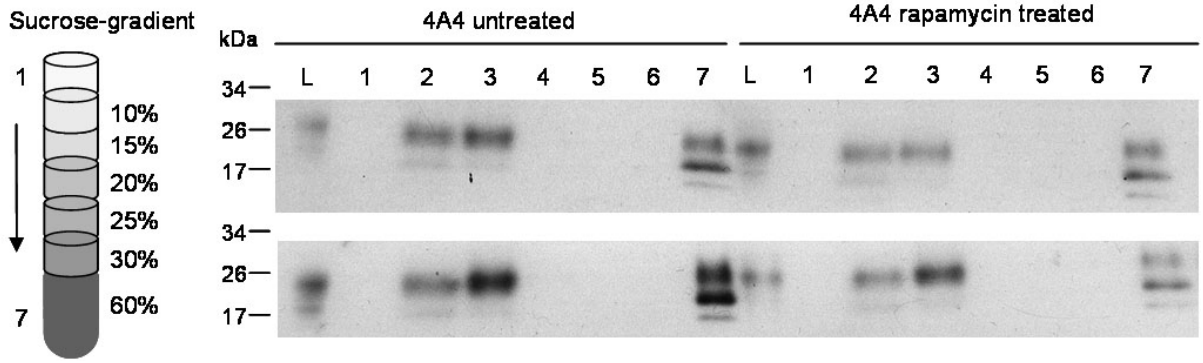

Fig. 40 Rapamycin treatment has no influence on the size of PrP aggregates. Western blot of sucrose gradients from cell lysates (L) of untreated and rapamycin treated ScN2a cells (4A4). ScN2a cells were lysed in 10 mM Tris pH 7.5, 1% Sarcosyl, 150 mM NaCl, 1 mM $MgCl_2$ and floated on sucrose gradient. The distribution of PrP was analyzed by immunoblotting in two independent experiments (upper panel and lower panel).

4 Discussion

In the present thesis, the heterogeneity of PrP^{C} was demonstrated *in vivo* and, in particular, the two conformers ^{Ntm}PrP and ^{Ctm}PrP were be further characterized. Moreover, it was demonstrated which signal transduction pathway is involved in the clearance of PrP^{Sc}. Thus, the objectives were achieved, i.e. the heterogeneity of PrP^{C} was proven *in vivo* and ^{Ntm}PrP was characterized with respect to localization, specific binding partners and expression pattern even if its function is still left unknown. Regarding the effect of α-tocopherol succinate on the clearance of PrP^{Sc} we were able to indentify a relevant signal transduction pathway and to narrow down the possible targets regulated by this pathway.

Although much progress has been made over the last few years regarding the physiological function of the cellular prion protein, it remains enigmatic. Many hypotheses have been proposed. To gain insight into the function of PrP, knock out mice have been generated. These PrP-deficient mice are viable and develop normally (Bueler *et al.*, 1992). Subsequently, investigations with mice expressing an N-terminally truncated version of PrP^{C} on the null background showed neuronal degeneration soon after birth, suggesting that PrP^{C} may play an important role in the maintenance and regulation of neuronal functions (Shmerling *et al.*, 1998). In addition, functions in copper metabolism (Brown *et al.*, 1997, Vassallo and Herms 2003), neurotransmitter metabolism, signal transduction (Mouillet-Richard *et al.*, 2000, Krebs *et al.*, 2006), cellular protection against oxidative stress (Wong *et al.*, 2000, Roucou and LeBlanc, 2005, Krebs *et al.*, 2007), differentiation (Graner *et al.*, 2000) and programmed cell death (Paitel *et al.*, 2002, Kim *et al.*, 2004, Solforosi *et al.*, 2004, Roucou *et al.*, 2005) have been proposed. These seemingly very diverse functions of PrP^{C} could for a large part be unified by the existence of a conformationally heterogenous population of PrP^{C}. *In vitro* translation studies have shown, that PrP^{C} can adopt several stable conformations, i.e. the secretory GPI-anchored ^{Sec}PrP and the two transmembrane isoforms ^{Ntm}PrP and ^{Ctm}PrP (Hegde *et al.*, 1998) which could perform different functions.

4.1 Topological isoforms of PrP^C

Progress in the molecular analysis of PrP conformers is linked to the technical abilities to detect and characterize these alternative folded isoforms of PrP^C. Due to the limited sensitivity of detection and the fact that only a very small part of PrP^C that is synthesized at the ER is folded into ^{Ntm}PrP or ^{Ctm}PrP, definite evidence of conformational heterogeneity of PrP^C *in vivo*, i.e. in normal brain has not been proven yet. Only the existence of ^{Ctm}PrP was demonstrated *in vivo* in association with progression of prion disease and Gerstmann-Sträussler-Scheinker syndrome (GSS) (Hegde *et al.*, 1999). In this thesis, questions concerning PrP conformers ^{Ntm}PrP and ^{Ctm}PrP could be answered with the help of two conformation-specific monoclonal α-PrPAb.

Monoclonal antibody 19B10 which was generated against recombinant hamster PrP, was found to bind specifically ^{Ntm}PrP in an immunoprecipitation (IP) with *in vitro* translated PrP (Korth and Lingappa, unpublished data). First experiments showed that 19B10 is a truly conformational antibody, i.e. recognized a distinct three-dimensional epitope constituted by nonadjacent amino acid residues and not a linear peptide sequence that is only exposed in the Ntm conformer and buried in all other conformations (see Fig. 7). This was in agreement with the fact, that the epitope of mAb19B10 could not be mapped with a PrP peptide library, which included only linear epitopes (Korth, unpublished data).

Binding studies showed that mAb19B10 precipitated an unglycosylated PrP species that overlapped with ^{Ntm}PrP from *in vitro* translation studies (see Fig. 6). This observation could be confirmed in a serial IP with ^{Ntm}PrP specific mAb19B10 after immunodepletion with the universal α-PrP mAb 6H4. In addition, the ability of the mAb19B10 to detect a specific subpopulation of PrP (^{Ntm}PrP) could be demonstrated (see Fig. 9). So far, mAb6H4 has been regarded as universal PrP antibody, because its epitope comprises inside of helix 1 of the prion protein, which is an exposed domain in PrP^C. The finding that the seemingly "universal" mAB 6H4 did not deplete

the 19B10 antigen from brain homogenates proved that different conformers of the prion protein existed in wild type mouse brain *in vivo* .

A pull down experiment with scFv19B10 identified two putative specific binding partners for ^{Ntm}PrP , Reticulon3A (RTN3a) and Ras-related protein 1a (Rap1a). These specific ligands could give insight into the physiological function of ^{Ntm}PrP. The subsequent experiments were focused on the reticulon family of proteins, because reticulons (RTNs) are known to play a role in neuronal outgrowth and plasticity and in the pathogenesis of the most common neurodegenerative disease (Alzheimer´s Disease). In that context, it is also interesting to note that it has been postulated that PrP^C has a putative role in neurogenesis (Steele *et al.*, 2006).

The reticulon familiy (RTN1 – RTN4), a group of proteins defined by the presence of a C-terminal reticulon-homology domain (RHD), are largely regarded as membrane-bound proteins shaping the tubular networks of the ER (Voeltz *et al.*, 2006). However, RTNs can also be found along the secretory compartments and on the cell surface in lipid rafts at lower levels (Oertle and Schwab, 2003, Dodd *et al.*, 2005). One other characteristic of RTNs is that they include a di-lysine ER retention/retrieval signal at the N-terminus and lack an N-terminal signal sequence. The most recognized reticulon is Nogo/RTN-4A. Nogo-A inhibits neuronal outgrowth and restricts the plasticity of the central nervous system (Chen *et al.*, 2000; GrandPre *et al.*, 2000). Nogo-A, -B, and -C are generated from the Nogo/RTN-4 gene and share a highly conserved C-terminal domain. The most predominant proteins that interact with Nogo-A are Nogo-B and Nogo-C (Dodd *et al.*, 2005). Nogo-B (55kDa), a splice variant of Nogo-A, is ubiquitously expressed in many tissues. It has been suggested to function in vascular remodeling (Acevedo *et al.*, 2004) and in apoptosis (Li *et al.*, 2001). Nogo-B which is enriched in caveolae and/or lipid rafts was discovered as an inhibitor of vascular remodeling (Acevedo *et al.*, 2004).

RTN3-A is expressed mainly in neurons of the cerebral cortex, hippocampus, hypothalamus, and cerebellum of the adult mouse brain (Cai *et al.*, 2005). It shares some significant similarity with RTN4-A in exon structure, tissue distribution, and brain expression profile (Cai *et al.*, 2005). It is localized not only in the ER

compartment but also in the Golgi (He *et al.*, 2004; Wakana *et al.*, 2005), axons, dendrites and growth cone (Hu *et al.*, 2007). This intracellular localization of RTN3 in the ER and the Golgi would be in line with the finding that ^{Ntm}PrP is solely localized intracellular in undefined vesicles near the nucleus (see Fig. 13).

A recent study showed that RTN3 plays a role in Alzheimer´s disease (AD) (Murayama *et al.*, 2006; He *et al.*, 2004). AD is the most common neurodegenerative dementia, characterized pathophysiologically by senile plaques, neuofibrillary tangles and neuronal loss. Recent studies suggest that cerebral accumulation of amyloid ß-protein (Aß), the main constituent of senile plaques, plays an initiating role in the molecular pathology of AD (Selkoe, 2002). Aß is generated through serial cleavage of its precursor, the amyloid precursor protein (APP). Cleavage of APP by ß-secretase (ß-site APP cleaving enzyme 1, BACE1) generates Aß40 and Aß42. Recent studies suggested that RTN3 and RTN4B can modulate the activity of BACE1 and affect secretion of amyloid-ß peptide, i.e. the interaction of the RTNs with BACE1 inhibit the processing of APP to Aß peptides (He *et al.*, 2007). An alternative role of RTN3 in AD pathogenesis could be that large amounts of Aß aggregates promote the formation of RTN3 immunoreactive dystrophic neurites (RIDNs) (Hu *et al.*, 2007). RIDNs are accumulations of RTN3 in a distinct population of dystrophic neurites. The occurrence of RIDNs is concomitant with the formation of high-molecular-weight RTN3 aggregates in brains of AD cases. This could mean that aggregation of RTN3 contributes to Alzheimer´s disease pathogenesis by inducing neuritic dystrophy (Hu *et al.*, 2007).

A co-immunoprecipitation experiment of RTN3a with ^{Ntm}PrP as a validation of the initially obtained results from the mass spectrometry (MS) analysis identified RTN3a as a specific ligand for ^{Ntm}PrP (see Fig. 19). In the following paragraph the putative role of ^{Ntm}PrP in conjunction with RTN3 will be discussed.

As described before, it is known that members of the reticulon family often interact with each other (Dodd *et al.*, 2005). It could be shown that in addition to RTN3a also RNT4B/NogoB interacts with ^{Ntm}PrP. RTN3 as well as NogoB are described as specific binding partners of BACE1 (He *et al.*, 2004, Murayama *et al.*, 2006, He *et al.*,

2007). They act as negative modulators of BACE1 and affect therefore the secretion of Aß. Due to the fact that RTN3 and NogoB are specific ligands for both BACE1and ^{Ntm}PrP the association of ^{Ntm}PrP to the BACE1-RTN complex should be examined in future experiments.

A different view on these results includes the aspect that RTN3 and NogoB are also known to be associated with FADD (Fas-associated death domain) which participates as part of a complex with MORT (mediator of receptor-induced toxicity) in the initiation of apoptosis signal transduction (Xiang*, et al.*, 2006). ER bound RTN3 protein recruits FADD to the ER membrane and subsequently initiates caspase-8-cascade, including activation of caspase-8, processing of Bid and release of cytochrom c from mitochondria (Xiang *et al.*, 2006). One function postulated for PrP^C is also a regulatory function in apoptosis. It has been proposed that the physiological function of endogenous cellular prion protein could be the regulation of p53-dependent caspase-3-mediated neuronal cell death (Paitel *et al.*, 2004). The resulting hypothesis would be that ^{Ntm}PrP also play a role in the regulation of apoptosis whereas both a stimulatory or inhibitory effect is conceivable (Saghafi, 2007).

For different reticulons it is known that they are up- or down-regulated during different periods of development. For RTN3 it has been shown that the expression of differentially spliced variants is highly regulated during development (Di Scala*, et al.*, 2005). A number of studies have also examined the expression of PrP^C during postnatal development. It could be shown that the PrP^C protein levels are very low at birth in contrast to the strong and wide expression of mRNA transcripts (McKinley *et al.*, 1988). PrP^C protein expression then increases from the day of birth through adulthood (Sales *et al.*, 2002, Miele *et al.*, 2003; Laffont-Proust *et al.*, 2007). Furthermore, it has been shown that PrP^C is highly regulated in the developing brain and could be stimulated by nerve growth factors (Kretzschmar *et al.*, 1986, Mobley *et al.*, 1988). The induction of PrP mRNA occurs between embryonic day E 8.5 and E9, during the period of transition from anaerobic to aerobic metabolism (Miele*, et al.*, 2003).

Since both, the specific binding partner of ^{Ntm}PrP, RTN3 and total PrP^{C} are highly regulated during development, the expression of ^{Ntm}PrP during embryonic development in mice brain was examined in this thesis. It could be shown that the expression of ^{Ntm}PrP increases continuously during embryonic and postnatal development (see Fig. 11) which fits to the findings which showed that mRNA levels of PrP increase slowly during embryogenesis and even faster from the day of birth through adulthood (Sales *et al.*, 2002; Miele *et al.*, 2003; Laffont-Proust *et al.*, 2007). No distinct point of time during the embryogenesis was detectable where ^{Ntm}PrP was specifically up-regulated in comparison to total PrP.

The analysis of ^{Ntm}PrP expression in undifferentiated and differentiated human fetal cord stem cells showed a decrease of ^{Ntm}PrP expression during differentiation (see Fig. 10). At first view this result is contrary to the hypothesis that the expression of the *Prnp* gene in the nervous system of Prnp-LacZ Tg mice begins only in post-mitotic neural cells after neuronal differentiation (Tremblay *et al.*, 2007). But the hypothesis was derived from investigations of neural progenitors of the mitotically active ventricular zone and these cells are already more differentiated than fetal cord stem cells.

The ^{Ntm}PrP recognizing mAb19B10 could be optimized in the present work through expressing a single chain variable fragment (scFv) as a analytical and therapeutical tool. The advantage of the scFv19B10 in comparison to full length mAB19B10 was that scFv19B10 could be crosslinked to NHS sepharose which solved the problem of unintentional elution of the antibody, (especially the light chain, which has a similar in molecular size as ^{Ntm}PrP) together with PrP. A second advantage was the small size of scFv19B10 which enabled passage through the blood brain barrier (see Fig. 15). In case of scFv19B10, an in vivo induction of signal transduction leading to apoptosis by the binding of the scFv19B10 to ^{Ntm}PrP was not neurotoxic as it had been known for other bivalent anti-PrP antibodies with PrP^{C} (Solforosi*, et al.*, 2004), because no increase of apoptotic cell was detected after scFv19B10 treatment (see Fig. 16).

It has been shown that mAb directed primarily against PrP^{C} prevent *de novo* scrapie infection and abrogate prion infectivity and PrP^{Sc} from chronically scrapie-infected

neuroblastoma cells (Enari *et al.*, 2001; Müller-Schiffmann & Korth, unpublished). The PrP^{Sc} level is thought to be a steady state equilibrium between formation and degradation, so that the protection of PrP^{C} by binding of anti PrP^{C} antibody can interrupt the propagation of PrP^{Sc} (Enari*, et al.*, 2001). Treatment with mAb19B10 or scFv19B10 resulted only in a faint reduction of the PrP^{Sc} amount. Therefore, it can be concluded that 19B10 has not the ability to serve as a therapeutic tool for the clearance of PrP^{Sc} by preventing *de novo* scrapie infection. This is in line with the fact that the majority of (convertible) PrP^{C} is not recognized by 19B10, and that PrP which is recognized by mAb 6H4 is convertible into PrP^{Sc} (Enari*, et al.*, 2001).

The second monoclonal antibody (termed 19C3) which was characterized in this thesis recognized specifically a subpopulation of PrP which overlapped with ^{Ctm}PrP from *in vitro* translation studies (see Fig. 21) (Korth and Lingappa, unpublished data). This mAB had been generated by immunizing a PrP knockout mouse with recombinant mouse PrP and its epitope was mapped to residues comprising β-strand 2 of PrP (Breil and Korth, unpublished data). A structural modeling of PrP (see Fig. 22) explains why this epitope is protected in fully translocated PrP (^{Sec}PrP) but is exposed in ^{Ctm}PrP: In fully translocated PrP, β-strand 2 is inaccessible due to interactions with β-strand 1 and helix 3; when amino acids forming β-strand 1 are lacking due to a transmembrane helical conformation, β-strand 2 becomes exposed. The risk of the use of a conformation specific antibody which recognizes a hidden epitope is, that due to minimal changes of the tertiary structure of the protein by denaturation, the antibody could detect also other conformers which produce false positive results. To guarantee that the conformation of ^{Ctm}PrP is stable during immunoprecipitation experiments, but at the same time the binding of the antibody to its epitope is ensured, the buffer conditions for IP were optimized (see Fig. 23).

With the help of mAB 19C3 it could be shown that ^{Ctm}PrP exists in small amounts in wild type FVB mice (see Fig. 24), which hints that ^{CTM}PrP has a physiological role, eventually in mediating cell death (Saghafi, 2007). Additionally this antibody enabled the differentiation between the C-terminal fragment of PrP ("C1") and ^{Ctm}PrP (see Fig. 26). These are normally difficult to distinguish, because both are cold PK-resistant,

which so far was the only biochemical property for the distinction of ^{Ctm}PrP from the other PrP conformers.

^{Ctm}PrP was shown to be localized in KHII overexpressing cells in immunoreactive clusters (see Fig. 27). These clusters could possibly correspond with ER vesicles or Golgi cisternae which would be consistent with one published finding that ^{Ctm}PrP was in the endoplasmic reticulum and in cerebellar granule neurons from Tg(L9R–3AV) in the Golgi apparatus (Stewart*, et al.*, 2001; Stewart and Harris, 2005). L9R–3AV is a mutant of PrP in the N-terminal signal peptide (L9R) and the transmembrane domain (3AV) of PrP, which results in an exclusive synthesis of the ^{Ctm}PrP in transfected cell lines and about 50% ^{Ctm}PrP (with the rest of the PrP population consisting of ^{Sec}PrP) in cerebellar granule neurons of Tg(L9R–3AV) mice (Stewart *et al.*, 2001; Stewart and Harris, 2005). In L9R–3AV PrP transfected cell lines it could be shown that ^{Ctm}PrP is retained in the ER and subject to proteasomal degradation after retro-translocation into the cytosol. (Stewart *et al.*, 2001). This suggests that ^{Ctm}PrP may damage neurons by activating stress-induced signaling pathways that are triggered by the accumulation of misfolded proteins in the ER (Stewart *et al.*, 2001). One example for a stress-induced signaling pathway would be the induction of the transcription factor CHOP/GADD153 and phosphorylation of the translation initiation factor eIF-2 which can kill cells by apoptotoc mechanism (Chapman et al., 1998; Kaufman, 1999). The localization of ^{Ctm}PrP in the Golgi apparatus of cerebellar granule neurons in culture raises the possibility that the toxic effects of ^{Ctm}PrP in vivo may also involve this cell type (Stewart and Harris, 2005). Although apoptotic pathways are known to be triggered in the ER as a result of protein misfolding, the role of the Golgi in programmed cell death is less clear. The Golgi apparatus undergoes a dramatic disassembly process during apoptosis (Maag *et al.*, 2003; Machamer, 2003). In addition, there are several caspase substrates, at least one procaspase and a caspase inhibitor that reside in this organelle. Thus, it is possible that ^{Ctm}PrP in the Golgi directly initiates apoptotic signals or amplifies signals that originate elsewhere in the cell.

^{Ctm}PrP has been proposed to be a neurotoxic intermediate underlying prion-induced pathogenesis (Hegde *et al.*, 1998; Hegde *et al.*, 1999; Saghafi, 2007). Originally it

was assumed that PrP^{Sc} is the primary cause of neurodegeneration, based on the spatial and temporal correlation between the accumulation of this isoform and the degree of neuronal damage during the course of prion diseases (DeArmond, 1999). However, recent studies proposed that ^{Ctm}PrP was a key intermediate in infectious and inherited forms of prion disease. Several pieces of evidence have implicated ^{Ctm}PrP in the pathogenesis of prion diseases (Hegde *et al.*, 1998; Hegde *et al.*, 1999; Saghafi, 2007). First, transgenic mice were created that express PrP carrying mutations in or near the transmembrane domain that favor formation of ^{Ctm}PrP (Hegde *et al.*, 1998; Hegde *et al.*, 1999). Mice that produced ^{Ctm}PrP above a threshold level developed a spontaneous neurological disease without detectable prions / PrP^{Sc}. In addition, when these mice were inoculated with scrapie prions, the amount of accumulating PrP^{Sc} was inversely related to the amount of ^{Ctm}PrP present, indicating that ^{Ctm}PrP rather than PrP^{Sc} was the proximate cause of neurodegeneration (Hegde *et al.*, 1999) . After scrapie inoculation of mice carrying a wildtype hamster PrP transgene that served as a reporter of ^{Ctm}PrP formation (hamster PrP can form ^{Ctm}PrP but not convert to PrP^{Sc}), ^{Ctm}PrP was found to accumulate during the course of the infection (Hegde *et al.*, 1999). Consistent with these findings was that in a human neurodegenerative disease caused by the A117V mutation [alanine (A) to valine (V) substitution at position 117] ^{Ctm}PrP generation in the ER was increased (Hegde *et al.*, 1998) without any relevant levels of PrP^{Sc}; brains of patients with the A117V mutation do not contain conventional PrP27–30 (the protease-resistant core of PrP^{Sc}) (Tateishi *et al.*, 1990). Taken together, these data imply that ^{Ctm}PrP is a component of a common pathway of neurodegeneration underlying both infectious and genetic forms of prion diseases, and that PrP^{Sc} is pathogenic because it enhances the formation of ^{Ctm}PrP (Hegde *et al.*, 1999) .

Recent findings suggest that neurodegeneration which is induced by the overexpression of ^{Ctm}PrP (Hegde *et al.*, 1998) causes by apoptosis (Saghafi, 2007). The hypothesis that ^{Ctm}PrP triggers apoptosis could be confirmed in this thesis by a co-staining of ^{Ctm}PrP overexpressing N2a cells with the ^{Ctm}PrP specific antibody 19C3 and a TUNEL staining (see Fig. 28). DNA fragmentation was observed in cells with a strong overexpression of ^{Ctm}PrP stained by mAb19C3.

The finding that ^{Ctm}PrP was precipitated in the presence of the detergent CTAB, which is known to precipitate nucleic acids led to the hypothesis that ^{Ctm}PrP could be associated to nucleic acids. This hypothesis is supported by the fact that the N-terminus of ^{Ctm}PrP is exposed to the cytosol. The main nucleic-acid binding sites of PrP are identified as two lysine clusters at the N-terminus of PrP (Mercey *et al.*, 2006) and also RNA binding and chaperoning properties of PrP were mapped to the N-terminal region of PrP (Gabus *et al.*, 2001). First experiments seemed to confirm this hypothesis (see Fig. 29), but the identification of a specific associated nucleic acid is still outstanding. It could be speculated that associated nucleic acids could be small modulatory dsRNAs (smRNAs) which possibly regulate the activity of ^{Ctm}PrP. smRNAs are currently discussed as an important subgroup of non coding RNAs as key regulators of cell behavior at both transcriptional and posttranscriptional levels (Kuwabara *et al.*, 2004).

4.2 Clearance of PrP^{Sc}

Previous studies had shown that tocopherols had anti-prion effects in ScN2a cells (Klingenstein & Korth, unpublished). It was found that the highly soluble tocopherol derivative α-tocopherol succinate revealed the highest antiprion potency. After treatment of ScN2a cells with α-tocopherol succinate, dose-dependent morphology changes were observed, however, it was unclear how α-tocopherol succinate effected the clearance of PrP^{Sc}. At least two ways of PrP^{Sc} reduction are known, first the reduction of PrP^{Sc} via interference of *de novo* formation of prions and second the degradation of pre-existing PrP^{Sc} via the lysosomal system (or a combination of both). The changes in morphology of ScN2a cells treated with α-tocopherol succinate indicated the induction of a signal transduction cascade. Therefore, antagonists of several signal transduction pathways were tested for their ability to antagonize the effect of α-tocopherol succinate on ScN2a cells. Rapamycin was identified as the only antagonizing component.

Rapamycin is the specific inhibitor of the serine-threonine protein kinase mTOR. The finding that rapamycin antagonized the effect of α-tocopherol succinate suggested that α-tocopherol succinate might activate the mTOR pathway resulting in a decreased amount of PrP^{Sc}. mTOR is known to regulate diverse cellular processes in response to environmental cues. Amongst others, autophagy is one process which is negatively regulated by mTOR. Autophagy is a catabolic process executing the degradation of a cell's own components like organelles or long-lived proteins through the lysosomal machinery. For PrP, it is known that at least part of the degradation takes place in the lysosomal system and that it plays a role in the deposition of PrP^{Sc}. As shown in ScN2a cells, although most PrP^{C} molecules turn over with a $t_{1/2}$ of ~6 h by a two-step degradation pathway (Caughey *et al.*, 1989; Taraboulos *et al.*, 1992), a small minority of PrP^{C} molecules (~ 5 %) escape degradation and acquire a protease-resistent core becoming become PrP^{Sc} (shown in ScN2a cells) (Borchelt *et al.*, 1990; Taraboulos *et al.*, 1990a; Borchelt *et al.*, 1992). Whether PrP^{Sc} is formed on the plasma membrane or during internalization of PrP^{C} is unknown (Caughey and Raymond, 1991 Caughey*, et al.*, 1991, Borchelt*, et al.*, 1992). PrP^{Sc} is further N-terminally trimmed in an acidic compartment (Caughey *et al.*, 1991; Taraboulos *et al.*, 1992) and accumulates primarily in secondary lysosomes (Taraboulos *et al.*, 1990b; McKinley *et al.*, 1991; Taraboulos *et al.*, 1992). These findings are in line with the findings that in scrapie-infected brain, lysosomes and lysosome-related structures are present in abnormally high numbers in neuronal cell processes and that these structures contain PrP (Laszlo *et al.*, 1992).

Due to these connections between PrP and the lysosomal degradation pathway, the hypothesis arose that α-tocopherol succinate could have an influence on the rate of autophagy via mTOR. The inhibition of autophagy via silencing of the two autophagy related proteins Atg7 and LC3 in cells did not alter the amount of PrP^{Sc} (see Fig. 39). Therefore, although additional and more detailed experiments have to be performed on that matter it is presently unlikely that the clearance of PrP^{Sc} induced by α-tocopherol succinate is caused by a decrease in autophagy.

To investigate whether the signal elicited by α-tocopherol succinate had an effect on the phosphorylation status of mTOR or the downstream p70 S6 kinase,

phosphorylation studies of α-tocopherol succinate and rapamycin treated ScN2a cells were performed. Western blot analysis (see Fig. 34A) suggested that α-tocopherol succinate has no influence on the phosphorylation status of mTOR or p70 S6 kinase, because no significant alteration of the phosphorylation rate was observed although sometimes a trend towards an increase in mTOR or S6 kinase phosphorylation was observed. By contrast, rapamycin induced a dephosphorylation of p70 S6 kinase at Thr 421 at a period of time from 2 h to 24 h after application and a dephosphorylation of mTOR at Ser 2481 3 h to 24 h after application irrespective of simultaneous treatment with α-tocopherol succinate.

Different pathways are conceivable of how α-tocopherol succinate executes its antiprion activity either upstream or downstream of mTOR. One model of activation of the mTOR pathway by α-tocopherol succinate was put forward in view to the fact that tocopherol succinate uptake is promoted by the tocopherol-associated protein (TAP) (Ni *et al.*, 2005). This protein is known to regulate PI 3-kinase/Akt signaling (Ni *et al.*, 2005) in connection with its function as a tumor suppressor. The binding of tocopherol succinate to its binding protein TAP could possibly lead to an activation of mTOR via TAP. The PI3 kinase/Akt signal pathway is also known to play a role in PrP^C signaling. Over the past years, evidence has been accumulating consistent with PrP^C triggering signal transduction pathways (Hetz *et al.*, 2003). This is not surprisin, as PrP^C is targeted to cholesterol-rich microdomains of the plasma membrane, regions that are abundant in receptors and signaling molecules (Walmsley *et al.*, 2003). Recently a link between PrP^C expression and phosphatidylinositol 3-kinase (PI 3-kinase) activation has been identified (Vassallo *et al.*, 2005). This is in agreement with the finding that PrP acts as a trans-interacting partner for neurons and elicits neurite outgrowth and neuronal survival via different transduction pathway including PI3 kinase/Akt signal, the nonreceptor Src-related family member $p59^{fyn}$, cAMP-dependent protein kinase A, and MAP kinase (Chen *et al.*, 2003). The overexpression of PrP at the cell surface increases neuronal survival (Chen *et al.*, 2003), which in turn involves the activation of the PI 3-kinase/Akt pathway.

The question arose if α-tocopherol succinate activates mTOR via the PI 3-kinase/Akt pathway similar to PrP^C (see Fig. 41). However, own experiments with wortmannin,

the specific inhibitor of PI 3-kinase (Wymann *et al.*, 1996), showed that α-tocopherol succinate did not regulate the PI 3-kinase, because Wortmannin was not able to antogonize the antiprion effect of α-tocopherol succinate (Klingenstein & Korth, unpublished data). Thus, it is presently not clear where α-tocopherol succinate acts, it could be upstream or downstream of mTOR (see Fig. 41). Notwithstanding, there might be signaling via a PrP^{C} / PI 3-kinase pathway but eventually executing a function that is not directly related to PrP^{Sc} conversion or clearance. In this thesis, it was shown that α-tocopherol succinate activates the mTOR pathway and increases the amount of PrP^{C} in the absence of PrP^{Sc} (see Fig. 32); this could be the result of an increased PrP^{C} synthesis triggered by the add up signal of PrP^{C} and α-tocopherol succinate over the mTOR pathway and triggered transcriptional events. These mechanisms have to be further elucidated.

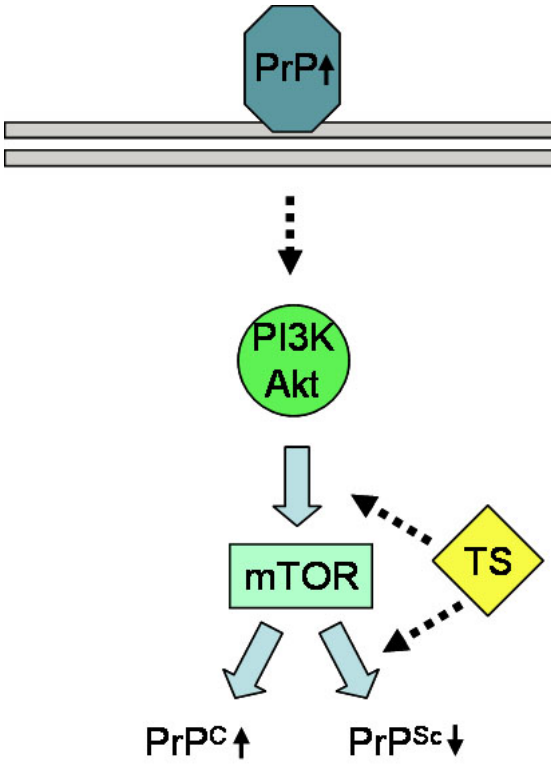

Fig. 41 Cartoon of the hypothesized position of α-tocopherol succinate in the mTOR signal transduction pathway. Tocopherol succinate (TS) regulates the pathway downstream of the PI 3-kinase/Akt (PI3K Akt) pathway and upstream or downstream of mTOR. PrP^{C} acts as a sensor and transmit signals via the PI 3-kinase/Akt pathway which may be independent of α-tocopherol succinate's effects on PrP conversion or clearance.

To investigate if the anti-prion effect of α-tocopherol succinate was caused by an increased clearance of PrP^{Sc} or a decreased conversion of PrP^{C} to PrP^{Sc}, rheb and the mutant rhebS20N together with MHM2 PrP were expressed in ScN2a cells. It is known that the binding of the small GTPase rheb to mTOR rescues mTOR from inactivation (Long *et al.*, 2005). Conversly, the dominant negative rheb mutant S20N, which also binds to mTOR, causes an inhibition of mTOR due to its lack of kinase activity (Long *et al.*, 2005). Therefore overexpression of the rheb mutant S20N should have a comparable effect on mTOR activity as the treatment with rapamycin. The pharmacological approach via rapamycin treatment as well as the genetic approach via overexpression of rhebS20N resulted in an inhibition of mTOR. This demonstrated that the activation state of mTOR influences the net PrP^{Sc} level. The finding that overexpression of the rheb mutant S20N increased PrP^{Sc} (see Fig. 35) suggested that inhibition of mTOR increased the conversion of PrP^{C} to PrP^{Sc}. This effect was dominant over the antiprion effect of α-tocopherol succinate (shown in Fig. 36). These results are consistent with the finding that rapamycin's effects, the pharmacological analogue of rheb S20N, were also dominant over the antiprion effect of α-tocopherol succinate.

Inhibition of mTOR, resulting from the overexpression of mutant rhebS20N, seemed to have no influence on the amount of PrP^{C} in murine or human neuroblastoma cells (see Fig. 38). This finding is based on only one experiment and has to be validated further. But if this result could be confirmed, it would be a further hint that α-tocopherol succinate leads to an increase of the amount of PrP^{C} by triggering PrP^{C} synthesis via mTOR, as the inhibition of mTOR does not alter the amount of PrP^{C}. If α-tocopherol succinate would cause a decelerated turn over of PrP^{C} by protein stabilization, the amount should decrease due to the inhibition of mTOR via rhebS20N.

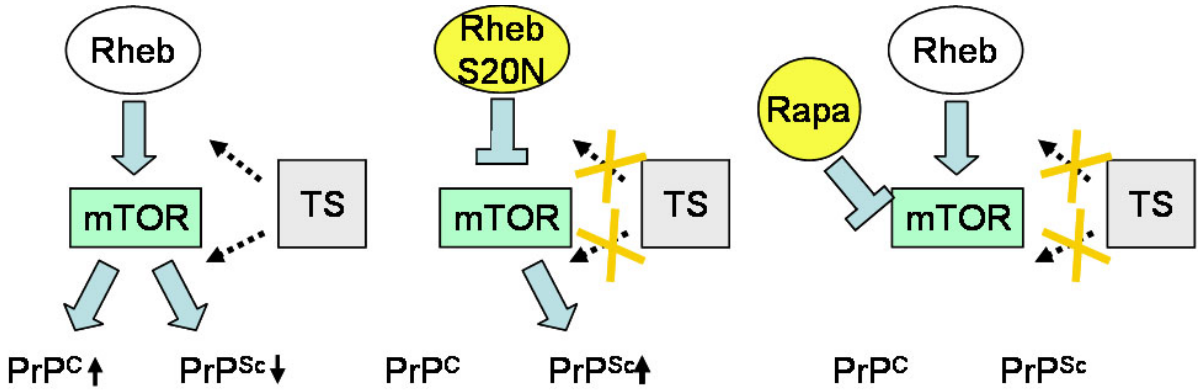

Fig. 42 Cartoon of the connections between the alterations in the amounts (black arrows) of PrP^{C}/PrP^{Sc} and the activation or inactivation of mTOR as a result of induction via α-tocopherol succinate or inhibition via rapamycin (Rapa), respectively, or the dominate negative rheb mutant S20N (rheb S20N).

In summary, the antiprion effect of α-tocopherol succinate can be antagonized both by pharmacological inhibition and genetic inhibition of mTOR (via rapamycin or the dominant negative rheb mutant S20N). Nevertheless, there seems to be a difference between the two ways of mTOR inhibition, because the overexpression of rhebS20N causes an increase in the amount of PrP^{Sc} which is not detectable with rapamycin treatment. Remarkably, even α-tocopherol succinate could increase PrP^{C} expression in some cell lines even though it negatively regulated PrP^{Sc}. This could be based on the fact that rheb and rapamycin form complexes with different interaction partners.

In conclusion this work provides important insights into the cellular clearance of PrP^{Sc} as well as the characterization and definite proof for PrP bioconformers *in vivo.*

5 Abstract

The prion protein, PrP, is unique since it can exist in several stable conformations ("conformers"). One of these conformers, PrP^{Sc}, is associated with prion disease, transmissible neurodegenerative diseases of humans and animals. This form has the exceptional ability to convert normal host PrP^{C} into the pathogenic PrP^{Sc} conformation. The function of normal PrP is still unknown and controversial functions of PrP (toxic and protective) have been proposed. These results could be explained by the fact that PrP^{C} itself can also adopt several stable conformations, i.e. secretory GPI-anchored ^{sec}PrP and the two transmembrane isoforms ^{Ntm}PrP (N-trans transmembrane) and ^{Ctm}PrP (C-trans transmembrane).

In this thesis, proof for the heterogeneity of PrP^{C} *in vivo* was demonstrated by utilizing two conformation specific monoclonal antibodies 19B10 (^{Ntm}PrP specific) and 19C3 (^{Ctm}PrP specific) for conformer characterization. Furthermore, I showed that the ability of the antibody 19C3 to detect the cold protease resistant fragment of ^{Ctm}PrP, but not of the C1 fragment of PrP^{C}, enables the clear distinction between both forms. ^{Ctm}PrP, previously assumed only to mediate neurotoxic signaling was surprisingly detected in small amounts also in the brain of wild typ mice suggesting a physiological function.

^{Ntm}PrP was demonstrated to be differentiation-dependend down and age-dependend upregulated and localized intracellularly. In addition, two members of the reticulon family (RTN3a and RTN4b) known to play a role in neurite outgrowth, vesicle trafficking and the pathogenesis of Alzheimer´s disease were identified as specific interaction partners for ^{Ntm}PrP.

When investigating the cellular mechanisms regulating differential conformer expression, the mTOR pathway was identified to be critical for PrP^{Sc} presence. It was shown that α-tocopherol succinate reduced the amount of PrP^{Sc} via the mTOR mediated pathway since rapamycin the specific inhibitor of the kinase mTOR antagonised the effect of α-tocopherol succinate. A similar antagonizing effect on α-tocopherol succinate was observed by overexpression of a dominant negative mutant of the mTOR activating GTPase rheb (rhebS20N). The combined overexpression of rhebS20N together with an epitope tagged PrP showed that the mTOR dependent pathway influences the conversion of PrP^{c} into PrP^{Sc}.

In conclusion, by using novel mABs to PrP conformers, these could be demonstrated to perform different cellular functions with ^{Ctm}PrP being associated with cell death and ^{Ntm}PrP being associated with neuronal differentiation. The mTOR signal pathway was shown to critically regulate the presence of PrP^{Sc} and defined as a pharmacological target of the tocopherols.

6 Zusammenfassung

Das Prion Protein, PrP^{C}, ist einzigartig, da es in verschiedenen stabilen Konformationen vorkommt. Eines dieser Konformere, das PrP^{Sc} ist mit transmissiblen neurodegenerativen Erkrankungen, den Prionen-Erkrankungen von Mensch und Tier assoziiert. Diese Form hat die außergewöhnliche Eigenschaft normales Wirts PrP^{C} in die pathogene Konformation PrP^{Sc} zu konvertieren. Die Funktion des normalen Prion Proteins (PrP^{C}) ist bislang unbekannt, da sehr gegensätzliche Funktionen postuliert wurden (toxisch und protektiv). Dies lässt sich durch die Tatsache erklären, dass PrP^{C} in drei verschiedenen stabilen topologischen Formen vorkommt. Dem ^{sec}PrP (sekretorischen PrP), das über einen GPI Anker mit der Plasmamemban verbunden ist, und den zwei Transmembranformen, dem ^{Ctm}PrP (transmembranen PrP mit lumenalem C-Terminus), und dem ^{Ntm}PrP (transmembranen PrP mit lumenalem N-Terminus), die unterschiedliche Funktionen besitzen.

In dieser Arbeit konnte mit Hilfe der konformationsspezifischen Antikörper 19B10 (^{Ntm}PrP spezifisch) und 19C3 (^{Ctm}PrP spezifisch) erstmalig die Heterogenität von PrP^{C} in vivo gezeigt werden. Zudem konnte gezeigt werden, dass der Antikörper 19C3 das aus dem kalten Proteaseverdau resultierende resistente Fragment von ^{Ctm}PrP, aber nicht das des C1 Fragments von PrP^{C} bindet. Dies ermöglicht es uns erstmals, die beiden Formen eindeutig voneinander zu unterscheiden. ^{Ctm}PrP, für das zuvor gezeigt werden konnte, dass es Neurotoxizität vermittelt, konnte überraschenderweise in kleinen Mengen im Gehirn von Wildtyp Mäusen detektiert werden, was eine physiologische Funktion nahe legt.

Für ^{Ntm}PrP konnte gezeigt werden, dass es differenzierungsabhängig herunterreguliert und altersabhängig hochreguliert wird, und es ausschließlich intrazellulär lokalisiert ist. Des weiteren konnten die beiden Mitglieder der Retikulon Familie RTN3a und RTN4B von denen bekannt ist, dass sie eine Rolle beim Neuritenwachstum, dem Vesikeltransport und der Pathogenese der Alzheimer Erkrankung spielen, als spezifische Interaktionspartner von ^{Ntm}PrP identifiziert werden.

Bei der Untersuchung zellulärer Mechanismen, welche die Expression verschiedener Konformere regulieren, wurde der mTOR Signalweg als entscheidend für das Vorhandensein von PrP^{Sc} identifiziert. Es konnte gezeigt werden, dass α-Tocopherol Succinat über den mTOR vermittelten Signalweg die Menge von PrP^{Sc} beeinflusst, da Rapamycin, der spezifische Inhibitor der Kinase mTOR, die Wirkung von α-Tocopherol Succinat antagonisierte. Der gleiche antagonisierende Effekt auf α-Tocopherol Succinat konnte durch die Überexpression des genetischen Analogons von Rapamycin, der dominant negativen Mutante von Rheb, einer mTOR regulierenden GTPase, erzielt werden. Die kombinierte Überexpression der dominant negativen Mutante von Rheb mit Epitop markierten PrP konnte zudem zeigen, dass der mTOR abhängige Signalweg einen Einfluss auf die Konversion von PrP^{c} zu PrP^{Sc} hat.

Zusammenfassend konnte mit Hilfe neuartiger, monoklonaler Mausantikörper gegen verschiedene PrP Konformere gezeigt werden, dass diese verschiedene, zelluläre Funktionen erfüllen, wobei ^{Ctm}PrP mit Zelltod und ^{Ntm}PrP mit neuronaler Differenzierung assoziiert ist. Darüber hinaus wurde gezeigt, dass der mTOR Signalweg bedeutend in der Regulierung des PrP^{Sc} Vorkommens ist und als pharmakologisches Ziel der Tocopherole definiert werden konnte.

7 References

Acevedo, L., Yu, J., Erdjument-Bromage, H., Miao, R. Q., Kim, J. E., Fulton, D., Tempst, P., Strittmatter, S. M. and Sessa, W. C. 2004. Nat Med. 10 (4): 382-388

Amiel, S. A. 1976. Br J Exp Pathol. 57 (6): 653-662

Bai, X., Ma, D., Liu, A., Shen, X., Wang, Q. J., Liu, Y. and Jiang, Y. 2007. Science. 318 (5852): 977-980

Borchelt, D. R., Scott, M., Taraboulos, A., Stahl, N. and Prusiner, S. B. 1990.J Cell Biol. 110 (3): 743-752

Borchelt, D. R., Taraboulos, A. and Prusiner, S. B. 1992. J Biol Chem. 267 (23): 16188-16199

Brandner, S., Isenmann, S., Raeber, A., Fischer, M., Sailer, A., Kobayashi, Y., Marino, S., Weissmann, C. and Aguzzi, A. 1996. Nature. 379 (6563): 339-343

Brown, D. R., Qin, K., Herms, J. W., Madlung, A., Manson, J., Strome, R., Fraser, P. E., Kruck, T., von Bohlen, A., Schulz-Schaeffer, W., Giese, A., Westaway, D. and Kretzschmar, H. 1997. 390 (6661): 684-687

Bruckener, K. E., el Baya, A., Galla, H. J. and Schmidt, M. A. 2003. J Cell Sci. 116 (Pt 9): 1837-1846

Bueler, H., Fischer, M., Lang, Y., Bluethmann, H., Lipp, H. P., DeArmond, S. J., Prusiner, S. B., Aguet, M. and Weissmann, C. 1992. Nature. 356 (6370): 577-582

Cai, Y., Saiyin, H., Lin, Q., Zhang, P., Tang, L., Pan, X. and Yu, L. 2005. Molecular Brain Research. 138 (2): 236-243

Caughey, B., Race, R. E., Ernst, D., Buchmeier, M. J. and Chesebro, B. 1989. J Virol. 63 (1): 175-181

Caughey, B. and Raymond, G. J. 1991. J Biol Chem. 266 (27): 18217-18223

Caughey, B., Raymond, G. J., Ernst, D. and Race, R. E. 1991. J Virol. 65 (12): 6597-6603

Chapman, R., Sidrauski, C. and Walter, P. 1998. Annu Rev Cell Dev Biol. 14 459-485

Chen, M. S., Huber, A. B., van der Haar, M. E., Frank, M., Schnell, L., Spillmann, A. A., Christ, F. and Schwab, M. E. 2000. 403 (6768): 434-439

Chen, S., Mangé, A., Dong, L., Lehmann, S. and Schachner, M. 2003. Molecular and Cellular Neuroscience. 22 (2): 227-233

Come, J., Fraser, P. and Lansbury, P., Jr. 1993. Proceedings of the National Academy of Sciences. 90 (13): 5959-5963

DeArmond, S. a. I., JW. 1999. Prion Biology and Diseases. Cold Spring Harbor Laboratory, NY

De Fea, K. A., Nakahara, D. H., Calayag, M. C., Yost, C. S., Mirels, L. F., Prusiner, S. B. and Lingappa, V. R. 1994. J Biol Chem. 269 (24): 16810-16820

Di Scala, F., Dupuis, L., Gaiddon, C., De Tapia, M., Jokic, N., Gonzalez de Aguilar, J. L., Raul, J. S., Ludes, B. and Loeffler, J. P. 2005. Biochem J. 385 (Pt 1): 125-134

Dodd, D. A., Niederoest, B., Bloechlinger, S., Dupuis, L., Loeffler, J.-P. and Schwab, M. E. 2005. J. Biol. Chem. 280 (13): 12494-12502

Dick, T. P., Nussbaum, A. K., Deeg, M., Heinemeyer, W., Groll, M., Schirle, M., Keilholz, W., Stevanovic, S., Wolf, D. H., Huber, R., Rammensee, H. G. and Schild, H. 1998. J Biol Chem. 273 (40): 25637-25646

Donofrio, G., Heppner, F. L., Polymenidou, M., Musahl, C. and Aguzzi, A. 2005. J Virol. 79 (13): 8330-8338

Ellis, R. J. and Hartl, F. U. 1996. Faseb J. 10 (1): 20-26

Enari, M., Flechsig, E. and Weissmann, C. 2001. Proc Natl Acad Sci U S A. 98 (16): 9295-9299

Ertmer, A., Gilch, S., Yun, S.-W., Flechsig, E., Klebl, B., Stein-Gerlach, M., Klein, M. A. and Schatzl, H. M. 2004. J. Biol. Chem. 279 (40): 41918-41927

Eskelinen, E. L. 2005. Autophagy. 1 (1): 1-10

Gabus, C., Derrington, E., Leblanc, P., Chnaiderman, J., Dormont, D., Swietnicki, W., Morillas, M., Surewicz, W. K., Marc, D., Nandi, P. and Darlix, J. L. 2001. J Biol Chem. 276 (22): 19301-19309

Gilch, S., Wopfner, F., Renner-Muller, I., Kremmer, E., Bauer, C., Wolf, E., Brem, G., Groschup, M. H. and Schatzl, H. M. 2003. J. Biol. Chem. 278 (20): 18524-18531

GrandPre, T., Nakamura, F., Vartanian, T. and Strittmatter, S. M. 2000. 403 (6768): 439-444

Graner, E., Mercadante, A. F., Zanata, S. M., Forlenza, O. V., Cabral, A. L., Veiga, S. S., Juliano, M. A., Roesler, R., Walz, R., Minetti, A., Izquierdo, I., Martins, V. R. and Brentani, R. R. 2000. Brain Res Mol Brain Res. 76 (1): 85-92

Hara, K., Maruki, Y., Long, X., Yoshino, K., Oshiro, N., Hidayat, S., Tokunaga, C., Avruch, J. and Yonezawa, K. 2002. Cell. 110 (2): 177-189

Hay, B., Barry, R. A., Lieberburg, I., Prusiner, S. B. and Lingappa, V. R. 1987a. Mol Cell Biol. 7 (2): 914-920

Hay, B., Prusiner, S. B. and Lingappa, V. R. 1987b. Biochemistry. 26 (25): 8110-8115

Head, M. W. and Ironside, J. W. 2000. Trends in Microbiology. 8 (1): 6-8

He, W., Lu, Y., Qahwash, I., Hu, X. Y., Chang, A. and Yan, R. 2004. Nat Med. 10 (9): 959-965

He, W., Shi, Q., Hu, X. and Yan, R. 2007. J. Biol. Chem. M704181200

Hegde, R. S., Mastrianni, J. A., Scott, M. R., DeFea, K. A., Tremblay, P., Torchia, M., DeArmond, S. J., Prusiner, S. B. and Lingappa, V. R. 1998. Science. 279 (5352): 827-834

Hegde, R. S., Tremblay, P., Groth, D., DeArmond, S. J., Prusiner, S. B. and Lingappa, V. R. 1999. 402 (6763): 822-826

Heppner, F. L., Musahl, C., Arrighi, I., Klein, M. A., Rulicke, T., Oesch, B., Zinkernagel, R. M., Kalinke, U. and Aguzzi, A. 2001. Science. 294 (5540): 178-182

Hetz, C., Maundrell, K. and Soto, C. 2003. Trends Mol Med. 9 (6): 237-243

Hershko, A. and Ciechanover, A. 1998. Annu Rev Biochem. 67 425-479

Holz, M. K. and Blenis, J. 2005. J Biol Chem. 280 (28): 26089-26093

Hough, R., Pratt, G. and Rechsteiner, M. 1986. J Biol Chem. 261 (5): 2400-2408

Hu, X., Shi, Q., Zhou, X., He, W., Yi, H., Yin, X., Gearing, M., Levey, A. and Yan, R. 2007. Embo J. 26 (11): 2755-2767

Jacinto, E., Loewith, R., Schmidt, A., Lin, S., Ruegg, M. A., Hall, A. and Hall, M. N. 2004. Nat Cell Biol. 6 (11): 1122-1128

Kabeya, Y., Mizushima, N., Ueno, T., Yamamoto, A., Kirisako, T., Noda, T., Kominami, E., Ohsumi, Y. and Yoshimori, T. 2000. Embo J. 19 (21): 5720-5728

Kaufman, R. J. 1999. Genes Dev. 13 (10): 1211-1233

Kim, B. H., Lee, H. G., Choi, J. K., Kim, J. I., Choi, E. K., Carp, R. I. and Kim, Y. S. 2004. Brain Res Mol Brain Res. 124 (1): 40-50

Klionsky, D. J. 2007. Nat Rev Mol Cell Biol. 8 (11): 931-937

Komatsu, M., Waguri, S., Chiba, T., Murata, S., Iwata, J.-i., Tanida, I., Ueno, T., Koike, M., Uchiyama, Y., Kominami, E. and Tanaka, K. 2006. 441 (7095): 880-884

Krebs, B., Dorner-Ciossek, C., Schmalzbauer, R., Vassallo, N., Herms, J. and Kretzschmar, H. A. 2006. Biochem Biophys Res Commun. 340 (1): 13-22

Krebs, B., Wiebelitz, A., Balitzki-Korte, B., Vassallo, N., Paluch, S., Mitteregger, G., Onodera, T., Kretzschmar, H. A. and Herms, J. 2007. J Neurochem. 100 (2): 358-367

Kretzschmar, H. A., Prusiner, S. B., Stowring, L. E. and DeArmond, S. J. 1986. Am J Pathol. 122 (1): 1-5

Kretzschmar, H. A., Ironside, J. W., DeArmond, S. J. and Tateishi, J. 1996. Arch Neurol. 53 (9): 913-920

Kuwabara, T., Hsieh, J., Nakashima, K., Taira, K. and Gage, F. H. 2004. Cell. 116 (6): 779-793

Laffont-Proust, I., Fonta, C., Renaud, L., Hassig, R. and Moya, K. L. 2007. J Comp Neurol. 504 (6): 646-658

Laszlo, L., Lowe, J., Self, T., Kenward, N., Landon, M., McBride, T., Farquhar, C., McConnell, I., Brown, J., Hope, J. and et al. 1992. J Pathol. 166 (4): 333-341

Lehmann, S. and Harris, D. A. 1995. J Biol Chem. 270 (41): 24589-24597

Li, Q., Qi, B., Oka, K., Shimakage, M., Yoshioka, N., Inoue, H., Hakura, A., Kodama, K., Stanbridge, E. J. and Yutsudo, M. 2001. Oncogene. 20 (30): 3929-3936

Li, Y., Corradetti, M. N., Inoki, K. and Guan, K. L. 2004. Trends Biochem Sci. 29 (1): 32-38

Loewith, R., Jacinto, E., Wullschleger, S., Lorberg, A., Crespo, J. L., Bonenfant, D., Oppliger, W., Jenoe, P. and Hall, M. N. 2002. Mol Cell. 10 (3): 457-468

Long, X., Lin, Y., Ortiz-Vega, S., Yonezawa, K. and Avruch, J. 2005. Curr Biol. 15 (8): 702-713

Lopez, C. D., Yost, C. S., Prusiner, S. B., Myers, R. M. and Lingappa, V. R. 1990. Science. 248 (4952): 226-229

Luzio, J. P., Pryor, P. R. and Bright, N. A. 2007. 8 (8): 622-632

Maag, R. S., Hicks, S. W. and Machamer, C. E. 2003. Curr Opin Cell Biol. 15 (4): 456-461

Machamer, C. E. 2003. Trends Cell Biol. 13 (6): 279-281

Manning, B. D. and Cantley, L. C. 2003. Trends Biochem Sci. 28 (11): 573-576

Martin, D. E. and Hall, M. N. 2005. Curr Opin Cell Biol. 17 (2): 158-166

McKinley, M. P., Bolton, D. C. and Prusiner, S. B. 1983. Cell. 35 (1): 57-62

McKinley, M. P., Lingappa, V. R. and Prusiner, S. B. 1988. Ciba Found Symp. 135 101-116

McKinley, M. P., Taraboulos, A., Kenaga, L., Serban, D., Stieber, A., DeArmond, S. J., Prusiner, S. B. and Gonatas, N. 1991. Lab Invest. 65 (6): 622-630

Mercey, R., Lantier, I., Maurel, M. C., Grosclaude, J., Lantier, F. and Marc, D. 2006. Arch Virol. 151 (11): 2197-2214

Meijer, A. J. and Codogno, P. 2004.Int J Biochem Cell Biol. 36 (12): 2445-24
Mercey, R., Lantier, I., Maurel, M. C., Grosclaude, J., Lantier, F. and Marc, D. 2006. Arch Virol. 151 (11): 2197-2214

Miele, G., Alejo Blanco, A. R., Baybutt, H., Horvat, S., Manson, J. and Clinton, M. 2003. Gene Expr. 11 (1): 1-12

Mobley, W. C., Neve, R. L., Prusiner, S. B. and McKinley, M. P. 1988. Proc Natl Acad Sci U S A. 85 (24): 9811-9815

Mouillet-Richard, S., Ermonval, M., Chebassier, C., Laplanche, J. L., Lehmann, S., Launay, J. M. and Kellermann, O. 2000. Science. 289 (5486): 1925-1928

Murayama, K. S., Kametani, F., Saito, S., Kume, H., Akiyama, H. and Araki, W. 2006. Eur J Neurosci. 24 (5): 1237-1244

Naslavsky, N., Stein, R., Yanai, A., Friedlander, G. and Taraboulos, A. 1997. J. Biol. Chem. 272 (10): 6324-6331

Ni, J., Wen, X., Yao, J., Chang, H.-C., Yin, Y., Zhang, M., Xie, S., Chen, M., Simons, B., Chang, P., di Sant'Agnese, A., Messing, E. M. and Yeh, S. 2005. Cancer Res. 65 (21): 9807-9816

Nixon, R. A., Cataldo, A. M. and Mathews, P. M. 2000. Neurochem Res. 25 (9-10): 1161-1172

Nunziante, M., Gilch, S. and Schatzl, H. M. 2003. Chembiochem. 4 (12): 1268-1284

Oertle, T. and Schwab, M. E. 2003. Trends in Cell Biology. 13 (4): 187-194

Ott, C. M. and Lingappa, V. R. 2004. Biochemistry. 43 (38): 11973-11982

Scott, M. R., Kohler, R., Foster, D. and Prusiner, S. B. 1992. Protein Sci. 1 (8): 986-997

Paitel, E., Alves da Costa, C., Vilette, D., Grassi, J. and Checler, F. 2002. J Neurochem. 83 (5): 1208-1214

Paitel, E., Sunyach, C., Alves da Costa, C., Bourdon, J. C., Vincent, B. and Checler, F. 2004. J Biol Chem. 279 (1): 612-618

Pan, K., Baldwin, M., Nguyen, J., Gasset, M., Serban, A., Groth, D., Mehlhorn, I., Huang, Z., Fletterick, R., Cohen, F. and Prusiner, S. 1993. Proceedings of the National Academy of Sciences. 90 (23): 10962-10966

Peretz, D., Williamson, R. A., Kaneko, K., Vergara, J., Leclerc, E., Schmitt-Ulms, G., Mehlhorn, I. R., Legname, G., Wormald, M. R., Rudd, P. M., Dwek, R. A., Burton, D. R. and Prusiner, S. B. 2001. Nature. 412 (6848): 739-743

Prusiner, S. B. 1989. Annu Rev Microbiol. 43 345-374

Prusiner, S. B. 1998. Brain Pathol. 8 (3): 499-513

Prusiner, S. B., Scott, M. R., DeArmond, S. J. and Cohen, F. E. 1998. Cell. 93 (3): 337-348

Qin, Z.-H., Wang, Y., Kegel, K. B., Kazantsev, A., Apostol, B. L., Thompson, L. M., Yoder, J., Aronin, N. and DiFiglia, M. 2003. Hum. Mol. Genet. 12 (24): 3231-3244

Riesner, D. 2003. Br Med Bull. 66 21-33

Roucou, X., Giannopoulos, P. N., Zhang, Y., Jodoin, J., Goodyer, C. G. and LeBlanc, A. 2005. Cell Death Differ. 12 (7): 783-795

Roucou, X. and LeBlanc, A. C. 2005. J Mol Med. 83 (1): 3-11

Sachse, M., Ramm, G., Strous, G. and Klumperman, J. 2002. Histochem Cell Biol. 117 (2): 91-104

Saghafi, S. 2007 dissertation, University of Cologne

Safar, J., Wille, H., Itri, V., Groth, D., Serban, H., Torchia, M., Cohen, F. E. and Prusiner, S. B. 1998. Nat Med. 4 (10): 1157-1165

Sales, N., Hassig, R., Rodolfo, K., Di Giamberardino, L., Traiffort, E., Ruat, M., Fretier, P. and Moya, K. L. 2002. Eur J Neurosci. 15 (7): 1163-1177

Sarbassov, D. D., Ali, S. M., Kim, D. H., Guertin, D. A., Latek, R. R., Erdjument-Bromage, H., Tempst, P. and Sabatini, D. M. 2004. Curr Biol. 14 (14): 1296-1302

Selkoe, D. J. 2002. J Clin Invest. 110 (10): 1375-1381

Shmerling, D., Hegyi, I., Fischer, M., Blättler, T., Brandner, S., Götz, J., Rülicke, T., Flechsig, E., Cozzio, A., von Mering, C., Hangartner, C., Aguzzi, A. and Weissmann, C. 1998. Cell. 93 (2): 203-214

Sigurdsson, E. M., Brown, D. R., Daniels, M., Kascsak, R. J., Kascsak, R., Carp, R., Meeker, H. C., Frangione, B. and Wisniewski, T. 2002. Am J Pathol. 161 (1): 13-17

Silveira, J. R., Raymond, G. J., Hughson, A. G., Race, R. E., Sim, V. L., Hayes, S. F. and Caughey, B. 2005. Nature. 437 (7056): 257-261

Smith, D. M., Kafri, G., Cheng, Y., Ng, D., Walz, T. and Goldberg, A. L. 2005. Mol Cell. 20 (5): 687-698

Solforosi, L., Criado, J. R., McGavern, D. B., Wirz, S., Sanchez-Alavez, M., Sugama, S., DeGiorgio, L. A., Volpe, B. T., Wiseman, E., Abalos, G., Masliah, E., Gilden, D., Oldstone, M. B., Conti, B. and Williamson, R. A. 2004. Science. 303 (5663): 1514-1516

Stahl, N., Borchelt, D. R., Hsiao, K. and Prusiner, S. B. 1987. Cell. 51 (2): 229-240

Steele, A. D., Emsley, J. G., Ozdinler, P. H., Lindquist, S. and Macklis, J. D. 2006. Proc Natl Acad Sci U S A. 103 (9): 3416-3421

Stewart, R. S., Drisaldi, B. and Harris, D. A. 2001. Mol. Biol. Cell. 12 (4): 881-889

Stewart, R. S. and Harris, D. A. 2005. J. Biol. Chem. 280 (16): 15855-15864

Sunyach, C., Cisse, M. A., da Costa, C. A., Vincent, B. and Checler, F. 2007. J. Biol. Chem. 282 (3): 1956-1963

Supattapone, S., Muramoto, T., Legname, G., Mehlhorn, I., Cohen, F. E., DeArmond, S. J., Prusiner, S. B. and Scott, M. R. 2001. J Virol. 75 (3): 1408-1413

Supattapone, S., Nguyen, H. O., Cohen, F. E., Prusiner, S. B. and Scott, M. R. 1999. Proc Natl Acad Sci U S A. 96 (25): 14529-14534

Taraboulos, A., Raeber, A. J., Borchelt, D. R., Serban, D. and Prusiner, S. B. 1992. Mol Biol Cell. 3 (8): 851-863

Taraboulos, A., Scott, M., Semenov, A., Avrahami, D., Laszlo, L. and Prusiner, S. B. 1995. J Cell Biol. 129 (1): 121-132

Taraboulos, A., Serban, D. and Prusiner, S. B. 1990b. J Cell Biol. 110 (6): 2117-2132

Taraboulos, A., Rogers, M., Borchelt, D. R., McKinley, M. P., Scott, M., Serban, D. and Prusiner, S. B. 1990a. Proc Natl Acad Sci U S A. 87 (21): 8262-8266

Tateishi, J., Kitamoto, T., Doh-ura, K., Sakaki, Y., Steinmetz, G., Tranchant, C., Warter, J. M. and Heldt, N. 1990. Neurology. 40 (10): 1578-1581

Tatzelt, J., Prusiner, S. B. and Welch, W. J. 1996. Embo J. 15 (23): 6363-6373

Tilly, G., Chapuis, J., Vilette, D., Laude, H. and Vilotte, J. L. 2003. Biochemical and Biophysical Research Communications. 305 (3): 548-551

Tobler, I., Gaus, S. E., Deboer, T., Achermann, P., Fischer, M., Rulicke, T., Moser, M., Oesch, B., McBride, P. A. and Manson, J. C. 1996. 380 (6575): 639-642

Tremblay, P., Bouzamondo-Bernstein, E., Heinrich, C., Prusiner, S. B. and DeArmond, S. J. 2007. Brain Res. 1139 60-67

Tzaban, S., Friedlander, G., Schonberger, O., Horonchik, L., Yedidia, Y., Shaked, G., Gabizon, R. and Taraboulos, A. 2002. Biochemistry. 41 (42): 12868-12875

Vassallo, N. and Herms, J. 2003. J Neurochem. 86 (3): 538-544

Vassallo, N., Herms, J., Behrens, C., Krebs, B., Saeki, K., Onodera, T., Windl, O. and Kretzschmar, H. A. 2005. Biochem Biophys Res Commun. 332 (1): 75-82

Vey, M., Pilkuhn, S., Wille, H., Nixon, R., DeArmond, S. J., Smart, E. J., Anderson, R. G., Taraboulos, A. and Prusiner, S. B. 1996. Proc Natl Acad Sci U S A. 93 (25): 14945-14949

Vincent, B., Paitel, E., Saftig, P., Frobert, Y., Hartmann, D., De Strooper, B., Grassi, J., Lopez-Perez, E. and Checler, F. 2001. J Biol Chem. 276 (41): 37743-37746

Voeltz, G. K., Prinz, W. A., Shibata, Y., Rist, J. M. and Rapoport, T. A. 2006. Cell. 124 (3): 573-586

Walmsley, A. R., Zeng, F. and Hooper, N. M. 2003. J. Biol. Chem. 278 (39): 37241-37248

Weissmann, C., Bueler, H., Fischer, M., Bluethmann, H. and Aguet, M. 1993. Dev Biol Stand. 80 53-54

Weissmann, C., Raeber, A. J., Montrasio, F., Hegyi, I., Frigg, R., Klein, M. A. and Aguzzi, A. 2001. Philos Trans R Soc Lond B Biol Sci. 356 (1406): 177-184

White, A. R., Enever, P., Tayebi, M., Mushens, R., Linehan, J., Brandner, S., Anstee, D., Collinge, J. and Hawke, S. 2003. 422 (6927): 80-83

Wigley, W. C., Fabunmi, R. P., Lee, M. G., Marino, C. R., Muallem, S., DeMartino, G. N. and Thomas, P. J. 1999. J Cell Biol. 145 (3): 481-490

Winklhofer, K. F. and Tatzelt, J. 2000. Biol Chem. 381 (5-6): 463-469

Wong, B.-S., Pan, T., Liu, T., Li, R., Petersen, R. B., Jones, I. M., Gambetti, P., Brown, D. R. and Sy, M.-S. 2000. Biochemical and Biophysical Research Communications. 275 (2): 249-252

Wullschleger, S., Loewith, R. and Hall, M. N. 2006a. Cell. 124 (3): 471-484

Wullschleger, S., Loewith, R. and Hall, M. N. 2006b. Cell. 124 (3): 471-484

Wymann, M. P., Bulgarelli-Leva, G., Zvelebil, M. J., Pirola, L., Vanhaesebroeck, B., Waterfield, M. D. and Panayotou, G. 1996. Mol Cell Biol. 16 (4): 1722-1733

Xiang, R., Liu, Y., Zhu, L., Dong, W. and Qi, Y. 2006. Apoptosis. 11 (11): 1923-1932

Yost, C. S., Lopez, C. D., Prusiner, S. B., Myers, R. M. and Lingappa, V. R. 1990. Nature. 343 (6259): 669-672

Zhang, C. C., Steele, A. D., Lindquist, S. and Lodish, H. F. 2006. Proc Natl Acad Sci U S A. 103 (7): 2184-2189

8 Abbreviations

Ab	anitbody
Aß protein	amyloid ß-protein
AD	Alzheimer´s Disease
Amp	ampicillin
APP	amyloid precursor protein
Atg7	autophagy-related protein
BACE1	ß-site APP cleaving enzyme 1
ßME	2-mercaptoethanol
BSA	bovine serum albumine
CAM	chloramphenicol
Carb	carbenicillin
CO_2	corbon dioxide
CTAB	Cetryl-trimethy-ammonium bromide
^{Ctm}PrP	C-terminal transmembran PrP
CV	column volumes
DAB	diamino benzidine
DMSO	Dimethylsulfoxid
DNA	deoxyribonucleic acid
DNAse	deoxyribonuclease
DOC	deoxycholat
ECL	chemiluminescent subtrate for western blot
EDTA	ethylene-diamine-tetra-acetic acid
E.coli	*Escherichia coli*
eIF4E	effectors eukaryotic initiation factor 4E
FADD	Fas-associated death domain
FCS	fetal calf serum
FITC	Fluorescein isothiocyanate
FKBP	FK506-binding protein
g	earth´s gravity

GPI	glycosylphosphatidyl inositol
GSS	Gerstmann-Sträussler-Scheinker syndrome
h	hour
IEC	Ion-exchange chromatography
IPTG	Isoproyl ß-D-1-thiogalactopyranoside
HEPES	4-(2-hydroxyethyl)-1-piperazineethanesulfonic acid
HRP	horserdish peroxidase
IgG	immunoglobulin G
IP	immunoprecipitation
Kan	kanamycin
kDa	kilo Dalton
KCl	potassium cloride
KHII	ShaPrP, K110I, H111I
LC3	rat microtubule-asociated protein 1 light chain 3
LB	Luria Bertani broth
LST8	lethal with sec thirteen 8
M	Mol
mAb	monoclonal antibody
mg	microgramm
MHM2	mouse PRP with syrian hamster epitope [L108M, V111M]
min	minute
mL	milliliter
mM	milli molar
MORT	mediator of receptor-induced toxicity
mTOR	mammalian target of rapamycin
mTORC1	mTOR complex 1
mTORC2	mTOR complex 2
ng	nanogramm
NHS	N-hydroxylsulfosuccimide
Ni-NTA	nickel-nitrilotriacetic acid
^{Ntm}PrP	N-terminal transmembrane PrP
o.n.	over night
P	postnatal

PA	protein A
PA beads	protein A-coupled –agarose beads
pAB	polyclonale antibody
PAGE	polyacrylamidegel-electrophoresis
PBS	phoshate buffered salineic
PBST	PBS with Tween-20
PCR	polmerase chain reaction
PFA	paraformaldehyde
PG	protein G
PG beads	protein G-coupled –agarose beads
PGPH	postglutamylpeptide hydrolysis
PI	protease inhibitor
PK	proteinase K
PMSF	phenylmethylsulfonyl fluoride
Prion	proteinaceous infectious particles
Prl	prolactin
Prl SN-> QT	mutaded prolactin substitutions: S20N, Q21T
$Prnp^{-/-}$	PrP knockout mice
PrP	prion protein
PrP^{C}	cellular prion protein
PrP^{Sc}	disease causing PrP
µg	microgramm
µL	microliter
µm	micrometer
µM	Micromolar
MS	mass spectrometry
Rap1a	Ras-related protein 1a
RHD	reticulon-homology domain
Rheb	Ras homolog enriched in brain
RIDNs	RTN3 immunoreactive dystrophic neurites
RNA	Ribonucleic acid
RNase	Ribonuclease
RTN	Reticulon

RTN3a	Reticulon-3-A
rpm	rotations per minute
RT	room temperature
RTN	Reticulon
scFv	single-chain variable-fragment
SDS	sodium dodecyl sulfate
^{Sec}PrP	secretory PrP
SHaPrP	Syrian hamster PrP
S6K1	S6 kinase 1
smRNAs	small modulatory dsRNAs
SUP	supernatant
TBS	Tris-buffered Saline
TBST	TBS with Tween-20
TCA	trichloroacetic acid
TECP	Tris(2-carboxyethyl)phosphine
Tg	transgenic
TRIS	tris-(hydroxymethyl)-aminomethane
TSC1/TSC2	Tuberous Sclerosis heterodimers
TUNEL	terminal UDP-mediated nick end labeling
u	units
UPS	ubiquitin proteasome system
v/v	volume/volume
w/v	weight/volume
wt	wild type
ΔSTE	SHaPrP, Δ104-113

9 Acknowledgement

I owe my gratitude to all those people who have made this dissertation possible.

First of all I would like to thank PD Dr. Carsten Korth for the excellent mentoring throughout the entire thesis, for the stimulating discussions and for all his ideas which enriched my project.

I thank Prof. Dr. Dieter Willbold for the mentoring of my thesis as a member of the “mathematisch naturwissenschaftliche Fakultät”.

I want to thank Prof. Dr. Reifenberger for the opportunity to develop this thesis at the Institute of Neuropathology.

Also special thanks to Prof. Vishwanath Lingappa for the collaboration and the very stimulating discussions, which led to further progress of my project.

I thank Prof. Dr. Hans-Werner Müller, Dr. Bruce Onisko, Prof. Dr. Heinrich Sticht and Prof. Dr. Lothar Stitz, with whom I have had opportunities to collaborate on various subjects.

I am also grateful to the former or current staff of the Institute of Neuropathology for their various forms of support during my doctor thesis. Dr. Ralf Klingenstein, Dr. Rutger Leliveld, Dr. Andreas Müller-Schiffmann and Ingrid Prikulis have provided me with necessary assistance and very helpful information.

I also would like to thank Dr. Verian Bader, Barbara Giesen, Dr. Stephanie Grubenbecher and Dr. Marietta Wolters, who supported me by proofreading this thesis.

I would also like to thank the graduate school (GRK1033) of the DFG (Deutsche Forschungsgemeinschaft) for there financial support and further education.

I extend many thanks to my colleagues and friends, Dr. Stephanie Grubenbecher, Dr. Ariane Trampe-Kieslich and Dr. Barbara Klink. They have helped me stay sane through the last three years. Their support and care helped me overcome setbacks and stay focused on my thesis. I greatly value their friendship.

Most importantly, none of this would have been possible without the love and patience of my parents and my partner Thorsten Kutzsche, they have been a constant source of love, concern, support and strength all these years and I deeply appreciate their belief in me.

10 Erklärung

Hiermit erkläre ich, dass ich die vorgelegte Dissertation eigenständig und ohne unerlaubte Hilfe angefertigt habe.
Die Dissertation wurde in der vorgelegten oder in ähnlicher Form noch bei keiner anderen Institution eingereicht. Ich habe bisher keine erfolglosen Promotionsversuche unternommen.

Düsseldorf, den 1. Juli 2008

(Janine Muyrers)